DISSERTATION

submitted to the

Combined Faculties for the Natural Sciences and for Mathematics

of the Ruperto-Carola University of Heidelberg, Germany

for the degree of

Doctor of Natural Sciences

presented by

Diploma-Biophysicist Frauke Christiane Leitner

born in Karlsruhe

Odor processing in the lateral entorhinal cortex revealed by two-photon calcium imaging

Referees:
Prof. Dr. Peter Seeburg
Prof. Dr. Hannah Monyer

Date of Oral Exam:

Declarations according to § 8 (3) b) and c) of the doctoral degree regulations: a) I hereby declare that I have written the submitted dissertation myself and in this process have used no other sources or materials than those expressly indicated, b) I hereby declare that I have not applied to be examined at any other institution, nor have I used the dissertation in this or any other form at any other institution as an examination paper, nor submitted it to any other faculty as a dissertation.

Heidelberg, _____

Contents

Nomenclature

5HT3aR	ionotropic serotonin receptor 5HT3a
A	**A**myl acetate
Aβ	**A**myloid-β
AAV	**A**deno **A**ssociated **V**irus
AD	**A**lzheimer's **D**isease
AP	**A**ction **P**otential
APP	**A**myloid-β **P**recursor **P**rotein
B	**B**enzaldehyde
BSA	**B**ovine **S**erum **A**lbumin
C	**C**ineole
CA	**C**ornu **A**mmonis
CB	**C**al**B**indin
CC	**C**orrelation **C**oefficient
CR	**C**al**R**etinin
CTB	**C**holera **T**oxin **S**ubunit B
DAB	**D**i**a**mino **b**enzidine
DG	**D**entate **G**yrus
Dp	**D**orsal pallial divison, **P**osterior zone
E	**E**ugenol
EB	**E**thyl **B**utyrate
EC	**E**ntorhinal **C**ortex
FG	**F**luoro**G**old
FS-cell	**F**ast-**S**piking cell

GABA	**G**amma-**A**mino**B**utyric **A**cid
GAD	**G**lutamic **A**cid **D**ecarboxylase
GECI	**G**enetically **E**ncoded **C**alcium **I**ndicators
GFP	**G**reen **F**luorescent **P**rotein
H	**H**exanal
ISI	**I**nter**S**timulus **I**nterval
LEC	**L**ateral **E**ntorhinal **C**ortex
LOT	**L**ateral **O**lfactory **T**ract
MEC	**M**edial **E**ntorhinal **C**ortex
NeuN	**NEU**ronal **N**uclei
NFT	**N**euro**F**ibrillary **T**angles
NPY	**N**euro**P**eptide **Y**
NRR	**N**ormal **R**at **R**inger solution
OB	**O**lfactory **B**ulb
PBS	**P**hosphate **B**uffered **S**aline
PIR	**PI**riform **C**ortex
PV	**P**ar**V**albumin
RF	**R**eceptive **F**ield
ROI	**R**egion **O**f **I**nterest
SEM	**S**tandard **E**rror of the **M**ean
SOM	**SOM**atostatin
Vv	**V**entral nucleus of the **v**entral telencephalon

Abstract

Recent studies ascribed to the lateral entorhinal cortex (LEC) an important function in object recognition and novelty detection and confirmed the involvement of the LEC in odor processing. In this thesis, I investigated the contribution of LEC layer II neurons in sensory processing. Using immunohistochemical staining methods I could show that excitatory neurons in LEC layer II can be distinguished based on the expression of two marker proteins, namely Reelin and calbindin (CB). In combination with retrograde tracer injections, I revealed distinct projection patterns of these two excitatory cell types, with Reelin$^+$ neurons projecting to the hippocampus and CB$^+$ neurons providing feedback to structures of the olfactory system. Inhibitory GABAergic neurons in layer II of the LEC comprise a variety of molecularly defined subtypes. My goal was to analyze the participation of the defined cell classes in stimulus-triggered network activity. Therefore, I implemented *in vivo* two-photon imaging of genetically encoded calcium indicators in the LEC of anesthetized mice. This approach allowed me to investigate the activity of small neuronal networks in response to olfactory stimulation. I demonstrated that Reelin$^+$ excitatory neurons transmitting information directly to the hippocampus respond with high selectivity to different odors. A markedly less selective response profile is exhibited by excitatory CB$^+$ neurons that convey feedback to upstream targets in the olfactory pathway. It was possible to contrast these response patterns of excitatory neurons with that of their inhibitory counterparts. Thus, GABAergic neurons responded the least selective to various odors. Furthermore, we established *in vivo* whole-cell patch-clamp recordings under visual guidance. This enabled us to particularly target excitatory and GABAergic odor-responsive cells and to characterize them based on electrophysiological and morphological criteria. In summary, I defined and characterized here different neuronal subtypes in the LEC that are functionally involved in the processing and transmission of odor information.

Zusammenfassung

Studien jüngeren Datums schreiben dem lateralen entorhinalen Kortex (LEC) eine wichtige Rolle beim Erkennen von Objekten und der Wahrnehmung von neuen Inhalten zu und untermauern die Beteiligung des LEC bei der Verarbeitung von Düften. In dieser Dissertation untersuchte ich die Mitwirkung von Neuronen in Schicht II des LEC bei der Verarbeitung sensorischer Inhalte. Mithilfe immunohistochemischer Färbemethoden konnte ich zeigen, dass exzitatorische Neurone in Schicht II des LEC basierend auf der Expression von zwei Proteinmarkern - Reelin und Calbindin (CB) - unterschieden werden können. In Kombination mit der Injektion retrograder Indikatoren konnte ich unterschiedliche Projektionsmuster nachweisen, insofern dass Reelin$^+$ Neurone zum Hippocampus projizieren, wohingegen CB$^+$ Neurone Rückmeldung zu Strukturen des olfaktorischen Systems geben. Inhibitorische GABAerge Neurone in Schicht II des LEC bestehen aus einer Vielzahl von Untergruppen, die sich durch die Expression molekularer Proteinmarker unterscheiden lassen. Mein Ziel bestand darin, die Teilnahme dieser definierter Zellklassen bei der von einem Stimulus induzierten Netzwerkaktivität zu untersuchen. Dazu habe ich 'Calcium Imaging' mittels genetisch kodierter Kalzium Indikatoren und Zwei-Photonen-Mikroskopie im LEC anästhesierter Mäuse implementiert. Diese Vorgehensweise machte es möglich, die Aktivität kleiner neuronaler Netzwerke nach Duftstimulation zu untersuchen. Ich konnte zeigen, dass exzitatorische Reelin$^+$ Neurone, die Information direkt an den Hippocampus übermitteln, mit hoher Selektivität auf verschiedene Düfte reagieren. Ein deutlich weniger selektives Antwortprofil bot sich bei den exzitatorischen CB$^+$ Neuronen, welche Information an Regionen übermitteln, die im olfaktorischen Signalweg dem LEC vorgeschaltet sind. Es war möglich einen Vergleich zwischen dem Antwortverhalten exzitatorischer Neurone mit dem ihrer inhibitorischen Gegenspieler anzustellen. Demnach antworteten inhibitorische Zellen am wenigsten selektiv auf verschiedene Düfte. Darüberhinaus etablierten wir *in vivo* die Patch-Clamp-Technik mit optischem Zugang. Dies ermöglichte ein gezieltes Anvisieren von exzitatorischen und GABAergen

Zellen, welche zuvor auf Düfte reagiert hatten, und eine Charakterisierung dieser Zellen basierend auf elektrophysiologischen und morphologischen Kriterien. Zusammenfassend definierte und charakterisierte ich hier verschiedene neuronale Populationen im LEC, die funktionell in die Verarbeitung und Weiterleitung von Duftinformation involviert sind.

1 INTRODUCTION

It is a typical situation everyone knows from their own experience: The smell of a trivial object can suddenly conjure up entire scenes from the past. The faint scent of sun screen on the skin suddenly evoke memories of this most beautiful beach where joyful holidays were spent during childhood. The lingering perfume of someone passing by on the street can recall past moments that were spent with the grandma who used to put this perfume on. The most famous example of this phenomenon is found in the literature when Marcel Proust describes the moment a madeleine, that was dipped in tea, fills the narrator's mouth (Proust, 1919). Immediately, the narrator is transported back into his own childhood when he used to get such madeleines from his aunt. He experiences moments of happiness, which Proust describes in such vivid words that the term "Proustian phenomenon" was coined for the idea that distinct odors have extraordinary power to help us recall distant memories. Neuroscientists were intrigued by this phenomenon and tried to reveal underlying brain areas and neuronal mechanisms. Several studies have shown a strong link between smell and memory with a particular involvement of the piriform cortex (PIR) (Gottfried et al., 2004) and the lateral entorhinal cortex (LEC) (Igarashi et al., 2014), two areas that are part of the olfactory system. In particular, the LEC might have an important role to play, considering its direct connectivity with the hippocampus, an area most relevant for the coding and retrieval of memories (Steward and Scoville, 1976). However, knowledge about the LEC is very limited. Its functional role in odor processing is not clear yet, and even more basic questions regarding its neuronal network and cellular composition have not been answered yet. Therefore, we address these fundamental questions in this project to help elucidating the significance of the LEC in odor processing.

1.1 Stages of olfactory processing in the brain

The first stage in olfactory processing is the olfactory epithelium, which lines the nasal cavity. Receptor neurons situated here express different receptors that bind odorous molecules and transduce the chemical signal into an electrical signal carried by neurons. In the genome of the mouse and the rat, approximately 1.000 genes for olfactory receptor neurons have been identified (Buck and Axel, 1991), but each receptor neuron is thought to express only one of these genes (Serizawa et al., 2000, 2003). Therefore, there are $\sim$1.000 different olfactory receptor neurons in mouse (Ressler et al., 1993) and rat (Vassar et al., 1993). These are distributed within a particular spatial zone of the olfactory epithelium in a seemingly random arrangement. They all send one unbranched axon to a single glomerulus in the olfactory bulb (OB) (Klenoff and Greer, 1998), and at this stage, an astonishing sorting occurs. Axons from olfactory receptor neurons expressing the same receptor type converge in a focal spot where their axons form a glomerulus (Ressler et al., 1994; Vassar et al., 1994; Mombaerts et al., 1996). In the mouse, $\sim$1.800 of these glomeruli are situated at the surface of the right and the left OB, and for most odorant receptor types there are generally two glomeruli per OB. There is approximate mirror symmetry between the bulbs such that glomeruli being innervated by the same type of receptor cell are found in approximately the same position in the left and in the right OB (Ressler et al., 1994; Belluscio and Katz, 2001). This layout seems to be evolutionarily conserved to a certain extent, as it is similar but not identical between animals and closely related species such as rat and mouse (Soucy et al., 2009). Furthermore, glomeruli that are responsive to specific molecular features and therefore overlap in their odor specificity seem to form domains in the bulb (Stewart et al., 1979; Rubin and Katz, 1999; Wachowiak and Cohen, 2001). However, neighboring glomeruli within such a domain have a similar likelihood to respond to the same odor as glomeruli far apart, such that on this finer scale no particular spatial arrangement is apparent (Soucy et al., 2009).

In a glomerulus, mitral cells receive sensory information about odor identity and transmit this information to downstream brain regions (Miyamichi et al., 2011; Sosulski et al., 2011). The piriform cortex (PIR) is considered to function like 'association cortex' in other sensory systems and receives the olfactory information from the OB via the lateral olfactory tract (LOT). One distinguishes between the anterior and the posterior PIR, with the former presumably being involved

in coding odor identity and the latter having a more pronounced role in coding odor quality (Gottfried et al., 2006). Interestingly, it was shown that the specific arrangement of glomeruli forming domains that is present in the OB is not preserved in the PIR. Instead, the PIR exhibits a 'salt and pepper' layout, where neurons, responsive to a given odor, are distributed without apparent spatial preference (Stettler and Axel, 2009). These neurons reveal a discontinuous receptive field, in that they can be activated by odors with a broad spectrum of molecular structures. This might be explained by the convergent input from distinct OB glomeruli onto pyramidal cells in PIR (Apicella et al., 2010; Sosulski et al., 2011). A particular odorant seems to be represented by a unique and distributed ensemble of neurons that no longer displays the spatially segregated pattern observed in the OB. Additional processing of olfactory information is accomplished in the downstream area, the LEC.

1.2 The LEC as part of the olfactory cortex

The connectivity between olfactory structures and the LEC is astonishing, considering the spatial extent between the first station in the brain in olfaction, the OB being located at the most anterior part of the brain, and the LEC, at the most posterior tip of the cerebral cortex. In the 1960s, lesion studies observing the degeneration of fibers could show for the first time that a direct projection exists both from the OB and the PIR to the LEC (Powell et al., 1965; White, 1965; Heimer, 1968). Already back then it was observed that the input from PIR and OB arrives in layer I in a complementary laminar pattern with the OB input arriving in layer Ia and the PIR input enervating layer Ib and to a lesser extent layer III. This pattern seems to be preserved across all cortical structures of the forebrain that receive input from both structures. Thus, the OB targets distal segments and the PIR proximal segments of apical dendrites without any overlap (Price, 1973). A few years later, Haberly and Price (1977) identified both mitral and tufted cells as the projecting cells of the OB. The later reevaluation, however, forwarded the notion that apparently only mitral cells project to the LEC (Igarashi et al., 2012). Nevertheless, this seminal study proved that the LEC is by definition part of the olfactory cortex as it is a direct target area of mitral cell terminals (**Figure 1.1A**). [1]

[1] The question if the MEC is also involved in olfactory transmission could not be fully clarified until today, with some reports showing no projections to the MEC and no effect of MEC de-

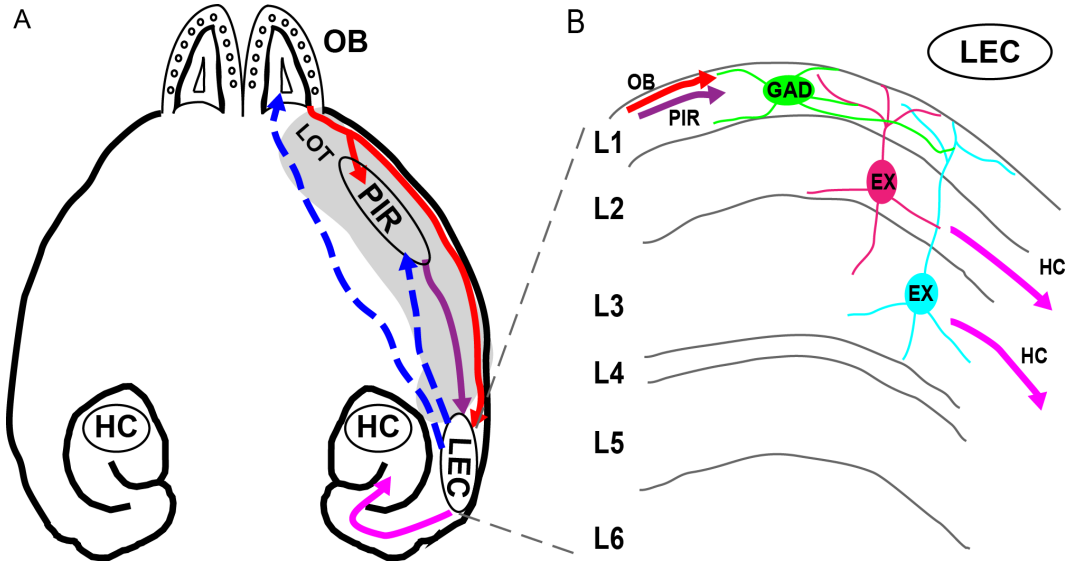

Figure 1.1. Connectivity between olfactory structures (A) Schematic drawing showing the reciprocal connections between the LEC and other olfactory structures. Mitral cells in the olfactory bulb (OB) send their axons (red) via the lateral olfactory tract (LOT, grey) to the piriform cortex (PIR) and the lateral entorhinal cortex (LEC). The LEC receives also input from the PIR (purple). Neurons in the LEC project back to both structures (dotted) and relay the information to the hippocampus (HC) (magenta). **(B)** The input from the OB and the PIR arrives in layer I of the LEC. Synapses are formed on GABAergic neurons (GAD, green) in layer I and apical dendrites from principal cells in layer II (EX, pink) and layer III (EX, cyan). Neurons in layer II and layer III project to the hippocampus.

Several cell types in the LEC receive input from fibers originating in the OB. Layer II spinous multipolar neurons and layer III spinous pyramidal neurons were shown to receive direct input at their distal dendrites located in layer Ia (Wouterlood and Nederlof, 1983). With this finding, for the first time an important idea was put forward - namely, the possibility of a neuronal chain consisting of three elements: the output neurons of the OB, i.e. the mitral cells, transmit information to neurons located in layer II and III in the EC that further convey the olfactory signal to the hippocampus (**Figure 1.1B**). This hypothesis was supported when fan cells (at that time still referred to as stellate cells), but not pyramidal cells, were shown to be contacted by OB projection neurons and in turn send their axon to the hippocampus, supporting this disynaptic olfactory input to the hippocampus (Schwerdtfeger et al., 1990). Also GAD^+ neurons located in layer Ia form synaptic contacts with fibers originating from the OB (Wouterlood et al.,

struction onto olfactory activation (Wilson and Steward, 1978; Habets et al., 1980a; Hintiryan et al., 2012) and other researchers arguing strongly for olfactory projections reaching the MEC (Kosel et al., 1981; Wouterlood and Nederlof, 1983).

1985). The PIR provides the strongest input to the LEC of all cortical areas, which constitutes 30% of the total afferent input. Neurons in layer II of the PIR form the axonal projections to the LEC (Beckstead, 1978; Burwell and Amaral, 1998a; Kerr et al., 2007).

Interestingly, the reciprocal connectivity is similarly strong as the LEC provides the heaviest projections to the PIR (Agster and Burwell, 2009). These projections terminate mainly in deep layer I and to a lesser extent in layer III. There is a prevalence of projections originating from the anterior part of the LEC compared to the posterior part of LEC to PIR. The origin of these cells that reciprocally connect the PIR with the LEC seems to be in all layers with a prevalence in layer II, III (rostrally) and layer IV (caudally) (Witter and Groenewegen, 1986; Insausti et al., 1997; Hintiryan et al., 2012). Projections to the OB arise in the LEC in layer II and III and to a lesser extent in layer IV, but more detailed knowledge about the identity of these projecting neurons is lacking (de Olmos et al., 1978; Shipley and Adamek, 1984; Witter and Groenewegen, 1986; Insausti et al., 1997). Although neurons projecting to the OB and the PIR can be located in the same LEC lamina, so far there is no evidence for neurons projecting to both structures simultaneously (Chapuis et al., 2013).

As mitral cells are the output cells of the OB, providing both the PIR and the LEC with olfactory information, it is worth taking a closer look at the projection patterns of OB mitral cells in order to anticipate possible network responses in the target regions. For the PIR, a diffuse projection pattern was shown without apparent spatial preference. Single mitral cells were found to make powerful connections with pyramidal cells in layer II and III, so that the coinciding input from few mitral cells is sufficient to elicit spikes (Sosulski et al., 2011; Franks and Isaacson, 2006). Considering that the activation of mitral cells is highly molecule specific, this argues for a model in which complex odors, i.e. odors consisting of numerous different molecules, are represented by pyramidal cells in the PIR in a broad and distributed manner. This would result in a dispersed coding of the complex odor (Stettler and Axel, 2009). How the decoding of such distributed patterns of activity is achieved, is not resolved yet, nor is there a satisfying answer as to which brain area might be responsible for that task.

Much less is known about the projection patterns from mitral cells to the LEC. Extensively arborizing axons are observed in layer Ia, but overall their number is lower in more caudal structures such as the LEC compared to their number in

rostral structures such as the anterior olfactory nucleus and the PIR (Hintiryan et al., 2012). Whether the projections follow a specific spatial layout and if so, what this spatial arrangement might look like, has not been determined. Therefore, the question remains if odors are represented in a distributed or spatially restricted and localized manner in the LEC.

1.3 Olfactory computation in other species

For some questions, it can be advantageous to address them in species less complex and less evolutionary evolved than rodents. In particular, both zebrafish and locusts such as *drosophila melanogaster* have proven to be especially useful when investigating the olfactory system. With respect to the first three olfactory processing stages - olfactory sensory neurons, mitral cells, and the olfactory cortex - numerous similarities can be observed.

In the OB of zebrafish, odors evoke fast oscillatory population activity and distinct firing rate patterns across mitral cells. Due to phase-locking of this activity pattern to the oscillatory field potential, mitral cells can form ensembles that show oscillatory synchrony. It was shown that these ensembles transmit information about molecular categories, i.e. the type and position of functional groups carried by the molecule. On the contrary, patterns of non-synchronized spiking mitral cells become decorrelated and provide information about precise odor information such as odor identity (Friedrich and Laurent, 2004). Mitral cells in the OB project to two distinct targets, the ventral nucleus of the ventral telencephalon (VV), a subpallial area, and the posterior zone of the dorsal telencephalon (Dp), a pallial area homologous to olfactory cortex. Thereby, chemotopic organization in the OB is translated into broad and sparse activity patterns in higher order brain areas that both lack obvious topography. An imaging study showed that individual Dp neurons combine information of various glomeruli converging onto them and form a unified percept of a mixture of odors rather than representing a single odor component (Yaksi et al., 2009). Interestingly, Dp neurons are largely insensitive to the oscillatory synchrony between mitral cells, as they act as low-pass filter. Hence, only their spike timing can be influenced by the oscillatory synchrony of mitral cells, but not their depolarization or firing rate (Blumhagen et al., 2011). As a consequence of these tranformational processes and the temporal filtering by Dp neurons, activity patterns evoked

by similar odors are more distinct in Dp than in OB, which allows a specific and decorrelated odor representation, a prerequisite for pattern storage. It has been suggested that perception could be directly determined by the output of Dp and that Dp neurons are directly involved in the storage of odor information (Friedrich, 2013).

In locusts, projection neurons in the antennal lobe, which is comparable to the OB, send their axons to Kenyon cells in the mushroom body, a homolog of the PIR, as well as to the lateral horn. Kenyon cells are innervated by broadly tuned projection neurons, but fire only very sparsely, as about 100 concurrent projection neuron inputs might be needed to drive Kenyon cells above spike threshold. Each Kenyon cell is on average connected to approximately 50% of all projection neurons (Jortner et al., 2007). For a long time, olfactory input to the mushroom body was considered to be random (Murthy et al., 2008; Caron et al., 2013), but recent studies challenged this perspective and indicated at least a coarse spatial segregation and some functional bias (Jefferis et al., 2007; Gruntman and Turner, 2013). Interestingly, the same neurons form highly stereotyped connections in the lateral horn, which is thought to be involved in behavior and innate odor responses (Fisek and Wilson, 2014). This is reminiscent of the amygdala in rodents, which is also innervated in a stereotypical manner (Miyamichi et al., 2011; Sosulski et al., 2011) and is believed to be important for fear responses (Herry et al., 2008).

In summary, it is noteworthy that the flow of information and the brain areas involved in processing of olfactory content downstream of the Dp in zebrafish and the mushroom body in locusts is still largely unresolved. Despite the experimental advantages provided in zebrafish and locusts, it is necessary to investigate the prospective function of the LEC and its unique role in olfactory processes in rodents, as no clear homology to the LEC could be determined so far.

1.4 Anatomy of the LEC

In rodents, the entorhinal cortex (EC) is part of the medial temporal lobe. It is partly enclosed by the rhinal (olfactory) sulcus, which gave this structure its name. In his seminal studies Ramón y Cajal observed a strong interconnectivity between EC and the hippocampal formation. The EC is the major gateway

between the neocortex and the hippocampus. He believed that the EC was part of the olfactory system and he assumed that whatever physiological significance one of the structures would have, the other one would share or inherit. Therefore, he expected the hippocampus to be an olfactory structure as well (Ramón y Cajal, 1902). This view was discarded with the discovery that the hippocampus was crucially involved in memory processing as revealed in the famous case of HM, who lost his declarative memory skills after a surgeon had removed parts of his hippocampi and neighboring areas trying to cure him from epileptic seizures (Scoville and Milner, 1957). Thereafter, two major discoveries resulted in renewed attention in the EC. In the 1980s, one of the most threatening diseases of mankind was related to the EC as it was shown that Alzheimer's Disease manifests itself in pathological abnormalities in the EC already at very early stages in the course of the disease (Hyman et al., 1984; Braak and Braak, 1985). More recently, spatially modulated cells were discovered in the medial part of EC (Fyhn et al., 2004) and since then the interest in formation, occurrence and stability of these so-called grid cells has led to a wealth of studies about the EC (Hafting et al., 2005; Giocomo et al., 2011; Stensola et al., 2012; Heys et al., 2014).

In general, the EC is divided into a medial and a lateral part (MEC and LEC), but a note of caution should be made regarding the different classification schemes that have been in use during the last decades. Initially, the parcellation of the EC was done on the basis of morphological features such as cell size and layering, sometimes resulting in subdivisions of LEC and MEC that can still be encountered in the literature. Nowadays, LEC and MEC are mostly characterized by their different input and output pattern (Insausti et al., 1997; Burwell and Amaral, 1998a; Kerr et al., 2007). The LEC is extensively connected to perirhinal cortex and PIR, as well as to insular cortex, frontal cortex and amygdala. On the contrary, the MEC has its most abundant connections with postrhinal cortex, presubiculum, visual association and retrosplenial cortices. These two divisions of the EC together provide the major input to the hippocampus via the perforant path. Neurons that are located in layer II send their axons to the dentate gyrus (DG), where they terminate in the outer 1/3 of the molecular layer (Wilson and Steward, 1978). Granule cells in the DG receiving input from the EC are connected via mossy fibers to pyramidal cells located in Cornu Ammonis (CA) 3, which in turn convey the information to CA1 pyramidal cells via Schaffer collaterals. CA1 neurons constitute the major output of the HC, projecting back to

the EC via the subiculum. This trisynaptic circuit emphasizes the strong interdependency between entorhinal and hippocampal structures. Additionally, layer III neurons in the LEC project directly onto pyramidal cells in CA1 via the temporoammonic pathway (Witter et al., 1986; Canto et al., 2008). 1/3 of the total afferent input to the LEC originates in hippocampal areas. Both the dorsal and the ventral hippocampus contribute to this input, but the ventral hippocampus provides the major input to the LEC (Kerr et al., 2007). The MEC, on the other hand, seems to be more strongly connected to dorsal hippocampal structures (Agster and Burwell, 2013). Also along the transverse axis, the projection pattern differs, as the LEC sends more projections to distal CA1 and the proximal subiculum, whereas the MEC is stronger connected with the proximal CA1 and the distal subiculum (van Strien et al., 2009).

1.4.1 Excitatory cell types in the LEC

From the perspective of a neuroanatomist, the EC is a transitional structure between paleocortex like the PIR and neocortex. Just like in the PIR, for example, afferent input to the LEC arrives extensively in layer I, contrary to the neocortex. But similar to neocortex, the EC is a six-layered cortex, whereas the PIR is organized in three layers. Based on cytoarchitectonical features, it is possible to distinguish between MEC and LEC and also other adjacent structures, but several markers need to be taken into account for a clear separation. Layer IV is an almost cell-free layer and therefore called lamina dissecans, and it is sharper delineated and easier to distinguish in MEC than in LEC (Witter et al., 1989). Also in layer I the neuronal density is very sparse and most neurons are GABAergic neurons. The other layers comprise a variety of different neuron types. In layer II, three morphological neuronal types can be distinguished: Fan cells, pyramidal cells, and multiform cells (Tahvildari and Alonso, 2005). Fan cells, the most abundant cell type in layer II, are equivalent to stellate cells in the MEC and are characterized by dendrites extending horizontally towards the pia. Pyramidal cells posses an apical dendrite ascending towards the pia, and basal dendrites extending into layer III. Multiform cells do not fit in either category. All three types exhibit dendritic spines, which reveals their excitatory nature (Tahvildari and Alonso, 2005). In layer III, pyramidal cells predominate. Fan cells in layer II and pyramidal cells predominantly in layer III provide the majority of projections to the hippocampus via the perforant path and via the temporoammonic path-

way, respectively. However, it was shown that the perforant path is not purely excitatory as a small population of sparsely spinous horizontal cells at the outer rim of layer II and multipolar cells in layer II and layer III, which are GABAergic, also project to the hippocampus (Germroth et al., 1989; Melzer et al., 2012).

Several recent studies contributed to our knowledge of excitatory cell types in the EC, and although the focus of investigation was the MEC and not the LEC it is worth taking a closer look at these findings. The expression of two specific molecular markers, calbindin (CB) and Reelin, was correlated with the layer II pyramidal cell and stellate cell phenotype respectively (Kitamura et al., 2014; Ray et al., 2014). These studies further supported the idea of a modular organization in this area, specifically the arrangement of CB^+ neurons in islands, a finding which sank into oblivion after the first description at the end of the last century (Fujimaru and Kosaka, 1996). While the functional significance of this arrangement in the MEC still needs to be determined, it is not known if a similar organizational principle exists in the LEC.

1.4.2 GABAergic cell types in the LEC

Excitation in the brain is tightly controlled and counterbalanced by inhibition provided by an abundant amount of inhibitory neurons. Depending on the brain region, the layer, and the species, these inhibitory neurons account for 10-30 % of the whole neuronal population (DeFelipe, 1997; DeFelipe et al., 2002; Meyer et al., 2011). Synapses of the majority of inhibitory neurons contain the neurotransmitter gamma-aminobutyric acid (GABA) that is released at the presynapse, leading to an inhibition in the postsynaptic cell. Interneuron research has been proven to be quite challenging, partly due to the heterogeneity of these cells. They show a broad range of different electrophysiological characteristics, molecular identities and morphological phenotypes and they can be classified according to all of these parameters (reviewed by e.g. Rudy et al. (2011); Markram et al. (2004); Kubota (2014)). It has become acknowledged that this variety of cell types might be related to a variety of different functions (see Isaacson and Scanziani, 2011). However, the tools for studying the function of different cell types in an intact circuit have just been developed in the last few years such that in interneuron research, the attempt can be made to match form to function.

In the LEC, knowledge about the identity of GABAergic cells in this area is still sparse. Most of the studies investigating GABAergic cells in the EC focused on the MEC and its cellular composition. The LEC as a separate structure was often neglected or treated stepmotherly. The little we know today about the interneuronal network in the LEC is mainly based on immunohistochemical studies investigating the distribution of different subtypes expressing known molecular markers. Neurons are often classified according to the expression of neuropeptides such as somatostatin (SOM) and neuropeptide Y (NPY) or calcium-binding proteins like parvalbumin (PV), calbindin (CB) or calretinin (CR). GABAergic neurons are located in all layers in the rodent entorhinal cortex, with few in layer I, and the majority in layer II and superficial layer III (Miettinen et al., 1996). In layer I in the LEC, several studies have shown that a large fraction of the cells express CR, however, there are contradictory observations regarding their excitatory or inhibitory nature (Miettinen et al., 1997; Wouterlood et al., 2000, 2007). The morphology of layer I neurons is either bipolar or multipolar and the distance between single neurons can be up to 500 μm (Miettinen et al., 1997; Wouterlood et al., 2000). In the rat cortex, SOM is expressed in a separate population of neurons and no coexpression with CR was shown (Rogers, 1992). In layer I, only few SOM$^+$ neurons are present, which are mostly located close to the border to layer II (Wouterlood and Pothuizen, 2000). The majority of SOM$^+$ neurons in the EC consists of small spherical cells, and in contrary to studies investigating colocalization of SOM with GAD or GABA in the hippocampus and the neocortex, in the EC only 18 % seem to coexpress SOM and GABA, and a large proportion of SOM$^+$ cells may consist of non-GABAergic, excitatory interneurons (Wouterlood and Pothuizen, 2000).

PV is a marker that is not encountered in layer I, but in layer II the expression level is exceptionally high. In contrary to the MEC, which is very strongly stained for PV, the LEC exhibits only a lighter staining (van Groen, 2001). The highest number of PV$^+$ neuron is reported for the dorsal LEC, the lowest for ventral LEC (Wouterlood et al., 1995). Their axons form typical basket-like structures, building a dense plexus around principal cell bodies providing strong inhibitory control (Jones and Buhl, 1993; Wouterlood et al., 1995). In the entorhinal cortex PV is a marker exclusively for GABAergic neurons (van Groen, 2001; Miettinen et al., 1996). For example, basket cells as well as chandelier cells with a bipolar or bitufted arbor found in layer II/III often express PV. In layer II, SOM is often detected in multipolar neurons, but GABAergic SOM$^+$ neurons are small

spherical neurons (Wouterlood and Pothuizen, 2000). CR is expressed in few mostly bipolar neurons with dendrites perpendicular to the surface of the LEC (Ma et al., 2008). Additionally, there are horizontal-bipolar inhibitory cells at the outer rim of layer II and multipolar cells in layer II and III that have been shown to contribute to the perforant path, rendering it not exclusively excitatory as was believed for a long time (Germroth et al., 1989; Melzer et al., 2012). Other neuronal markers like NPY, VIP, substance-p, CCK and ENK were also found to be expressed in superficial layers of the EC (Köhler and Chan-Palay, 1982, 1983; Köhler et al., 1985, 1986). However, comprehensive descriptions of expression profiles of neuronal subtypes and specifically their functional correlate in local circuits are still missing.

It is noteworthy that in the MEC groundbreaking progress was made just recently concerning the connectivity between interneurons and principal neurons, which will change the field of understanding and modeling grid cell formation deeply (Couey et al., 2013; Buetfering et al., 2014). As often, research in the LEC lags behind, and to determine how various neuronal players are interconnected is adamant.

1.5 The functional role of the LEC

1.5.1 Spatial navigation and object processing

Next, I would like to address the question what is currently known about the function of the LEC. Located in the direct vicinity of the MEC, and sharing some features both in terms of neuronal composition as well as projection patterns to the hippocampus, it was hypothesized that the LEC might be involved in similar computational tasks as the MEC. Therefore, the interest was great to reveal if the LEC would also exhibit grid cells and play a role in spatial navigation.

The earliest findings were published in 2005 by Hargreaves and colleagues and were at that time quite surprising, as it was shown that there is a major dissociation between MEC and LEC input to the hippocampus: During an open field exploration task in a very simple environment, the MEC conveyed much more spatial information than the LEC (Hargreaves et al., 2005). When the open field was transformed into a cue-rich environment providing landmarks, they came

to the same conclusion (Yoganarasimha et al., 2010). However, after placing discrete objects into the open field, LEC neurons exhibited firing selectively at locations relative to objects, with stronger responses to novel or misplaced objects than MEC neurons (Deshmukh and Knierim, 2011). Moreover, LEC neurons continued their firing at locations where objects were previously placed, resembling the characteristic place specific firing of hippocampal place cells. Using a circular track that allowed manipulation of both global and local cues independently, Neunuebel and colleagues came to the conclusion that overall the spatial signal is not strong in the LEC. They suggested that the firing of LEC neurons is dominated by local cues, whereas the MEC rather processes global cues (Neunuebel et al., 2013).

The aforementioned studies used tetrodes to record multiple single units in either MEC or LEC. A study using lesions of either the MEC or the LEC to clarify their respective roles in spatial cognition found - as expected - that MEC lesions lead to severe deficits in the water maze and a path integration task (Van Cauter et al., 2013). Interestingly, LEC lesions did not affect navigation abilities in either of these tasks but altered spatial as well as non-spatial processing in an object exploration task. Lately, researchers investigating the functional role of the LEC drifted away from the idea of spatial navigation, and rather focused on the processing of objects in the LEC. Pharmacological inactivation experiments affecting the perforant path inputs from the MEC or the LEC into the hippocampus suggested that these inputs may not be fully functionally dissociable at the level of the hippocampus as there is already a lot of intermixing of information between MEC and LEC (Hunsaker et al., 2013). Nevertheless, lesions of the LEC primarily disrupted item novelty detection, whereas lesions of the MEC primarily affected contextual novelty detection (Hunsaker et al., 2013). Lesions of the LEC also affected the animal's ability to perform object-context recognition tasks, without impairing object recognition or context habituation (Wilson et al., 2013a). In a follow-up study, the same authors extended their work and demonstrated a wider role of the LEC in binding together several features of an event, showing a more general involvement in associative but not non-associative recognition memory (Wilson et al., 2013b). The processing of familiar or novel objects at familiar or novel locations in the LEC was investigated in further detail just recently by Tsao and colleagues (Tsao et al., 2013). They discovered that some LEC neurons fire at objects and that other LEC neurons develop specific firing at places where objects had previously been located. These object cells and

object-trace cells belong to two different classes as object-trace cells did not respond to an object as long as it was still present (Tsao et al., 2013). Object-trace cells showed persistence over many days during the phase of extinction, indicating the involvement in memory processes of the LEC. As also rate remapping in the hippocampus was impaired after lesions of the LEC (Lu et al., 2013), evidence is accumulating that the LEC codes for non-spatial parameters such as the diversity of experiences at specific locations.

1.5.2 Olfactory information processing

Based on anatomical data, the involvement of the LEC in olfactory information processing was described in previous sections. Here, I would like to focus on the available literature regarding the functional involvement in odor processing. It all started with the famous patient HM, who was not only a very important case for the study of memory functions in general, but also for research about olfactory learning specifically (Eichenbaum et al., 1983). After the surgery, HM was subjected to a battery of behavioral and cognitive tests, which revealed normal performance in odor detection, discrimination of odor intensity and adaptation to odors. However, he showed significant impairments in discrimination of distinct odors and odor identification. The damage to his brain was substantial and allowed only conclusions about the function of the medial temporal lobe as a whole, but even so, these findings triggered further investigations about the different compartments and their respective functional contributions to olfactory memory.

Today, it is well established that the entorhinal cortex and the hippocampus have distinct tasks in odor identification, both in humans (Kjelvik et al., 2012) and mice (Staubli et al., 1984; Eichenbaum et al., 1988; Otto and Eichenbaum, 1992). A large body of evidence derived from behavioral studies suggests that the LEC plays an important role in olfactory learning. However, interpretation of the available literature is not straightforward as the results are pointing in two apparently opposing directions. Lesioning the LEC leads to either impairment or facilitation of discrimination. On the one hand, it was reported that LEC lesions lead to impairments in retaining olfactory information over long (but not short) delays (Staubli et al., 1984, 1986; Otto and Eichenbaum, 1992). Although learning of new discriminations was disrupted, the ability to perform odor discriminations learned prior to the lesion was not affected (Staubli et al., 1984, 1986). On

the other hand, facilitation of olfactory learning was reported following bilateral lesion of the whole entorhinal cortex (Otto et al., 1991; Ferry et al., 1996) or more specifically the lateral entorhinal cortex (Wirth et al., 1998; Ferry et al., 2006). Using odor aversion paradigms, it was shown that EC lesions resulted in a higher tolerance to long interstimulus intervals, suggesting an extended duration of the memory trace (Ferry et al., 1996; Wirth et al., 1998; Ferry et al., 2006). In this respect, it is noteworthy that is has been suggested that the LEC exerts a main inhibitory effect on the processing of odors in connected brain areas (Mouly and Di Scala, 2006; Bernabeu et al., 2006; Chapuis et al., 2013). Electrical stimulations of the EC, the OB, or a combination thereof leads to inhibition in the PIR and the basolateral amygdala and it was hypothesized that this effect might concern the whole network of olfactory structures (Mouly and Di Scala, 2006). Using the opposite approach and suppressing activity in the LEC via muscimol infusion, activity in the anterior PIR was enhanced, but behavioral performance of lesioned animals was impaired, in particular for difficult but not for easy odor discrimination tasks (Chapuis et al., 2013).

The degree of coupling between different olfactory areas was investigated in numerous studies, showing the important role of the LEC as a bridging element between olfactory sampling in the OB and further processing in the hippocampus (Boeijinga and Lopes da Silva, 1989; Kay and Freeman, 1998; Chabaud et al., 2000; Martin et al., 2007; Chapuis et al., 2013). Just recently, a near-theta frequency oscillation in the hippocampus was described, which is coherent with nasal respiration and rhythmic field potentials of the OB and most likely mediated via the LEC (Yanovsky et al., 2014). Additionally, and with regards to memory and learning tasks, learning to master an odor-place association task is accompanied by evolving coherence of firing patterns in entorhinal-hippocampal circuits and this coherence is linked to ensemble representations for unique trial outcomes in distal CA1 and LEC (Igarashi et al., 2014).

An important question is to which extent the different types of excitatory and inhibitory neurons in the LEC take an active role in these odor-related processes. Classical papers indicate that in particular layer II neurons increase their firing rate upon odor stimulation (Wilson and Steward, 1978; Habets et al., 1980b). On a single cell level, only limited data is available but LEC neurons have been shown to respond selectively to particular odors, which is expressed by either an enhancement or a suppression of firing rate (Young et al., 1997; Petrulis et al., 2005; Xu and Wilson, 2012; Igarashi et al., 2014). These odor-selective neurons

were reported to be situated in superficial layers (Young et al., 1997), in both deep and superficial layers with odor responses most prominent in superficial layers (Petrulis et al., 2005), detectable throughout all layers of the LEC (Xu and Wilson, 2012), and in layer III specifically (Igarashi et al., 2014). However, it is still unknown whether one specific neuronal type located in different layers responds to odors or a heterogeneous group of neurons, and even less is known about the differential involvements of distinct neuronal types. For that matter, it is of interest to relate different response patterns elicited by odor stimulation to neurons with known identity, their protein expression profile and anatomical connectivity, to characterize such odor-responsive neurons in more detail.

1.6 The LEC and its involvement in neurological disorders

Next to the pressing question about the functional role of the LEC, its investigation is also of interest in regard to its known significance in the progression of Alzheimer's Disease (AD). I would like to touch upon this aspect of LEC research briefly. AD is defined by the pathological presence of amyloid-β (Aβ) plaques and neurofibrillary tangles (NFTs) in the brain. Plaques are composed of Aβ, which is a peptide derived by enzymatic cutting of amyloid-β precursor protein (APP). This combination of pathological changes in the brain represent the classic diagnostic hallmarks of AD as described by Alois Alzheimer beginning of the 19th century (Alzheimer et al., 1995). At the end of last century, the EC gained attention when it emerged as the site of very early pathological changes in the brain (Hyman et al., 1984; Braak and Braak, 1985). In particular, cells connecting the EC with the hippocampus were strongly affected. Braak and Braak showed that layer II projections to the hippocampus were almost completely destroyed at early stages of the disease (Braak and Braak, 1985) and NFTs developed in these cells that constitute the origin of the perforant path (Hyman et al., 1984). The severity of pathological changes were found to be maximal in the entorhinal area and the hippocampus and a peculiar involvement of olfactory areas lead to the suspicion that olfactory pathways might play a particular role in the progression of AD (Pearson et al., 1985). In the years to come, it became more and more apparent that AD patients develop pronounced deficits in the detection, identification, and discrimination of odors already early in the course

of the disease (Kesslak et al., 1988; Murphy, 1999). However, it is unclear which role can be attributed to the LEC, as there is still a lack of knowledge why the disease impacts olfaction. In a mouse model overexpressing a mutated form of the human APP progressive olfactory deficits were shown to correlate with Aβ burden (Wesson et al., 2010). Interestingly, of all olfactory areas investigated, LEC and hippocampus were the only areas where significant correlations for all three olfactory deficits tested - investigation, habituation and discrimination - were revealed. The longstanding question, whether both the LEC and the MEC are affected in preclinical AD, was answered by an elegant study that exploited a high-resolution functional magnetic resonance imaging variant (Khan et al., 2013). This study did not only identify the LEC as the entorhinal subdivision being primarily affected in preclinical AD, but it has also found further evidence for the LEC being the anatomical source from which the disease could spread. Of uttermost importance to my study are furthermore findings that the number of neurons in layer II in the LEC is reduced in AD patients (Gómez-Isla et al., 1996) and in particular the number of Reelin$^+$ neurons in layer II as was shown in hAPP mouse models and aged rats with cognitive impairment (Chin et al., 2007; Stranahan et al., 2011a). In the hAPP mouse model, this finding was shown to rather reflect a decrease in Reelin expression than a loss of neurons (Chin et al., 2007). This opens the possibility that deficits in odor identification relying on hippocampus depending memory might be due to disrupted transmission of olfactory information, if Reelin$^+$ neurons take an active role in this process (Stranahan et al., 2011b).

1.7 Two-photon calcium imaging

For decades, the field of neuroscience has relied on electrical recordings of neuronal activity to investigate response patterns and the cellular composition of circuits involved in the processing of information. Action potentials (APs) have been recorded successfully using a variety of techniques. Extracellular recordings allow the recording from single neurons as well as cell ensembles composed of multiple, inseparable neurons. It has become possible to record from hundreds of neurons simultaneously (see Buzsaki, 2004), but the molecular identity or position of recorded cells cannot be resolved. Additionally, extracellular recordings suffer from the limitation of being blind to silent neurons, there-

fore prohibiting an estimation of the percentage of non-participating neurons in a network. Intracellular recording techniques such as whole-cell patch-clamp recordings can resolve subthreshold membrane potentials as well as firing properties, which can serve for classification of neuronal subtypes. However, this technique is limited to single neurons or pairs of neurons but cannot contribute to unraveling the activity state of small groups of nearby neurons, often referred to as microcircuit.

Therefore, the emergence of a new imaging technique at the end of the 20th century lead to a revolution in the measurements of neuronal network dynamics. Two-photon excited fluorescence laser scanning microscopy or in short two-photon microscopy enabled completely new paths of discovery (Denk et al., 1990). It allows fluorescence imaging in living animals and intact tissue several hundreds of micrometer deep (Theer et al., 2003; Mittmann et al., 2011). The spatial resolution is sufficient to discern not only neurons, but also dendrites and synapses (Engert and Bonhoeffer, 1999; Stettler et al., 2006), and measurements can be repeated over several months (Margolis et al., 2012; Kato et al., 2012). Particularly in combination with fluorescent reporters of neuronal activity, two-photon microscopy has developed into a key technology for studying rodent brains. For the first time, it had become possible to study entire local populations of neurons and their network dynamics in intact (Stosiek et al., 2003) and even awake animals (Greenberg and Kerr, 2009). I highly recommend a review by Lütcke and Helmchen (2011) to the interested reader, which was in part the basis for this introduction to two-photon calcium imaging.

The advantage of two-photon microscopy in comparison to other microscopy techniques such as confocal microscopy is its lower sensitivity to light scattering, which usually is the major problem when imaging biological tissue. To achieve 'two-photon excitation', simultaneous absorption of two near-infrared photons is required, which is a process with low probability. The high density of photons needed for sufficient excitation of fluorophores is usually achieved with a pulsed laser source. Two-photon excitation has a quadratic dependence on the average laser power, which results in fluorescence generation being confined to the focal spot of the size of microns (Denk et al., 1990). Additionally, the use of longer wavelengths has the advantage that excitation light is less scattered. The image is generated most typically by raster-like scanning across the x-y axis. This intrinsic optical sectioning allows to follow the detection strategy formulated by Helmchen and Denk (2005): 'collect as many photons as possible' as the origin

of fluorescence photons is well defined at any point in time.

The staining of cells with activity sensors was initially accomplished with small organic dyes such as Oregon Green BAPTA-1 (Stosiek et al., 2003; Kerr et al., 2005), but with the cloning of green fluorescent protein (GFP) from the jellyfish *Aequorea victoria* the use of genetically encoded sensors of neuronal activity became possible (Miyawaki et al., 1997). This approach offered a great advantage for several reasons. As proteins are encoded by DNA, they can be directly expressed in the tissue of interest allowing long term recordings. Additionally, expression can be targeted to specific cell types with the help of promoters controlling the DNA transcription and translation (Tian et al., 2009; Lütcke et al., 2010). Conditional gene expression is often very desirable and can be achieved with systems that couple gene expression to specific developmental stages, neuronal subtypes or even cell compartments. Organic dyes, however, stain indiscriminately all cell types, including astrocytes. This results in high background fluorescence as the dyes gradually leak from the cytosol into the extracellular space and substantial fluorescence is also encountered in neuronal processes. Nevertheless, Oregon Green BAPTA-1 was a very popular activity sensor for a long time as it offered the best kinetics for recording of action potential firing with a reasonable temporal resolution and a good signal-to-noise ratio. When a cell is excited to elicit an action potential, voltage-gated channels in the membrane open and allow calcium ions to enter the cell. The task of calcium indicators is to detect this brief influx of calcium ions and to report this transient via a modification of their conformation that leads to a change in their fluorescent intensity. The fluorescence response to a single AP can be described by a fast exponential onset and a slower exponential decay and only the newest generation of genetically encoded calcium indicators (GECIs) can keep up with the fast kinetics and high amplitude changes Oregon Green BAPTA-1 could offer (data given for GCaMP6s: ΔF/F$_0$ 1 AP: 23 $\pm$ 3.2%, decay $\tau_{1/2}$ 1 AP (ms): 550 $\pm$ 52, rise τ_{peak} 1 AP (ms): 179 $\pm$ 23, detection efficiency (at 1% false positive): 99 $\pm$ 0.5%) (Akerboom et al., 2012; Chen et al., 2013b).

These new GECIs have been generated relying on both rational design and directed mutagenesis, which was aided by resolving the crystal structure of the GCaMP calcium sensor (Akerboom et al., 2009). GECIs are classified into two groups based on the number of fluorescent proteins they contain. The Calcium-sensing protein itself is not fluorescent, but via a conformational change, the fluorescence of a single protein can be enhanced (or depressed). The most pop-

ular example of single fluorescent protein GECIs are members of the GCaMP family (Tian et al., 2009; Akerboom et al., 2012; Chen et al., 2013b). For the group of ratiometric GECIs, which use the ratio between two fluorescent proteins as readout, newly developed YC-Nano calcium sensors promise single AP resolution and might become important tools in the future, especially for *in vivo* imaging (Horikawa et al., 2010). Already now, it has become possible to image over weeks in awake behaving animals from the same population of neurons with high temporal resolution, which will help tremendously to increase our knowledge about the formation and stability of networks during learning (Huber et al., 2012).

The diverse and broad range of calcium indicators available nowadays is paralleled by different techniques for delivering these indicators to the target region. Among these techniques are intracellular loading, dye electroporation and multicell bolus loading (Stosiek et al., 2003). For numerous scientists, viral transfection by adeno-associated virus (AAV) for the delivery of GECIs has become the method of choice. For genetically encoded indicators, the injection is performed several days to few weeks prior to the actual experiment, and not the fluorescent product as such is injected, but cells are provided with the genetical material to produce the final product themselves. The DNA coding for the sensor is mediated via viral vectors, which can infect cells and use the internal cell machinery for transcription and translation of the viral genes. High levels of stable expression over weeks and months are observed in a large fraction of cell, thereby allowing long-term monitoring of neural network activity (Tian et al., 2009; Lütcke et al., 2010). Additionally, conditional gene expression can be achieved using the Cre-loxP system, a highly successful tool for genome manipulation. It consists of two components, the Cre recombinase, which is an enzyme that catalyzes recombination between two DNA recognition sites, called loxP sites, and a gene of interest flanked by these recognition sites. The gene of interest can be delivered to the neuron by viral injection or can be introduced in a transgenic animal, but importantly, expression takes only place upon a successful and site-specific recombination event mediated by Cre recombinase (Tian et al., 2009).

The increasing number of transgenic mouse lines expressing Cre recombinase under the control of cell-type specific promoters promises to broaden the scope of addressable cell types for selective investigations (e.g. Fuchs et al. (2007), Gong et al. (2007) or Gavériaux-Ruff and Kieffer (2007) for a review). There has

also been some progress in the generation ot transgenic mice expressing the calcium indicator itself in various neuronal subtypes, which has the advantage of homogeneous and stable expression circumventing an invasive procedure (Chen et al., 2012; Zariwala et al., 2012).

With large networks of hundreds and thousands of neurons labeled, the limiting factor has become the technical progress of the microscopic set-up. Among others, two aspects are of particular importance: the imaging speed that can be achieved for rastering the sample and the size of the field of interest, relating to the number of neurons that can be imaged within one frame. The goal is to maximize these parameters to increase both the temporal and the spatial resolution. Recent years have brought the advancement of novel scanning schemes that are superior to standard raster-like frame scanning. With this conventional scanning approach, it is usually possible to image field-of-views ranging from 100-800 µm covering networks of tens to hundreds neurons, accepting relatively slow frame rates of 1-10 Hz. New scanning approaches allow an increased scanning speed by collecting only signal from user-defined areas like cell bodies. Thereby, scanning speed could be accelerated to 20-300 Hz while collecting calcium signals from several tens of neurons (Göbel and Helmchen, 2007; Rothschild et al., 2010). Other strategies to further increase imaging speed explore new technologies for the time-optimized deflection of the laser beam, which can be accomplished by resonant galvanometric mirrors (Leybaert et al., 2005) or acousto-optical deflectors (Lechleiter et al., 2002). The latter allows the optical resolution of whole sets of action potential trains within local neuronal populations, reaching a temporal resolution almost comparable to electrical recordings (Grewe et al., 2010). Other approaches for improving the efficiency are multifocal techniques with several laser foci recording in parallel (Kurtz et al., 2006) or the extension of the free line scan into the third dimension in space (Göbel et al., 2007). In summary, slowly but surely these new high-end techniques will find their way into the laboratories and will be used for standard applications. One can expect to see further progress in the years to come that will enable two-photon calcium imaging to perform on temporal time scales comparable to electrophysiological recordings, but having the advantage of possible identification of neuronal subtypes involved in the network activity without the necessity for optogenetic stimulation.

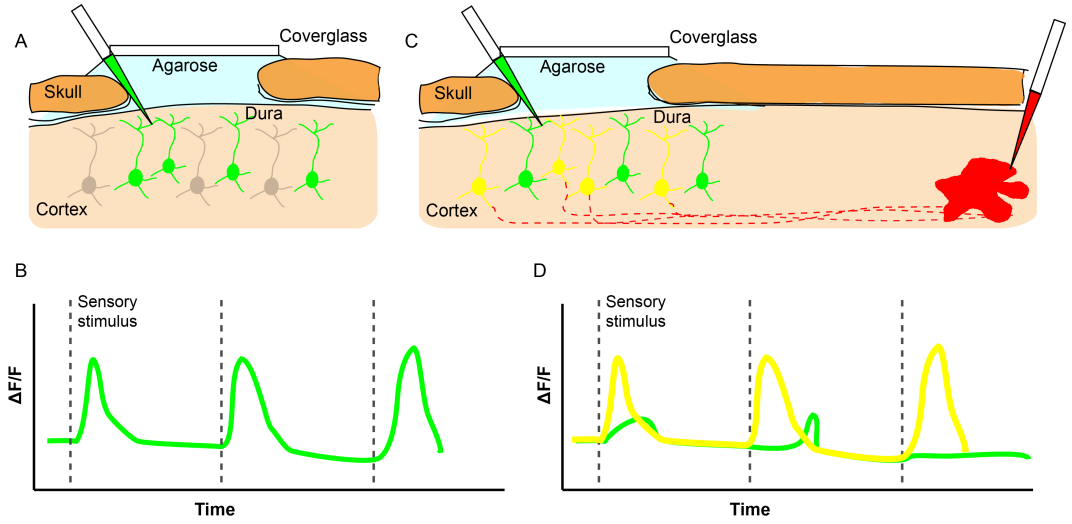

Figure 1.2. Labeling strategies to record from defined set of neurons (A) and (B) After injection of an AAV carrying a floxed version of a GECI into a transgenic animal expressing Cre recombinase in a defined neuronal subtype, only neurons of this type express the GECI (green). When calcium imaging is performed on the day of the actual experiment, all recorded stimulus-evoked calcium traces can be attributed to this specific neuronal type (green). **(C) and (D)** An AAV coding for an GECI (green) and a retrograde tracer (red) are injected prior to the experiment. The retrograde tracer is taken up by axons located at the injection spot. On the day of imaging, neurons in the field of view express the GECI unspecifically (green), and a subpopulation of these neurons is also labeled with the retrograde tracer (yellow) indicating their axonal projection pattern.

In particular, this last aspect of known neuronal identity will gain increasing importance in the future. Not only technical developments, but maybe even more so clever experimental design will gain further importance, making use of several labeling possibilities in parallel that enable us to advance our knowledge about the identity and connectivity of cells in the imaging area. In **Figure 1.2**, several of these labeling strategies are depicted. The left panel shows recording in a transgenic animal, that expresses Cre recombinase in a defined set of neurons, and thus reveals celltype-specific labeling after injection of an AVV carrying a floxed version of a GECI. Thereby, the firing rate that is recorded after the delivery of a sensory stimulus can be attributed to a distinct neuronal cell type (**Figure 1.2B**). On the right side, neuronal specificity is achieved based on the connectivity pattern. After AVV injection, the calcium indicator is expressed unspecificly. However, by injection of a retrograde tracer into another brain area that is targeted by the area under investigation, somata of neurons projecting into this target region are double-labeled (**Figure 1.2C**). This allows to identify neurons with a known connectivity pattern and to relate functional activity to

anatomical layout (**Figure 1.2D**). This approach, exploiting labeling of connectivities, promises to increase our understanding of functional diversity and task distribution in the brain substantially (Huber et al., 2012; Chen et al., 2013a).

1.8 Aim of the study

The overarching aim of this study is to contribute to our understanding of the functional role of the LEC and in particular its involvement in olfaction. In order to do this, I used a variety of technical approaches, exploring the LEC from various perspectives. Firstly, I want to investigate the neuronal composition in the LEC exploiting immunohistochemical markers, to elaborate on the distribution of both excitatory and inhibitory neurons as well as subtypes thereof. Therefore, I will focus on typical neuronal marker proteins that have been shown to be expressed in the MEC. Secondly, electrophysiological and morphological properties of LEC neurons will be investigated *in vivo*, with particular interest in those neurons that were modulated by odor stimulation. Thirdly, I will establish two-photon calcium imaging in the LEC, developing a surgery that allows optical access and combining the recordings with the application of odorant stimuli. The exploration of odor-elicited responses in the LEC will be restricted to superficial layers, with a distinct focus on the distinction between different neuronal subpopulations. Our combinatorial approach will reveal the spatial layout of microcircuits in the LEC with different neuronal players and their respective functions in odor processing in an unprecedented detail. The conception of the functional role of superficial layers in the LEC is still vague and ambiguous, and we hope that with this study we can clarify some open questions.

2 MATERIALS AND METHODS

2.1 Materials

2.1.1 Mouse strains

5-HT3^{EGFP} (Inta et al., 2008)

CB^{Cre} (unpublished)

GAD67^{Cre} (Tolu et al., 2010)

GAD67^{EGFP} (Tamamaki et al., 2003)

Wildtype animals were taken from several lines with C57BL/6 background.

2.1.2 Viruses

All adeno-associated viruses (AAVs) were obtained from Penn Vector Core, University of Pennsylvania, Philadelphia. We would like to acknowledge that the AVVs were provided by the Genetically Encoded Neuronal Indicator and Effector (GENIE) Project and the Janelia Farm Research Campus of the Howard Hughes Medical Institute.

For the delivery of calcium indicators to the cells, we used the newest version of the GCaMP family available, AAV1.Syn.GCaMP6s in wild-type mice and the floxed version for injections into Cre-mice, AAV1.Syn.flex.GCaMP6s.

2.1.3 Antibodies

Primary and secondary antibodies were diluted in phosphate buffered saline (PBS, pH 7.4).

Antibody	Company	Concentration
Rabbit anti-CB	Swant, Marly, Switzerland	1:5000
Mouse anti-CR	Swant, Marly, Switzerland	1:1000
Rabbit anti-EGFP	Invitrogen, Darmstadt, Germany	1:5000
Mouse anti-NeuN	Merck Millipore, Billerica, MA	1:1000
Rabbit anti-NeuN	Merck Millipore, Billerica, MA	1:1000
Mouse anti-PV	Sigma-Aldrich, St. Loius, MO	1:1000
Rabbit anti-PV	Swant, Marly, Switzerland	1:1000
Mouse anti-Reelin	Merck Millipore, Billerica, MA	1:2000
Rat anti-SOM	Merck Millipore, Billerica, MA	1:1000
Mouse anti-GAD67	Merck Millipore, Billerica, MA	1:1000

Table 2.1. Primary antibodies CB: calbindin, CR: calretinin, EGFP: enhanced green fluorescent protein, GAD67: glutamic acid decarboxylase67, NeuN: Neuronal Nuclei, PV: parvalbumin, SOM: somatostatin.

Antibody	Company	Concentration
Cy3 goat anti-mouse	Jackson Immuno Research, West Grove; PA	1:1000
Cy3 donkey anti-rabbit	Jackson Immuno Research, West Grove; PA	1:1000
DyLight 649 goat anti-rabbit	Jackson Immuno Research, West Grove; PA	1:500
Alexa Fluor 488 goat anti-rabbit	Invitrogen, Germany	1:1000
Alexa Fluor 488 goat anti-mouse	Invitrogen, Germany	1:1000
Alexa Fluor 647 donkey anti-mouse	Invitrogen, Germany	1:1000
Alexa Fluor 647 donkey anti-rabbit	Invitrogen, Germany	1:1000

Table 2.2. Secondary antibodies

2.2 Methods

2.2.1 Virus injection and retrograde tracer injection

All mouse experiments were performed following the guidelines for animal treatment by the German law (Regierungspräsidium Karlsruhe, license Az G-74/13). The animals used in these experiments were all males and between 8 to 14 weeks old. They were kept singly or doubly housed on a 12 h light/dark cycle. All experiments were conducted during the light phase of the schedule. The protocol for stereotactic injections was described previously (Cetin et al., 2007).

Mice were anesthetized with a mixture of ketamine (120 mg/kg bodyweight, CP-Pharma, Burgdorf, Germany) and xylazine (16 mg/kg bodyweight, Bayer, Leverkusen, Germany) and the depth of anesthesia was constantly monitored via the absence of pain reflexes such as the toe pinch reflex. Animals were mounted in a stereotactic apparatus (David Kopf Instruments, Tujunga, California) with a heat pad to keep the body temperature constant and the eyes were covered with ointment. For the injection of the AAVs, two small craniotomies were made above the LEC using a dental drill. A glass micropipette with an outer diameter of 8-10 µm was filled with the virus and then inserted into the brain. The spots were located 3.8 mm posterior and 4.5 mm lateral from bregma and 3.5 mm and 4.8 mm lateral from bregma, and in each spot 300 nl of the virus was injected. The pipette was lowered to 2.3 mm below the surface and then retraced to 1.6 mm while continuously injecting the virus over a period of 5 min. After the injection, the micropipette was kept in place for additional 5 min before complete retraction. The scalp incision was sutured and buprenorphin was administered subcutaneously to prevent post operative pain. For the injection of retrograde tracers, a similar protocol was used as described above. As retrograde tracer, either cholera toxin subunit B (CTB) 488, CTB555 (Life Technologies, Carlsbad, USA) or FluoroGold (FG) (Fluorochrome, Denver, USA) was used for injection into the following brain areas: OB (CTB555 and CTB488, unilateral, 450 nl or FG, bilateral, 300 nl), DG (CTB555, unilateral, 100 nl), CA1 (CTB555, unilateral, 100 nl), PIR (CTB555, unilateral, 100 nl) and LEC (CTB555, unilateral, 100 nl). The tracer was injected within 5 min and after injection the micropipette was left in place before retraction for at least 15 min to avoid spreading of the tracer in areas other then the target area.

2.2.2 Immunohistochemistry

Mice injected with retrograde tracers were subjected to histological analysis 5-7 days (CTB555) or 2-3 weeks (FG) after the injection. Animals that were used for electrophysiological recordings or two-photon imaging were further processed directly after termination of the data recording experiments. Mice were deeply anesthetized with isoflurane (Baxter, Germany) or ketamine/xylazine and transcardially perfused with PBS, followed by 4% paraformaldehyde. The fixed brains were removed from the skull and kept in 4% paraformaldehyde at 4°C for 24 h. Using a vibratome (VT1000s vibratome, Leica, Germany), brains were sliced

horizontally in 50 µm thick sections. Free-floating sections were washed in PBS (pH 7.4) several times before they were permeabilized and blocked for 2 h in PBS (pH 7.4) containing 5% bovine serum albumin (BSA) and 0.2% Triton X-100. Sections were incubated with primary antibodies over night at 4°C in 600 ml PBS containing 0.1% Triton X-100. After thorough washing with PBS, sections were incubated with the secondary antibody. For double-labeling experiments, a combination of primary antibodies as well as a combination of secondary antibodies was used that would ensure correct binding without cross-talk. Sections were again washed with PBS, mounted on glass slides and covered with Aqua-Poly/Mount (Polysciences, Inc., Warrington, USA) or Mowiol 40-88 (Aldrich, Taufkirchen, Germany).

Brains from mice that were used for *in vivo* whole-cell patch-clamp experiments were further processed. After brain sections were stained using the method of immunofluorescence as described above, before mounting them they were further processed with diaminobenzedine (DAB) stainings. Sections were quenched in 1% H_2O_2 for 10 min followed by thorough washing with PBS, before being permeabilized with PBS containing 1% Triton X-100 for 1 h. After repeated washing, sections were incubated with avidin-biotin-horseradish peroxidase complex (Elite ABC, Vector Laboratories, Burlingame, USA) in PBS over night at 4°C. After washing with PBS, sections were incubated in a solution containing 35% DAB, 15% PBS, 49.6% ammonium chloride and 0.4% glucose oxidase to which 20 µl beta-D-glucose per well was added one minute after start of the reaction. Sections were shaken in the dark until darkening of them could be observed, which usually took between 15-45 min. Reaction was stopped by washing sections again in PBS, which was followed by mounting sections on glass slides using Moviol 40-88.

2.2.3 Surgical procedure

For the initial anesthesia, mice were anesthetized with a mixture of ketamine (120 mg/kg bodyweight) and xylazine (16 mg/kg bodyweight) and additional doses throughout the course of the surgery were administered if necessary. Animals were mounted in a stereotactic apparatus and placed on a heat pad to keep the body temperature constant. The eyes were covered with ointment, the skin disinfected and the fur cut using a razor blade. Dexamethasone (0.02 ml at 3 mg/ml PBS, CP-Pharma, Burgdorf, Germany) was intramuscularly in-

jected into the quadriceps to reduce cortical stress response during the surgery and prevent cerebral edema. Lidocaine (AstraZeneca, Wedel, Germany) was administered locally to the skull as additional anesthetic for pain reduction. A small cut of $\sim$1.5 cm was made in the skin and the underlying skull revealed. The skull was cleaned of periosteum and other tissue and subsequently a bone scraper was used for roughening the skull surface. Muscles located laterally at the right side of the skull were removed. Four miniature screws (Bilaney Consultants, Kent, UK) were screwed in the skull and fixed with cyano veneer, a 2-component dental cement (Hager Werken, Duisburg, Germany). Orthogonal to each other, two cap nuts were cemented on top of the screws as anchors for holding bars used in further stages of the surgery when ear bars could not be applied anymore. As the LEC is located laterally and ventrally in the mouse brain, the mouse had to be tilted by 90° to allow direct access to this area for which holding bars attached to the cap nuts were used. Thereby, the right LEC faced upwards and after fixing a head plate on top of this area, a small craniotomy was made using a dental drill. Regular rinsing with normal rat ringer solution (NRR) (in mM: 135 NaCl, 5.4 KCl, 5 HEPES, 1.8 CaCl2, pH = 7.2 adjusted with NaOH) was used to prevent the brain from overheating due to the drilling. The open area where the skull was removed will be called the imaging window from now on and had a size of $\sim$1.2 x 1.0 mm^2. Using fine forceps and spring scissors (FST, Heidelberg, Germany), the dura was removed leaving the underlying brain surface intact. Mild bleeding due to ruptured blood vessels in the skull or skin tissue could be stopped with the medicated sponge TachoSil (Takeda, Konstanz, Germany). For image stabilization and reduction of brain movements, 1.5% agarose in NRR was applied to the imaging window and a small round cover glass (thickness 100-150 µm, Warner Instruments, Hamden, USA) was put on top for holding the brain down and stable. Mice were transferred from the stereotactic apparatus to a movable plate with bar holders that were compatible with spatial restrains under the objectives of the two-photon microscope. During the time of recording neuronal activity, urethane (Sigma-Aldrich, ST. Louis, USA) was used for keeping the mouse anesthetized. However, in some instances the first few trials were recorded only under influence of the ketamine/xylazine mixture to avoid overdosing, when the mouse was still sufficiently anesthetized.

2.2.4 Two-photon calcium imaging

Two-photon imaging with olfactory stimulation was conducted 6 to 8 days after the virus injection. The calcium imaging experiments and the whole-cell patch-clamp recordings *in vivo* were performed using a ZEISS LSM 510 META NLO two-photon microscope (ZEISS, Jena, Germany). The excitation source was a Chameleon Ultra mode-locked Ti: Sapphire Laser (Coherent, Santa Clara, USA) with the wavelength set to 900 nm. Two different water immersion objectives were used for the acquisition of fluorescence images. For overview images of the recording position within an imaging window, a 10x/0.3 NA Plan-Neofluar was used and for recordings of neuronal activity an infrared-corrected 40x/1.0 NA objective (both ZEISS, Jena, Germany). NRR was used as immersion fluid. Fluorescence images of neuronal activity were acquired at 5 Hz frame rate and 100 x 100 pixel resolution. As reference image, a high resolution image of every area was taken (512 x 512 pixel, line average 4) at the beginning and after every 5 trials for control of position and focus. If necessary stacks of $\sim$10 µm, otherwise single plane images, were acquired for easier detection of neurons labeled with the retrograde tracer CTB555 for which the laser wavelength was set to 750 nm. Green fluorescence was detected using a longpass 515 nm filter. Spectral separation between signal emitted by GCaMP6 and CTB555 was achieved by using a bandpass 500 - 550 nm and a bandpass 575 - 640 nm filter cube. This filter cube was also used for the detection of TexasRed dye in the pipette for electrophysiological recordings. Imaging was continued for as long as image quality allowed, which was usually for 2 - 4 different areas per mouse. In some mice, Vybrant DiI cell-labeling solution (Life Technologies, Carlsbad, USA) was injected through the imaging window after the recording session to control the exact location of the window in regard to the LEC. Experiment was terminated at the end of the day by deeply anesthetizing the mouse with isoflurane before perfusing it as described previously. The brain was stored for analysis of injection sites, retrograde tracer labeling, immunohistochemical experiments and the location of the imaging window.

2.2.5 Image acquisition of brain slices

Images of all brain slices with fluorescence stainings, tracer or virus injections were taken with a confocal laser scanning microscope (LSM 700, ZEISS, Germany). This microscope is equipped with both 5x and 20x objectives, which were used either for overview images or high-resolution images with single cell resolution, respectively. Images for cell counting and analysis of co-expression of marker proteins and tracers were taken with the 20x objective (1024 x 1024 pixels). The software Fiji (NIH) was used for further processing of images. Image contrast and brightness were slightly adjusted if necessary, whereby single channel images and merged images were treated separately to display information as clearly as possible. Data are presented as mean $\pm$ SEM.

2.2.6 Building an olfactometer

The code for controlling the olfactometer was written in LabView. This work was done by Christian Kieser, Max Planck Institute for Medical Research (Heidelberg), with whom I worked closely together on this software and who implemented my specifications and guidelines.

The program 'Olfactometer: Valve control 1.0' offers the possibility to use seven valves for the delivery of odorized air and an eight valve was included for cleaning the tubing between different odors. Different settings can be chosen by the user: an initial delay, a period for opening of the valves and a following interstimulus interval during which valve eight is opened for cleaning the tubing. This setting also ensures continuous airflow so that switching between valves is not accompanied by a change in the overall airflow. The sequence of odors can be chosen manually or defined by the program using the randomization algorithm for the creation of new sequences determined by chance. Via the loop setting, such a trial can be repeated several times. There are two hardware triggers for start and stop of a sequence. The transition between opening and closing of two different valves can be adjusted with the parameter 'valve transition time' to compensate for differences in time constants. A sensor measures the air flow with 100 samples/second to control the overall air flow as well as peaks that can occur when switching from one valve to the next in a sequence. Recording is started via the two-photon imaging software together with the start of the valve sequence, and hereafter the pulsing is hardware triggered by a data acquisition

card (National Instruments, Austin, Texas). The communication between the PC and the valves is achieved via a microcontroller and a shift register that control the valve driver. Three data files are stored that contain all relevant information about the experiment: air flow data, valve settings, time points for start of a sequence and odor delivery.

2.2.7 Olfactory stimulation with a custom-built olfactometer

Single-molecule odors (i.e. odors consisting of a single odor component) with a broad spectrum of molecular features were chosen for stimulating neuronal activity in the LEC: ethyl butyrate (EB), amyl acetate (A), eugenol (E), cineole (C), hexanal(H), benzaldehyde (B) (Sigma-Aldrich, ST. Louis, USA). A custom-built olfactometer mixed saturated odor vapor of pure odors with filtered air. The carrier stream of clean air was set to a flow rate of 2 liter per minute, which was mixed with odorized air of 0.2 liter per minute for a final concentration of 10%. Odors were delivered by solenoid valves under computer control for 4 s/stimulus with an initial delay of 5 s for baseline recordings. Each stimulus was followed by an interstimulus interval (ISI) of 26 s to avoid sensory adaptation. Stimulus delivery was randomized and for every imaging area at least 15 trials were recorded with each trial consisting of 3 stimuli. Every series of trials included mock trials where pure filtered clean air was delivered. These mock trials served as control that no residual contaminating odors were lingering in the tubing. Changing between valves did not lead to increase or decrease in the total flow rate, which was controlled by a mass flow sensor for gases (First Sensor AG, Berlin, Germany).

2.2.8 Analysis of two-photon calcium imaging data

The analysis of the data obtained by two-photon calcium imaging was performed by our collaboration partners Henry Lütcke (ETH Zurich) and Prof. Fritjof Helmchen (University of Zurich).

Image analysis was performed in Matlab (Mathworks, Natick, MA) and ImageJ (NIH). All quantifications and statistical analyses were performed with Matlab. Cellular regions of interest (ROIs) were manually selected on high-resolution reference images. Calcium imaging movies were warped to high-resolution refer-

ence images by custom-written routines based on the non-linear image registration toolbox MIRT (https://sites.google.com/site/myronenko/research/mirt). For each ROI, the average fluorescence intensity was extracted and converted into relative change in calcium according to:

$$\Delta F/F = \frac{F - F_0}{F_0}$$

The baseline fluorescence F_0 was calculated as the 10th percentile of background subtracted fluorescence for each ROI. Odor-evoked receptive fields (RF) were computed by averaging calcium responses to all presentations of a specific odor and quantified as the peak average ΔF/F occurring within 20 s of odor onset. In addition, calcium events were determined on a single-trial basis as trials were ΔF/F exceeded the average pre-stimulus value by 5 standard deviations for at least 1 s. The event probability is the fraction of trials on which a calcium event occurred. The selectivity of responses to specific odors was quantified by normalizing all odors to the second-best odor. If a neuron responds very selectively to one odor, the normalized response to the second-best odor and all other remaining odors will be small. Means between different cell types were compared by two-sample t-tests. All p-values were adjusted for multiple comparisons using the Bonferroni procedure.

2.2.9 Electrophysiological recordings

All electrophysiological experiments were performed by Dr. Sarah Melzer in the department of Prof. Dr. Hannah Monyer.

Whole-cell patch-clamp recordings in the LEC were performed *in vivo*. Mice were anesthetized with ketamine/xylazine and a craniotomy above the LEC was performed as described for two-photon calcium imaging. Cells were patched in the LEC under visual guidance using the two-photon microscope, which allowed for specific selection of various cell types and different locations of cells. In some cases, movement of the brain was reduced by applying a thin layer of low melting point agarose (Thermo Fisher Scientific, Waltham, USA) with a concentration of 1.5% in NRR. Recording pipettes were pulled from borosilicate glass capillaries with resistances of 4.5 - 6 MΩ and were filled with intracellular solution containing (in mM) 130 K-gluconate, 10 Na-gluconate, 10 Hepes, 10 phosphocreatine, 4 NaCl, 4 Mg-ATP, 0.3 GTP, pH 7.2 adjusted with KOH.

TexasRed (4 µl/ml) was added to the intracellular solution to visualize the pipette under the microscope. No correction was applied for liquid junction potentials. Before penetration of the pia, high pressure (∼300 mbar) was applied to the pipettes to keep them clean. Directly after the pipette had penetrated the pia, the pressure was quickly reduced to 70 mbar. The pressure was further lowered to 50 mbar and 30 mbar as soon as the pipette was close to the cell and at the cell, respectively. For the analysis of firing patterns, 1 s current pulses were applied in current-clamp mode, with intersweep intervals of 3 s. The first sweep was elicited with -50 pA and followed by subsequent sweeps increasing the amplitude in 20 pA steps, until saturation were reached. Saturation was recognized as a decrease in action potential amplitudes. Matlab was used for the offline analysis of firing patterns. Signals were sampled at 10 kHz and filtered at 3 kHz. The software used for stimulus delivery and data acquisition was Pulse Software.

2.2.10 Biocytin filling and cell reconstruction

For morphological analysis of electrophysiologically identified target cells, whole-cell patch-clamped neurons were filled with biocytin (Aldrich, Taufkirchen, Germany; up to 10 mg/ml, dissolved in intracellular solution). Cells were filled for up to 8 min before retracting the pipette. Only one cell per mouse or per brain slice was patched and filled to avoid ambiguous overlap and crossing of dendritic and axonal networks. Following *in vivo* filling, mice were deeply anesthetized with isoflurane, and transcardially perfused with PBS and paraformaldehyde as described above. The dissected brain or the acute slices with filled cells were fixed overnight in 4% paraformaldehyde. Whole brains were sliced on a vibratome (VT1000s vibratome, Leica, Germany) into 50 µm thick horizontal slices and stained with antibodies against several protein markers before staining with DAB as described for the immunohistochemistry. Labeled cells were reconstructed using the Neurolucida tracing program (MicroBrightField, Colchester, Vermont).

3 RESULTS

3.1 Distinct cellular organization in the LEC

In the MEC two defined types of excitatory neurons, namely CB^+ and $Reelin^+$ neurons, can be detected by immunohistochemical experiments (Ray et al. (2014), Kitamura et al. (2014), Tang et al. (2014) and work in our own group). CB and Reelin expression in LII was shown to exhibit a very distinct pattern, with neurons expressing Reelin organized in a band-like structure, but with CB^+ neurons clustering together and thereby forming cellular modules. This modules appear like islands as they are nested in the band of RE^+ neurons. We wondered whether these neuronal markers would also be present in excitatory neurons in the LEC and if we would find comparable organization within LII. To test this, I performed immunostainings against Reelin and CB (**Figure 3.1**).

Comparable to the MEC, the LEC contains neurons that are positive for Reelin as well as CB, however, they are arranged in a different fashion. $Reelin^+$ neurons align in a band directly at the border to LI that seems to be the continuation of the band already present in MEC, running further anterior in the LEC. In dorsal slices, neurons are densely packed in this narrow band, in comparison to ventral slices, where this band appears to be broader (**Figure 3.1A**). Strikingly, however, CB^+ neurons are not intermingled within this band but form a distinct layer underneath. This layer seems to be part of LII as well, which is why it was termed LIIb (Fujimaru and Kosaka, 1996). In LIIb, CB^+ neurons can also form islands, but they are more rarely detectable than in the MEC. I combined immunostainings against Reelin (**Figure 3.1B**) and CB (**Figure 3.1C**) with immunostainings against the neuronal marker protein NeuN in *GAD67*^{EGFP} mice. The overview (**Figure 3.1B** left image) as well as the magnifications show clearly that in LIIa, NeuN and Reelin are co-expressed in basically all excitatory neurons ($EGFP^-$), indicating that LIIa consists of no other excitatory cell type than Reelin-expressing neurons. Note that NeuN is not expressed in all GABAergic

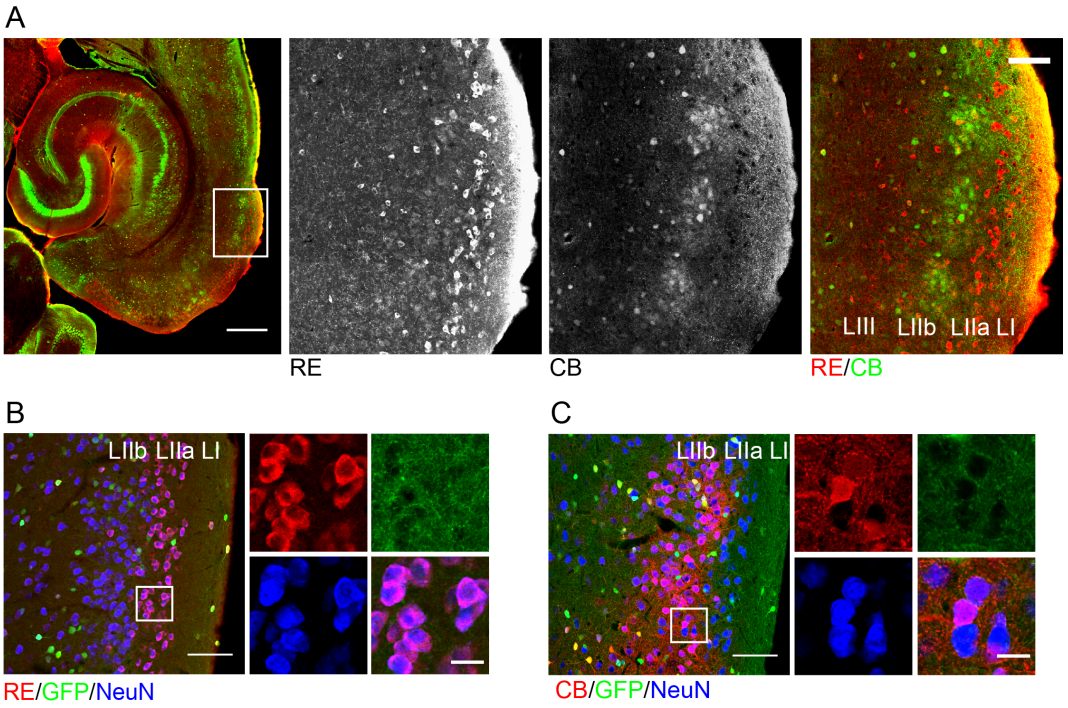

Figure 3.1. Distinct organization of superficial layers in LEC (**A**) The LEC with immunostaining against Reelin and CB in 50 µm thick horizontal sections. The left image shows an overview of the parahippocampal region. Higher magnifications of the boxed area (right) show a distinct organization of Reelin$^+$ and CB$^+$ neurons. Reelin$^+$ neurons are arranged in a band-like structure in LIIa whereas CB$^+$ neurons form islands and are situated in LIIb. Scale bar, 100 µm. (**B**) Immunostaining against Reelin and the neuronal marker protein NeuN in *GAD67*^{EGFP} mice. All NeuN$^+$ neurons co-express Reelin in LIIa. (**C**) Immunostaining against CB and NeuN in *GAD67*^{EGFP} mice. In LIIb, a subset of NeuN$^+$ neurons co-express CB. Note that GFP$^+$ GABAergic neurons in (**B**) and (**A**) often do not co-express NeuN but can be positive for both Reelin and CB. Scale bar, 50 µm and 20 µm in (**B**) and (**C**). Abbreviations: CB, calbindin; GFP, green fluorescent protein, L, layer; NeuN, neuronal nuclei; RE, Reelin.

neurons in the LEC. LIIb, on the other hand, consists of two types of excitatory neurons: CB$^+$ and CB$^-$ neurons (**Figure 3.1C**). The distribution of GABAergic neurons in superficial LEC layers will be presented later.

3.1.1 Distinct projection patterns: Reelin$^+$ but not CB$^+$ neurons project to the DG

The connectivity between entorhinal cortex and the hippocampus has been described in numerous publications and it is well established that LII neurons project to the DG and CA3 whereas LIII neurons send their axons to CA1 and

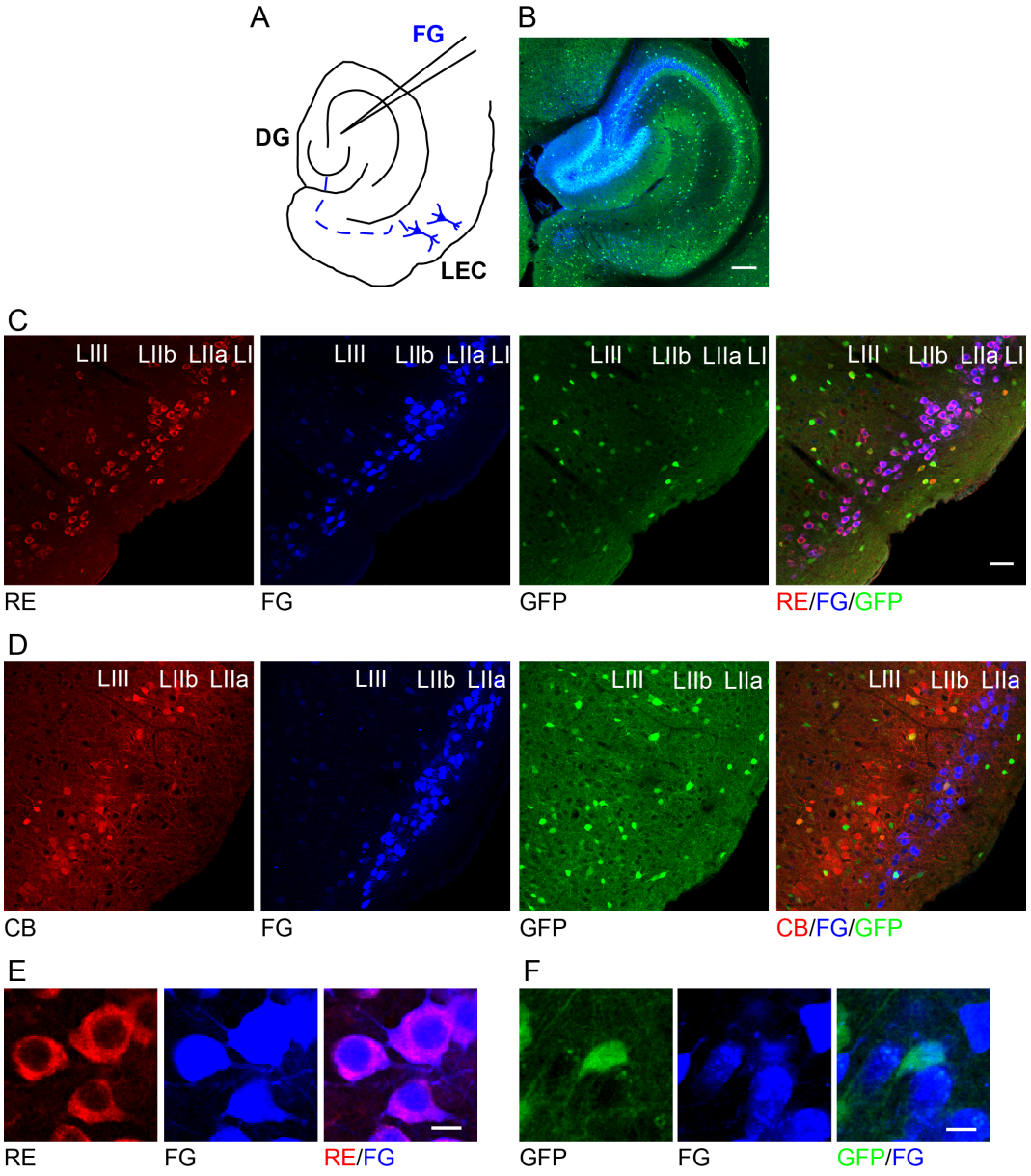

Figure 3.2. Reelin⁺ but not CB⁺ neurons project to the DG (**A**) Schematic drawing of the FG injection into the DG. (**B**) Confocal image of the injection site with the regrograde tracer FG shown in blue. Scale bar, 200 µm. (**C**) Immunostaining against Reelin after injection of FG into the DG in *GAD67*^{EGFP} mice. FG⁺ neurons overlap extensively with Reelin⁺ neurons in LIIa. (**D**) Same as in (**C**) but with immunostaining against CB. FG⁺ neurons are clearly separated from CB⁺ neurons. (**E**) Higher magnification of Reelin⁺/FG⁺ neurons. (**F**) EGFP⁺ GABAergic neurons projecting to the DG are rare. Scale bars, 50 µm in (**C**) and (**D**) and 10 µm in (**E**) and (**F**). Abbreviations: CB, calbindin; DG, dentate gyrus; FG, fluorogold; GFP, green fluorescent protein, L, layer; RE, Reelin.

the subiculum (Steward and Scoville, 1976). Having found two distinct types of excitatory neurons in LII in the LEC, the obvious question for us was whether

both or just one neuronal population would be the connecting element between EC and hippocampus. To address this question, I injected the retrograde tracer FG into the DG of *GAD67*^{EGFP} mice (**Figure 3.2A and B**) and performed immunohistochemical experiments, staining against Reelin and CB.

I found that the number of retrogradely labeled FG$^+$ neurons was high in LIIa, with 98.33 $\pm$ 0.60% FG$^+$ LIIa neurons being Reelin$^+$ (1097 FG$^+$ neurons in 2 hemispheres from 2 *GAD67*^{EGFP} mice) (**Figure 3.2C and E**). In LIIb, I observed dispersed neurons exhibiting a weak FG-labeling, which did not allow counting these neurons. The intensity of this signal was much reduced and not comparable to the signal in LIIa (**Figure 3.2D**). I also observed FG$^+$ neurons located in LIII, but far less than in LIIa (data not shown). As FG is taken up both by excitatory and inhibitory neurons unselectively, I also payed attention to GABAergic neurons in LII projecting to the DG. From previous studies it is known that at the border between LI and LII GABAergic neurons exist that project to the hippocampus (Germroth et al., 1989; Schwerdtfeger et al., 1990; Melzer et al., 2012), and indeed I detected few FG$^+$/EGFP$^+$ GABAergic neurons (7 EGFP$^+$ neurons of 1097 FG$^+$ neurons in 2 hemispheres from 2 *GAD67*^{EGFP} mice) (**Figure 3.2F**). With this findings, we could conclude that Reelin$^+$ neurons, but not CB$^+$ neurons form the perforant path to the DG. Logically, if CB$^+$ neurons do not project to the DG they must have one or several other target regions to which they send their axons and this is what we wanted to determine with the following experiment.

3.1.2 Distinct projection patterns: CB$^+$ and few Reelin$^+$ neurons project to the OB

The LEC is part of the olfactory cortex as it is directly innervated by mitral cells of the OB (Haberly and Price, 1978). The general reciprocal connectivity of LEC neurons projecting back to the OB in order to transmit feedback information about olfactory content has been described (de Olmos et al., 1978; Shipley and Adamek, 1984; Witter and Groenewegen, 1986; Insausti et al., 1997). However, further identification of the neuronal cell type establishing this connectivity is still lacking. We hypothesized that CB$^+$ neurons might be good candidate neurons for this task. Therefore, I injected the retrograde tracer CTB555 into the OB of *GAD67*^{EGFP} mice (**Figure 3.3A and B**) and performed immunohistochemical experiments staining against Reelin and CB. As it was shown that LEC projec-

tions to the OB are strictly ipsilateral (Chapuis et al., 2013), I performed bilateral injections to spare mice.

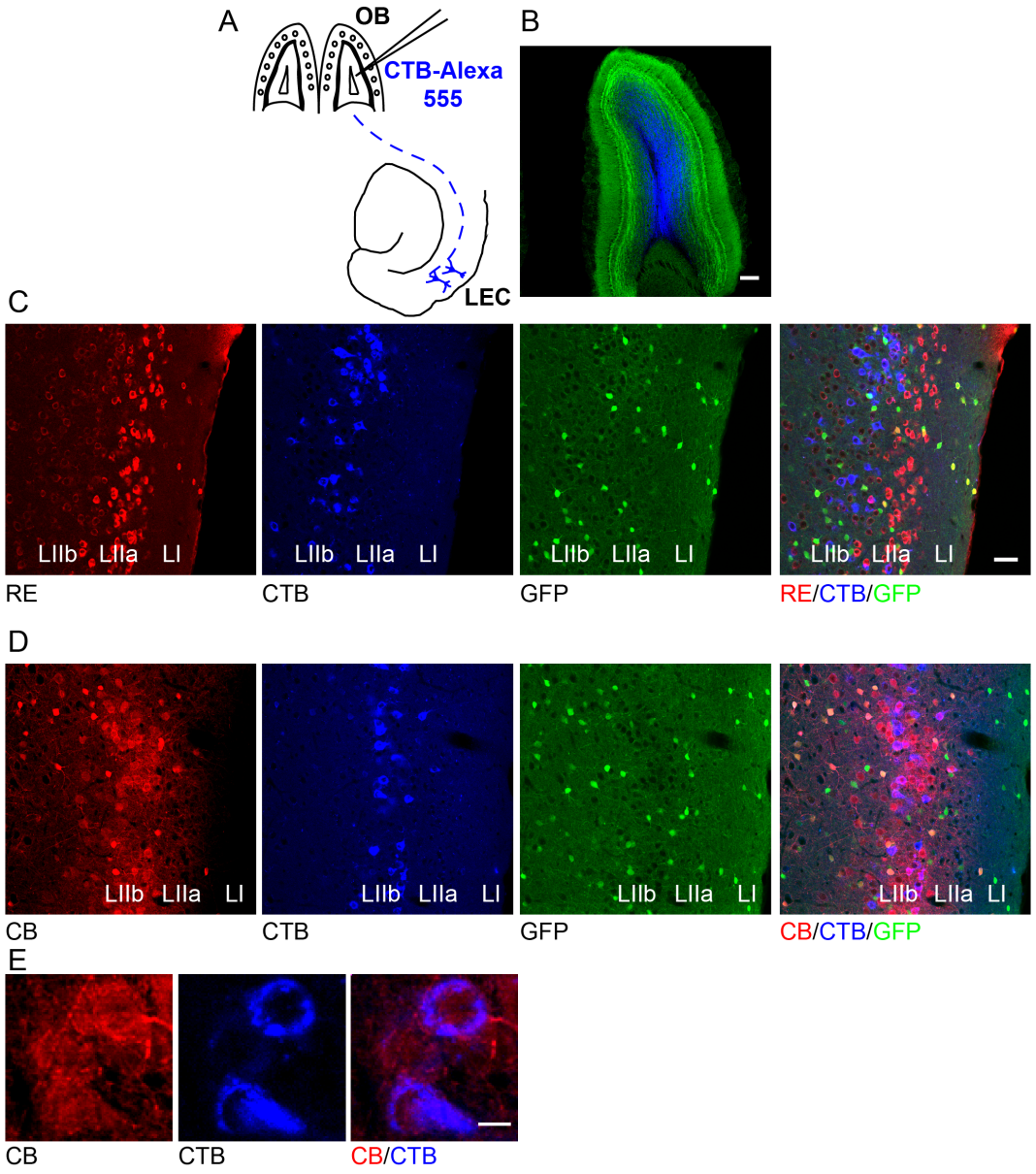

Figure 3.3. CB⁺ and few Reelin⁺ neurons project to the OB (**A**) Schematic drawing of the CTB injection into the OB. (**B**) Confocal image of the injection site with the regrograde tracer CTB shown in red. Scale bar, 200 µm. (**C**) Immunostaining against Reelin after injection of CTB into the OB in *GAD67*^{EGFP} mice. CTB⁺ neurons are found only rarely in Reelin⁺ neurons in LIIa. (**D**) Same as in (**C**) but with immunostaining against CB. CTB⁺ neurons often colocalize with CB⁺ neurons in LIIb. (**E**) Higher magnification of CB⁺/CTB⁺ neurons. Scale bar, 50 µm (**C**) and (**D**) and 10 µm in (**E**). Abbreviations: CB, calbindin; CTB, cholera toxin subunit B; GFP, green fluorescent protein, L, layer; OB, olfactory bulb; RE, Reelin.

The majority of retrogradely labeled CTB⁺ neurons could be detected in LIIb

(**Figure 3.3C, D and E**). Counting in slices from 4 hemispheres of 3 mice revealed that in LIIa 27.20 $\pm$ 3.62% of all CTB$^+$ neurons were Reelin$^+$ (total of 191 CTB$^+$ neurons in LIIa counted)(**Figure 3.3C**). In the slices stained against CB (**Figure 3.3D**), 1189 CTB$^+$ neurons were assigned to LIIb, of which 63.23 $\pm$ 5.76% were CB$^+$. From double-staining experiments we know that Reelin and CB can be co-expressed, therefore it is conceivable that a certain fraction of Reelin$^+$/CTB$^+$ LIIa neurons might have also been CB$^+$. I did not observe CTB$^+$/EGFP$^+$ (GABAergic) neurons in LIIb in the LEC. However, there was a striking tendency for LIIb CTB$^+$ neurons to be located in rather anterior parts of the LEC. In this experiment it was furthermore especially easy to distinguish LEC from further anterior regions: Not only the band of Reelin$^+$ neurons disappeared, which usually served as 'LEC marker' for me, but also the CTB$^+$ neurons were denser packed and located in deeper layers in the olfactory cortices located anteriorly to the LEC, which is in line with previous results (Shipley and Adamek, 1984). Of note, in the LEC also deeper layers than LIIb showed high numbers of FG$^+$ neurons, but as I focus in my study on the investigation of superficial layers in LEC, I did not examine these neurons any further.

3.1.3 CB$^+$ neurons in layer IIb project to the PIR and the contralateral LEC

Observations from our own group indicated that single CB$^+$ neurons in the MEC can target several regions in the brain, e.g. the medial septum and the contralateral MEC (personal communication by Dr. Elke Fuchs). Therefore, I set out to investigate the projection patterns of CB$^+$ neurons in the LEC in more detail to see if I would detect similar organizational principles as in the MEC. The reciprocal connection between LEC and PIR is known (Beckstead, 1978; Wyss, 1981; Burwell and Amaral, 1998b), however, so far it was not clear, which cell types in the LEC contribute to this projections to the PIR. The same is true for contralateral LEC-LEC projections, where functional connectivity has been described (Lacy and Stark, 2012) with little knowledge about the origin of projections and neurons participating in this interhemispheric information transfer. To address this question, I injected CTB555 in either the PIR (**Figure 3.4A**) or the LEC (**Figure 3.4B**) of wild-type mice and combined these injections with immunostainings against Reelin and CB (**Figure 3.4C and D**).

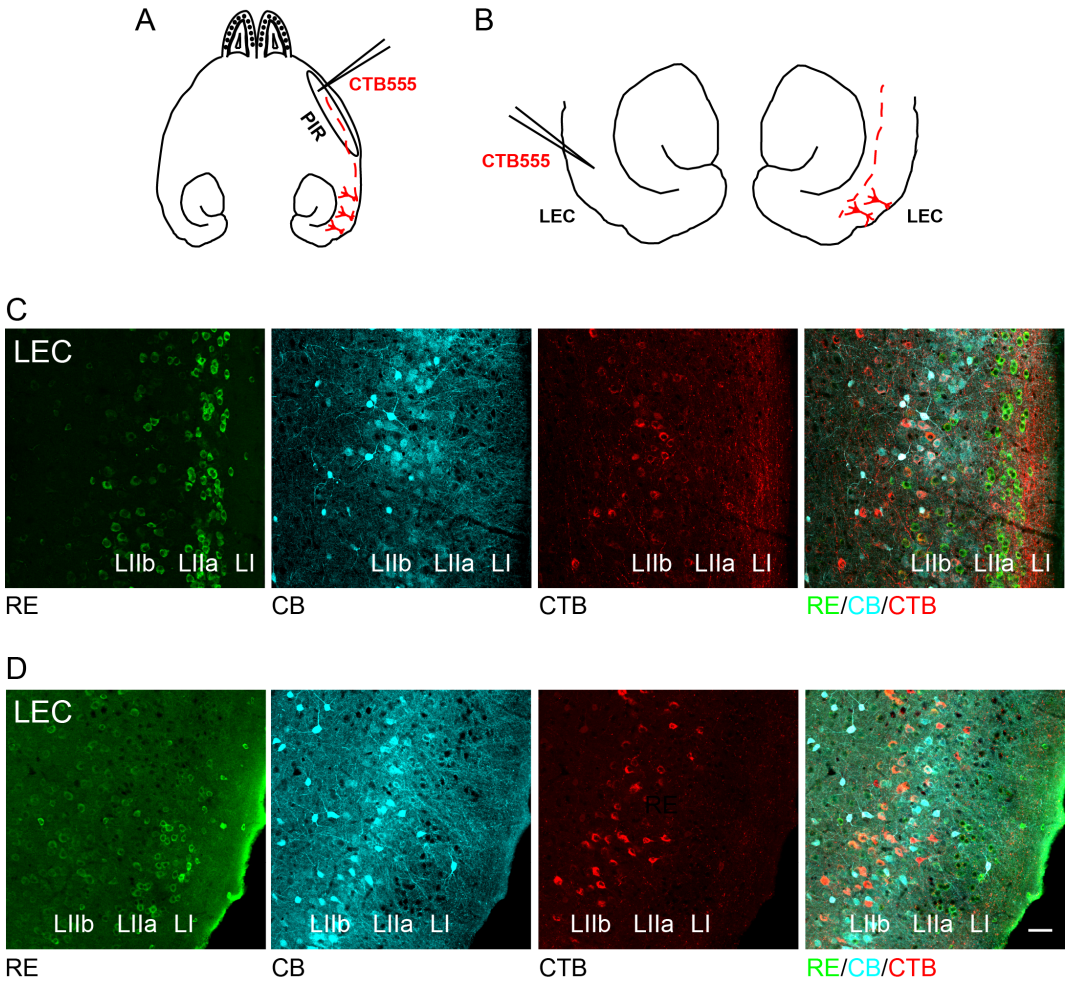

Figure 3.4. CB⁺ neurons project to the PIR and the contralateral LEC (**A**) and (**C**) Schematic drawing of the CTB injection into the PIR and respective immunostaining against Reelin and CB in wild-type mice. CTB⁺ neurons in LIIb are often also CB⁺. (**B** and **D**) Schematic drawing of the CTB injection into the contralateral LEC and respective immunostaining against Reelin and CB in wild-type mice. CTB⁺ neurons are found mostly in LIIb and deeper layers and are often CB⁺ in LIIb. Both in (**C**) and (**D**) Reelin⁺ neurons in LIIa are not CTB⁺. Scale bar, 50 µm. Abbreviations: CB, calbindin; CTB, cholera toxin subunit B; L, layer; OB, olfactory bulb; PIR, piriform cortex; RE, Reelin.

Injection of CTB into the PIR lead to labeling mainly in LIII and deeper layers in LEC, but also in LIIb a small fraction of CTB⁺ neurons was present (**Figure 3.4C**). 51.52 ± 4.62% of these were CB⁺ (206 CTB⁺ neurons in 3 hemispheres from 3 wild-type mice). On the contrary, in LIIa only sporadically labeling with CTB was detected. Injection of CTB into the LEC confirmed that there is a high degree of contralateral connectivity between the left and the right LEC (**Figure 3.4D**). However,the connectivity pattern regarding the origin of projections looked different to the connectivity seen with the PIR. The majority of

CTB$^+$ neurons were located in LIIb, and LIII contained the minor part of neurons that were projecting to the contralateral side as indicated by their CTB labeling. Neurons in LIIb could be both CB$^+$ and CB$^-$, but as we wanted to focus on the connectivity with olfactory structures, we did not investigate contralateral LEC-LEC projections any further. Note that CTB$^+$ neurons after either injecting CTB into the PIR or the contralateral LEC were only rarely seen in LIIa and therefore the contribution of Reelin$^+$ neurons in LIIa to these projections is negligible (**Figure 3.4C and D**).

3.1.4 Single CB$^+$ neurons in layer IIb send projections to both the OB and the PIR

We decided to combine injections into the OB with injections into the PIR using different fluorophores conjugated with CTB to address the following question: Having shown that CB$^+$ neurons in LIIb in the LEC send projections to the OB as well as to the PIR, we wondered if their might be some neurons that actually target both regions at the same time. These neurons would be in an ideal position to provide feedback information to both olfactory structures that are the direct input stations of the LEC. CTB555 was injected into the ipsilateral PIR and CTB488 into the ipsilateral OB (**Figure 3.5A**), and after immunostaining against Reelin or CB, I indeed could show that such cells are present.

Interestingly, there is a spatial segregation regarding these projections, and neurons projecting to the OB are located rather ventral whereas neurons providing feedback information to the PIR are found in more dorsal regions of the LEC. Nevertheless, there was a horizontal stripe with overlapping projections and for counting the number of neurons that are projecting to both areas at the same time, I took into account only slices where more than 4 neurons of each population were present in LIIb (**Figure 3.5B**). This resulted in 239 CTB488$^+$ neurons projecting to the OB and 50 CTB555$^+$ neurons projecting to the PIR (counted in one hemisphere of one wild-type mouse). Among these neurons, I detected 10 neurons that were positive for both CTB555 and CTB488, and of these 10 neurons 6 were CB$^+$. In **Figure 3.5B**, the magnifications show examples of CTB488$^+$/CTB555$^+$ neurons that are either CB$^-$ (area 1) or CB$^+$ (area 2), respectively. This result would indicate the existence of a population of CB$^+$ neurons that can provide the two main olfactory regions in the brain,

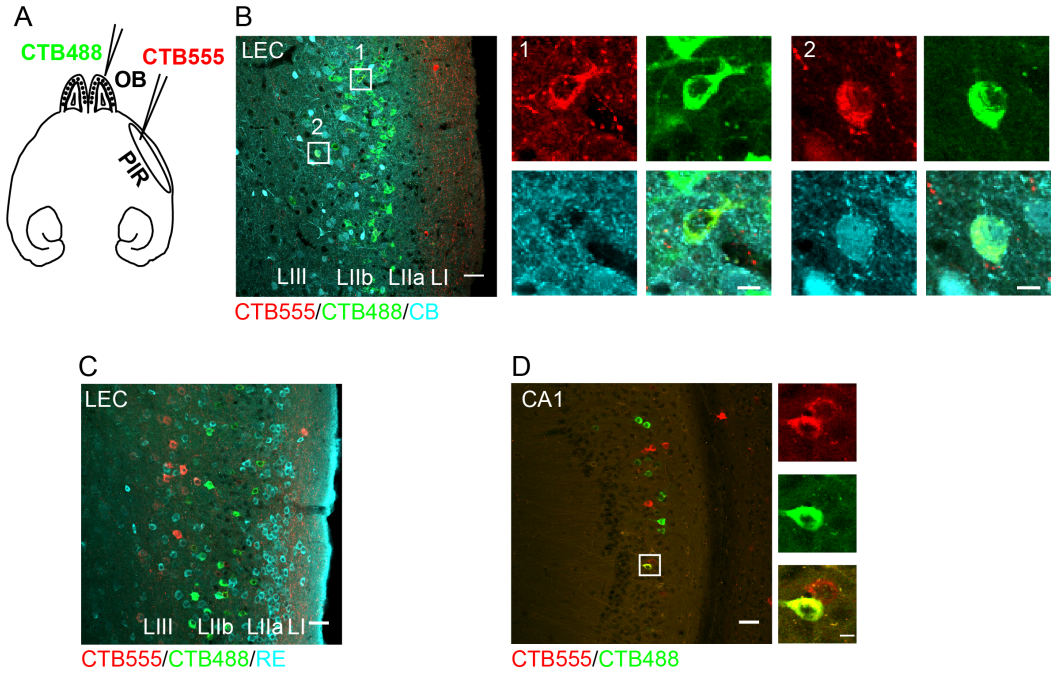

Figure 3.5. CB⁺ neurons send projections in parallel to both the OB and the PIR (**A**) Schematic drawing of the CTB injection into the OB and the PIR. Injections were ipsilateral and either CTB conjugated to Alexa488 or to Alexa555 was used. (**B**) Immunostaining against CB after injection of CTB555 into the PIR and CTB488 into the OB. Neurons in LIIb project both to the OB and the PIR, as shown by their CTB488 and CTB555 labeling. Magnifications of the boxed areas reveal that these neurons can be both CB⁻ (area 1) as well as CB⁺ (area 2). Scale bar, 50 µm and 10 µm. (**C**) Same as in (**B**) but with immunostaining against Reelin. The band of Reelin⁺ neurons is clearly separated from the population of neurons being CTB⁺. Scale bar, 50 µm. (**D**) In the hippocampal CA1 area, CTB488⁺ as well as CTB555⁺ neurons can be detected, and some of these neurons are even positive for both. Scale bar, 50 µm and 10 µm. Abbreviations: CB, calbindin; CA1, *Cornu Ammonis* 1; CTB, cholera toxin subunit B; L, layer; OB, olfactory bulb; PIR, piriform cortex; RE, Reelin.

the OB and the PIR, with feedback information in parallel processing streams. Reelin⁺ neurons in LIIa were only extremely rarely CTB488⁺ and I never detected Reelin⁺/CTB488⁺/CTB555⁺ neurons (**Figure 3.5C**). Interestingly, not only in the LEC but also in the hippocampus there were neurons that were either CTB4888⁺ or CTB555⁺ or even both (**Figure 3.5D**). These neurons were located in the CA1 area at the border close to the subiculum, however, their somata did not reside in the pyramidal layer. Therefore, they do not seem to be typical pyramidal CA1 neurons, but most probably they are also not GABAergic neurons (personal communication by Dr. Elke Fuchs).

3.1.5 Heterogeneous expression of GABAergic marker proteins in the LEC

The goal to understand the excitatory neuronal network and its underlying function in the LEC can only be accomplished by taking the opposing players, the inhibitory GABAergic neurons, into account. In the MEC, the excitatory network is under strict inhibitory control, provided mainly by the dense network of PV^+ neurons that constitute about 50% of the GABAergic population (Miettinen et al., 1996; Wouterlood et al., 1995). PV^+ cells typically form a dense plexus of processes within LII in the MEC, with a gradient in intensity both from medial to lateral as well as from dorsal to ventral (Wouterlood et al., 1995; Fujimaru and Kosaka, 1996). First attempts looking at the distribution of PV^+ revealed striking differences in the LEC, which lured us to take a closer look at the distribution of GABAergic markers in the LEC. I performed therefore immunohistochemical experiments to investigate the occurrence and distribution of the most common GABAergic markers such as PV, SOM, and CR. I also included stainings against Reelin and CB, because although we consider these proteins as markers for excitatory neurons in the LEC, they are also localized in a subpopulation of GABAergic neurons (**Figure 3.6**).

I focused on LI, LIIa and LIIb and counted in 4-5 hemispheres from 2-3 *GAD67*^{EGFP} mice. The percentages given are always derived from dividing the number of neurons expressing a respective marker in a certain layer by the total number of GABAergic neurons in this layer. The absolute values of how many neurons per layer and per marker were counted and the respective percentages are listed in **Table 3**. In the LEC, there is a dense PV^+ plexus, which is broadly spread across LIIa and LIIb, forming the typical basket surrounding both $Reelin^+$ and CB^+ cell bodies, sometimes resulting in PV^+ neuropil forming visible modules (**Figure 3.6A**). PV^+ somata are however absent in LI, very sparse in LIIa (17.36%), and more numerous in LIIb (30.34%). Therefore, the fraction of PV^+ neurons of the total GABAergic population is much lower than what has been reported for the MEC (Miettinen et al., 1996; Wouterlood et al., 1995). Staining against SOM revealed that LI contains very few positive neurons (3.67%), and that in LIIa and LIIb 6.82% and 14.33% respectively of all GABAergic neurons were SOM^+ (**Figure 3.6B**). CR^+ neurons showed a comparable distribution across layers as SOM^+ neurons, with few neurons in LI (3.67%), and increasing occurrence in LIIa (18.14%) and LIIb (27.01%) (**Figure 3.6C**). The same

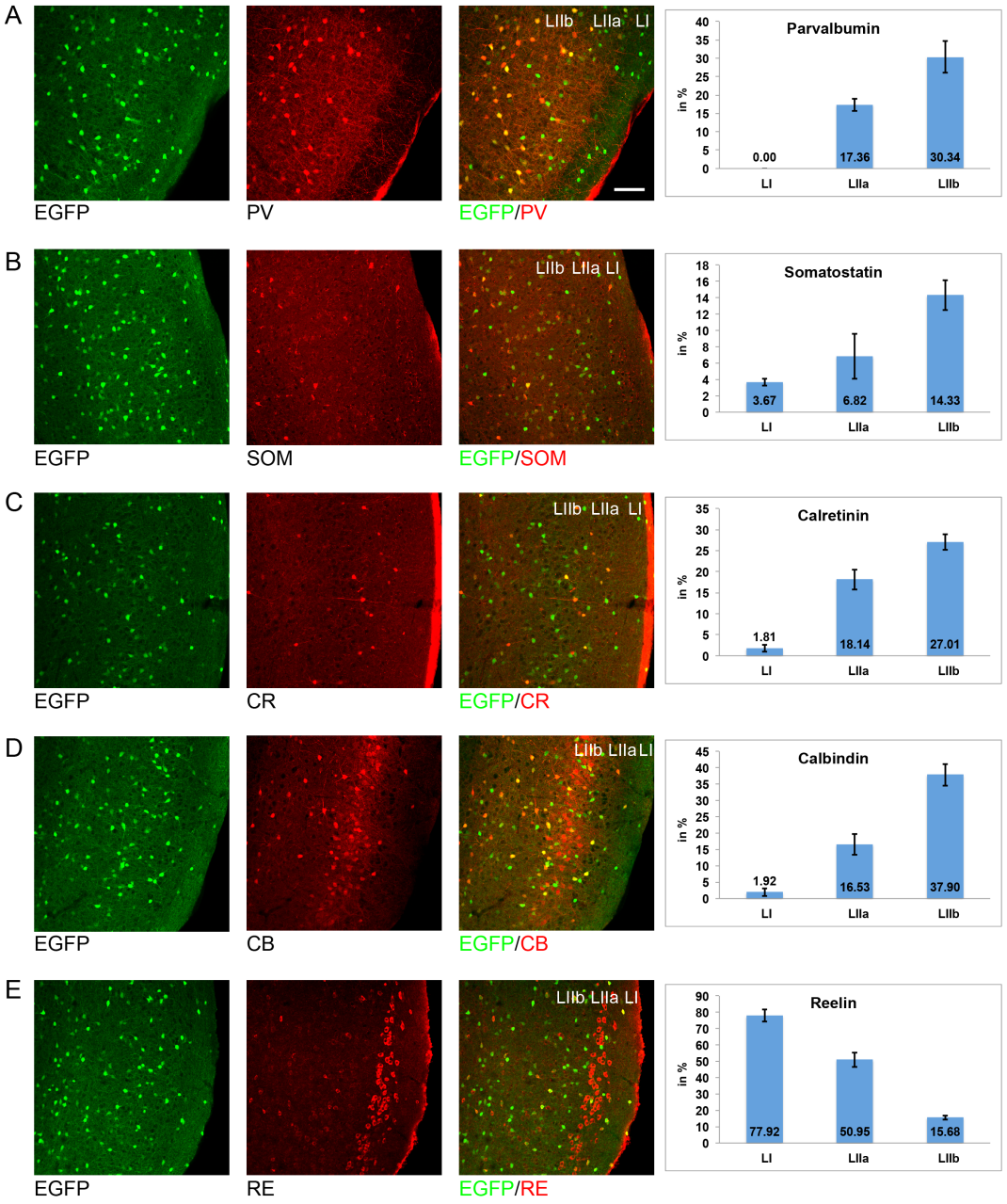

Figure 3.6. High diversity of interneuron markers in the LEC Immunostainings in *GAD67*^{EGFP} mice against (**A**) PV (**B**) SOM, (**C**) CR, (**D**) CB, (**E**) and Reelin with respective graphs showing the distribution across layers. Different markers can be coexpressed, which can explain higher added percentages than 100%. Scale bar, 100 µm. Abbreviations: CB, calbindin; CR, calretinin; GFP, green fluorescent protein; PV, parvalbumin; RE, Reelin; SOM, somatostatin.

holds true for CB$^+$/EGFP$^+$ neurons (**Figure 3.6D**). Layer I is basically free of CB$^+$/EGFP$^+$ neurons (1.92%) and in LIIa and LIIb, 16.53% and 37.90% respectively express CB. This numbers reveal that although CB is regarded as marker of excitatory neurons in LII in the entorhinal area, it is also present in a substan-

tial fraction of GABAergic neurons. All the markers presented so far showed quite low occurrence in LIIa, with percentages never higher than 20% of the GABAergic population in LIIa. Reelin, however, is not only expressed in most excitatory neurons in LIIa, but it is also detected in a large fraction of GABAergic neurons in superficial LEC (**Figure 3.6E**). LI contains 77.92% Reelin$^+$/EGFP$^+$ neurons, LIIa 50.95% and LIIb 15.68%.

Marker	LI		LIIa		LIIb		LI in %	LIIa in %	LIIb in %
	GAD+	GAD+/Marker+	GAD+	GAD+/Marker+	GAD+	GAD+/Marker+			
	by absolute values						by relative values		
PV	166	0	181	32	453	132	0.00 +/- 0.00	17.36 +/- 1.71	30.34 +/- 4.25
SOM	135	5	179	14	558	82	3.67 +/- 0.45	6.82 +/- 2.73	14.33 +/- 1.84
CR	203	4	248	45	869	237	1.81 +/- 0.87	18.14 +/- 2.44	27.01 +/- 1.82
CB	132	3	167	28	525	195	1.92 +/-1.13	16.53 +/- 3.13	37.90 +/- 3.37
Reelin	161	126	260	129	504	80	77.92 +/- 3.65	50.95 +/- 4.39	15.68 +/- 1.33

Table 3.1. Numbers of GABAergic neurons expressing different markers Abbreviations: PV, parvalbumin; SOM, somatostatin; CR, calretinin; CB, calbindin; GAD$^+$, *GAD67*^{EGFP}-positive neuron; L, layer.

Only recently it was shown that neurons expressing the ionotropic serotonin receptor 5HT3a (5HT3aR) constitute a major group of interneurons in the neocortex and in combination with the populations of SOM-expressing and PV-expressing neurons account for nearly 100% of neocortical GABAergic neurons (Rudy et al., 2011). It has been known that 5HT3a receptors are present exclusively in GABAergic neurons (Morales and Bloom, 1997; Ferezou et al., 2002) and that 5HT3aR-expressing cells are distinct from neurons expressing both PV and SOM (Ferezou et al., 2002). However, as there is no antibody to the 5HT3a receptor available, it has not been possible to use immunohistochemistry to investigate the size of the population of GABAergic neurons expressing 5HT3aR. The analysis of 5HT3aR-expressing neurons was facilitated for me by the availability of a transgenic mouse line expressing EGFP in these neurons (*5HT3aR-BAC*^{EGFP} mouse line) (Inta et al., 2010). I used immunohistochemical stainings against Reelin and against CB in *5HT3aR-BAC*^{EGFP} mice to separate between LIIa and LIIb (**Figure 3.7A**) and counted in these mice only 5HT3aR$^+$ neurons. To get an estimate of the percentage of 5HT3aR$^+$ neurons of the total GABAergic population, I compared the number of EGFP$^+$ cells in *5HT3aR-BAC*^{EGFP} mice versus the number of EGFP$^+$ cells in the *GAD67*^{EGFP} mice.

In these experiments, I had found that across LI-LIIb, the distribution of GABAergic neurons was as following: 17% of all GABAergic neurons counted in LI-LIIb reside in LI, 24% are encountered in LIIa, and the majority of 59% of GABAergic neurons are assigned to LIIb (number of neurons counted: 293 for LI, 427 for LIIa and 1029 for LIIb). Divided by the number of slices that were

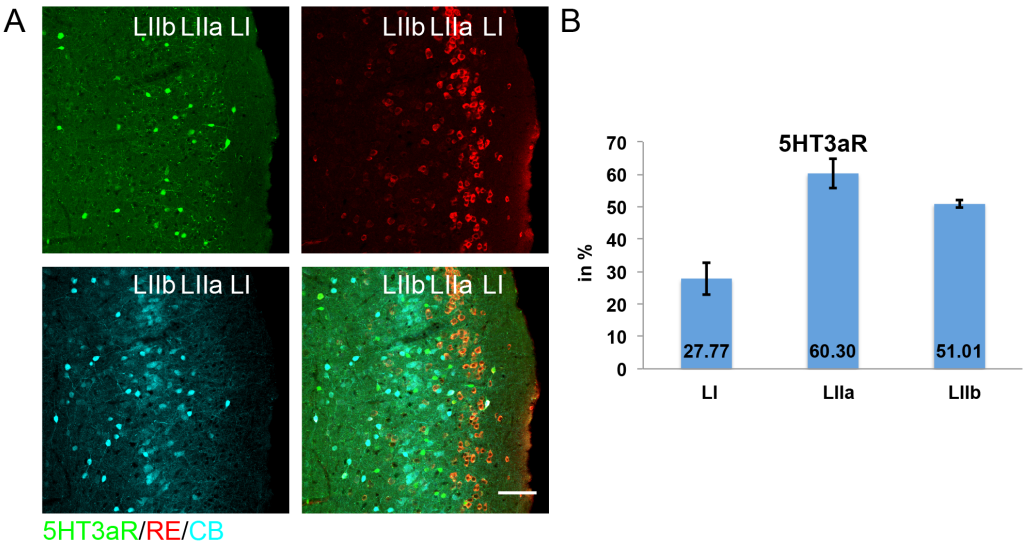

Figure 3.7. The distribution of 5HT3aR-expressing neurons (**A**) Immunostainings in *5HT3aR-BAC*^{EGFP} mice against Reelin and CB (as reference to locate cell bodies). (**B**) The relative percentage of 5HT3aR$^+$ neurons of estimated numbers of GABAergic neurons based on countings in *GAD67*^{EGFP} mice in LI-LIIb. Scale bar, 100 µm. Abbreviation: 5HT3aR, ionotropic serotonin receptor 5HT3a; CB, Calbindin; L, layer; RE, Reelin

taken into account for counting, this yields the number of GABAergic neurons per layer and per slice (approximate number of GABAergic neurons per slice area counted: 8.73 $\pm$ 0.85% in LI, 12.56 $\pm$ 1.26% in LIIa and 30.03 $\pm$ 0.97% in LIIb). This is what I consider as the estimated total number of GABAergic neurons for calculating the percentage of 5HT3aR-expressing neurons. Based on these calculations, 5HT3aR-expressing neurons are a large fraction of the GABAergic population, with 27.77 $\pm$ 4.95% in LI, 60.30 $\pm$ 4.63% in LIIa, and 51.01 $\pm$ 1.23% in LIIb (number of neurons counted: 64 in LI, 194 in LIIa and 386 in LIIb, in 3 hemispheres of 2 mice, (**Figure 3.7C**). With 5HT3aR, I have found a marker of GABAergic neurons that is expressed in LEC LII in a comparable percentage to the expression of PV in MEC LII (Miettinen et al., 1996; Wouterlood et al., 1995). It is noteworthy that the summation of PV$^+$, SOM$^+$ and 5HT3aR$^+$ neurons in LI-LIIb never exceeds 100%, which is in line with observations that these markers are expressed in distinct populations (Ferezou et al., 2002). Coexpression of other markers, however, was observed, as e.g. among Reelin$^+$ and CB$^+$ neurons, CB$^+$ and PV$^+$ neurons and among CR$^+$ and 5HT3aR$^+$ neurons (data not shown).

3.2 Two-photon calcium imaging of odor-evoked neuronal activity in the LEC

All studies to date that tried to elucidate the functional role of the LEC were based on single unit recordings, tetrode recordings or lesions of the LEC, but there is no publication so far that reported findings from imaging the LEC network activity *in vivo*. One of the reasons lies certainly in the major challenge that one faces trying to approach the LEC using microscopy techniques. I developed a surgical procedure that enabled us to overcome this obstacle. As described in the introduction, one of the major advantages of two-photon calcium imaging is the possibility to record from neurons with known identity and spatial layout. In the following part, I will present data that we gained from calcium imaging experiments in the LEC of anesthetized mice. Neurons projecting to the DG (presumably Reelin$^+$) are contrasted with CB$^+$ neurons and GABAergic neurons in respect to their responsiveness to odor-stimulation.

All in-depth data analysis of two-photon calcium imaging data was performed by Prof. Fritjof Helmchen and Dr. Henry Lütcke (Zürich).

3.2.1 Experimental setup

The LEC is located at ventral and posterior levels of the mouse brain, which prohibits direct access from top. Therefore, I developed a surgical procedure that involves tilting of the mouse by 90° that is schematically depicted in **Figure 3.8A**. The use of a 10x objective allowed the visualization of blood vessels, which served as guidelines for targeting the LEC, since this area is located ventrally to the caudal rhinal vein. All images were taken in the most ventral parts of the accessible imaging area and focused on posterior regions to ensure correct recordings in the LEC. A custom-built olfactometer allowed controlled and precisely timed odor-stimulations using 6 different volatile mineral oils (**Figure 3.8B**). Each trial consisted of an initial delay of 5 s, and 3 stimuli that were presented for 4 s followed by an interstimulus interval (ISI) of 26 s (**Figure 3.8C**). Presentation of different odors was randomized and controlled by custom-written software. Flowmeters recording the air flow in the tubing were used to control for steady and constant delivery of the stimulus (**Figure 3.8D**).

All the mice used for calcium imaging were injected with AAV.GCaMP6 (wildtype mice) or AAV.flex.GCaMP6 (*GAD67*^{Cre} and *CB*^{Cre}) in the LEC. Wild-type mice were additionally injected with CTB in the DG, and for the *in vivo* recordings I focused on cells in a depth ranging from 100 µm to 200 µm, where I encountered a dense population of GCaMP6^{+}/CTB^{+} neurons. The CTB-labeling served two purposes: Firstly, it allowed selective targeting of cells projecting to the DG, and secondly, the CTB-labeling indicated that these cells were most presumably

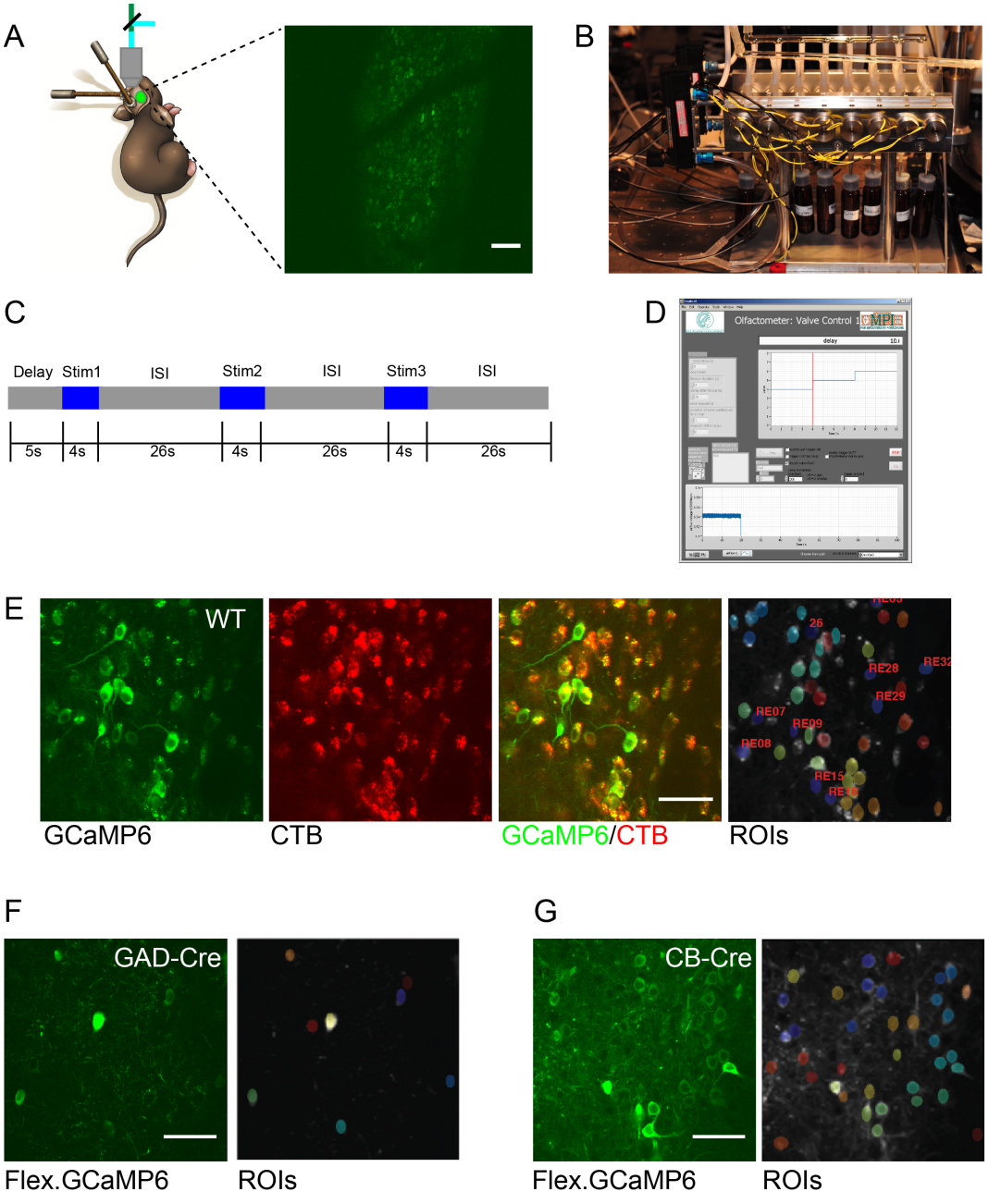

Figure 3.8. Experimental setup of two-photon calcium imaging in the LEC
Text continues on the next page.

Figure 3.8. (**A**) Experimental setup with image of brain surface and blood vessels visualized by a 10x objective. Scale bar, 100 µm. (**B**) Picture of the custom-built olfactometer. (**C**) Stimulation protocol. (**D**) The custom-written software called 'Olfactometer: Valve Control 1.0' allows randomized odor stimulation. (**E**) Imaging area in a wild-type mouse with neurons labeled with GCaMP6 and CTB555. ROIs are manually drawn and distinguish between GCaMP6^{+} neurons and GCaMP6^{+}/CTB^{+} neurons marked as 'RE'. (**F**) and (**G**) Imaging areas in a *GAD67*^{Cre} mouse and a *CB*^{Cre} mouse, respectively, both injected with AAV.flex.GCaMP6. Images with overlaid ROIs are shown to the right. Scale bars, 50 µm in (**E**), (**F**), and (**G**). Abbreviations: CTB, cholera toxin subunit B; Stim, stimulus; ISI, interstimulus interval; RE, Reelin; WT, wild-type; ROI, region of interest.

Reelin^{+} neurons (as shown in section **3.1.1**). The fluorophores of GCaMP6 and CTB can be excited best with 900 nm and 750 nm respectively, and spectral separation into a green and a red channel enabled us to differentiate between neurons labeled with GCaMP6, CTB555 or both. Selection of neuronal cell bodies was done manually, whereby such regions of interest (ROIs) were classified as either GCaMP6^{+}/CTB^{+} or GCaMP6^{+}/CTB^{-} (e.g. RE15 versus 26) (**Figure 3.8E**). The AAV carrying the GCaMP6 infects excitatory Reelin^{+} and CB^{+} as well as inhibitory GAD^{+} neurons (**Appendix Figure 1**). To selectively image different neuronal cell types, we used transgenic mice expressing Cre recombinase in a specific neuronal subtype and the floxed version of GCaMP6 to ensure cell-type specific GCaMP6 expression. GABAergic neurons were imaged in a depth between 100 µm and 220 µm in *GAD67*^{Cre} mice injected with AAV.flex.GCaMP6 (**Figure 3.8F**). CB^{+} neurons could be selectively imaged in *CB*^{Cre} mice injected with AAV.flex.GCaMP6 with all imaging planes located between 190 µm and 250 µm from the pia (**Figure 3.8G**). The day of imaging was scheduled the latest 8 days after the virus injection, as I noticed with longer waiting times an increased susceptibility to undesired nuclear filling, a correlate of cytomorbidity, in the neurons. This is in marked difference to other brain areas, where waiting times of two weeks (in my hands) or even longer (Chen et al., 2013b) did not lead to increased numbers of neurons with filled nuclei (**Appendix Figure 2**).

3.2.2 Characterization of the newly generated *CB*^{Cre} mouse line

As the *CB*^{Cre} mouse line had not been used in any other previous publication, we subjected it to thorough investigation to confirm the correct expression pat-

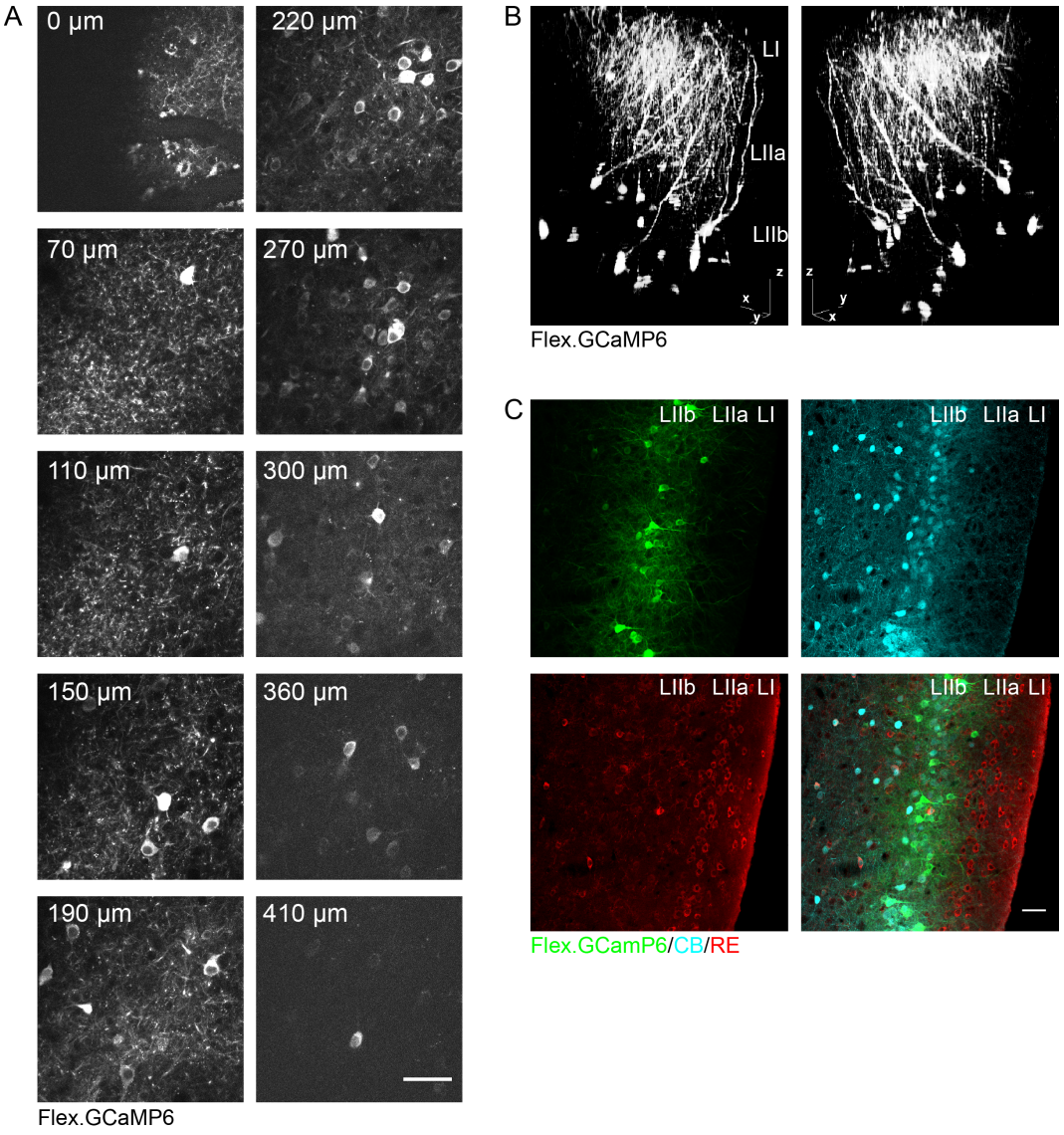

Figure 3.9. Characterization of the newly generated *CB*^{Cre} mouse line (**A**) Two-photon images *in vivo* in the *CB*^{Cre} mouse covering a depth between 0 µm and 400 µm from the pia surface. The most abundant labeling of cell bodies is observed between 190 µm and 270 µm. (**B**) 3D reconstruction of an image stack demonstrating *CB*^{Cre} cells with cell bodies located in LIIb and an apical dendrite extending towards the pia. Note that somata and dendrites often exhibit oblique orientation. (**C**) Confocal images of a *CB*^{Cre} mouse immunostained with Reelin and CB following injection of AAV.flex.GCaMP6 in the LEC confirm selective expression of the virus in CB^{+} neurons. Scale bars, 50 µm in (**A**) and (**B**). Abbreviations: CB, calbindin; L, layer; RE, Reelin.

tern. We showed in our immunohistochemical experiments that CB^{+} neurons are rarely located in LI and LIIa. The beginning of LIIb is marked by the appearance of a high number of CB^{+} neurons. In confocal images, this border is located approximately 160 µm below the pia (personal observation). With

the two-photon microscope, images in several depths were taken in the LEC of *CB*^{Cre} injected with AAV.GCaMP6, starting from the pia going down to a depth of 410 μm (**Figure 3.9A**). Till a depth of 150 μm single GCaMP6^{+} neurons were observed. In a range between 190 μm and 270 μm, high numbers of GCaMP6^{+} neurons were imaged and although the laser power had to be increased with increasing depth, no reduction in image quality was observed. With further increasing depth, the number of GCaMP6^{+} neurons declined and the image became darker, most probably due to light scattering in the tissue. Considering the shrinkage of processed tissue, these images are in accordance with the observation in slices stained against CB. A high-resolution stack that covered about the same range starting from the pia going down to a depth of about 350 μm reveals the dense dendritic network in LI and the oblique orientation of CB^{+} somata in LIIb (**Figure 3.9B**). Immunostainings against Reelin and CB confirm the selective expression of GCaMP6 in CB^{+} but not Reelin^{+}/CB^{-} neurons (**Figure 3.9C**). The only exception can occur in the center of the injection spot, where unusual GCaMP6 expression was also observed in LIIa Reelin^{+} neurons. In summary, these findings strongly support a correct expression of Cre-recombinase specifically in CB^{+} neurons.

3.2.3 Reelin^{+}, CB^{+} and GAD^{+} neurons respond to odors

The calcium transients following odor stimulation of 605 Reelin^{+} neurons, 407 CB^{+} neurons and 194 GAD^{+} neurons in LEC LII were recorded in 9 wild-type mice, 8 *CB*^{Cre} mice and 11 *GAD67*^{Cre} mice (in 24, 17 and 26 imaging areas, respectively). In all three different cell types odor stimulation elicited a change in neuronal activity as revealed by an increase in the calcium transients. These changes in the fluorescence intensity were usually time-locked to the onset of the stimulus, although occasionally I observed a decrease in firing activity or an increase after termination of the stimulus. For the further analysis, I focus on time-locked activity increases following odor delivery. Six Reelin^{+}, CB^{+} and GAD^{+} neurons of a respective imaging area are depicted as examples in **Figure 3.10A, B, and C**. Neurons varied in their responsiveness to odor stimulation, in their selectivity for different odors and in their calcium transient amplitude. Cell responses to none of the odors (e.g. CB29), to one odor (e.g. RE33, CB18), to two odors (e.g. RE12, CB07, GAD07) or to all three presented odors (e.g. CB28, GAD 05) can be observed across the different populations.

All odors could successfully drive activity in all three different cell types, as shown by the grand average odor-evoked receptive fields (RFs). Similar to the visual system, in the olfactory system RFs are used to describe by which odors

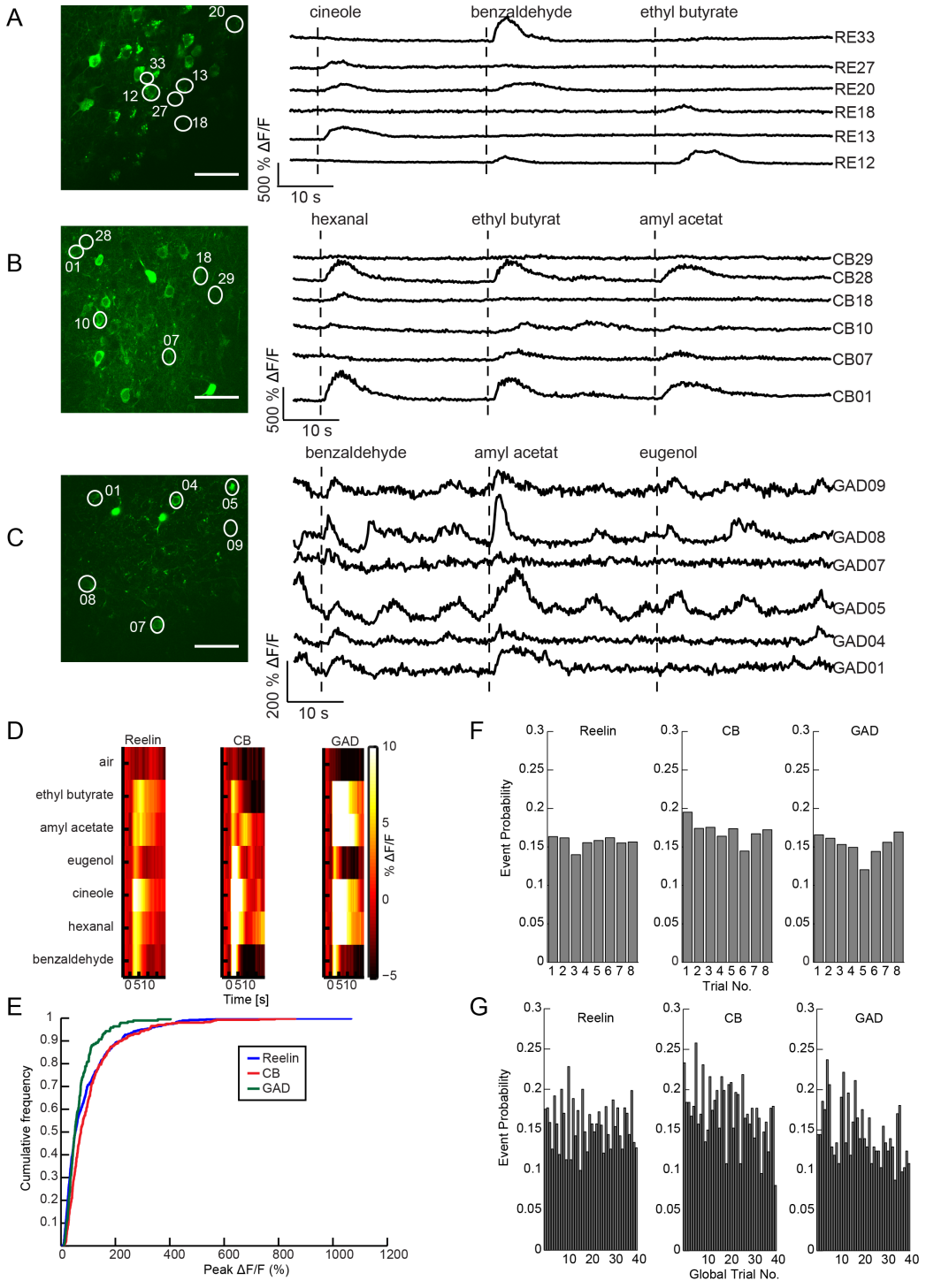

Figure 3.10. Reelin⁺, CB⁺ and GAD⁺ neurons respond to odors
Text continues on the next page.

Figure 3.10. Neurons of all three cell types investigated respond to odors. (**A**) Calcium transients of six Reelin$^+$ neurons outlined in the left panel following stimulation with three different odors. (**B**) Calcium transients of six CB$^+$ neurons outlined in the left panel following stimulation with three different odors. (**C**) Calcium transients of six GAD$^+$ neurons outlined in the left panel following stimulation with three different odors. Note the different scaling. (**D**) Grand average odor-evoked RFs for different cell types showing that all stimuli but air elicit reliable responses. (**E**) Cumulative distribution of trial-averaged peak ΔF/F demonstrating higher response amplitude of Reelin$^+$ and CB$^+$ neurons compared to GAD$^+$ neurons. (**F**) Event probability over repetition of the same odor for the different cell types. (**G**) Event probability over trial number irrespective of odor identity for the different cell types. Scale bars, 50 µm in (**A**), (**B**), and (**C**). Data analyzed jointly with Dr. Henry Lütcke.

a specific neuron or neuron population can be activated. Air as control stimulus did not lead on average to an increase in activity (**Figure 3.10D**). Peak ΔF/F is the maximal amplitude to an odor for each neuron, i.e. the amplitude of the average response evoked by the best stimulus. In the population of Reelin$^+$ neurons, more than 50% of the neurons exhibited peak ΔF/F lower than 73%. 50% of the CB$^+$ and GAD$^+$ neurons had peak ΔF/F lower than 51% (**Figure 3.10E**). Reelin$^+$ neurons and CB$^+$ showed larger odor-evoked responses than GAD$^+$ neurons, with peak ΔF/F as high as 1067% and 861% for single Reelin$^+$ neurons and CB$^+$ neurons, respectively and peak ΔF/F of 402% for GAD$^+$ neurons. Mean values for odor-evoked calcium transients were 92.91 $\pm$ 4.26%, 106.81 $\pm$ 5.41% and 68.21 $\pm$ 4.09% for Reelin$^+$, CB$^+$ and GAD$^+$ neurons, respectively (Reelin versus CB: p = 0.042, Reelin versus GAD: p = 0.002, CB versus GAD: p = 0.000, t-test, Bonferroni corrected).

The event probability, as the probability that one particular odor elicits a response in a specific neuron, was stable from the first to the last presentation of the odor in all neuronal populations (**Figure 3.10F**). On a global level, considering the number of odor stimulations irrespective of odor identity, we observed small differences between the three neuronal populations. The event probability stayed stable for Reelin$^+$ neurons, but for CB$^+$ and GAD$^+$ neurons, there was a small trend towards lower event probabilities with increasing repetitions (**Figure 3.10G**).

3.2.4 Reelin$^+$, CB$^+$ and GAD$^+$ neurons exhibit different selectivity in their response to odors

The observed differences in the response pattern of the three different cell types in single traces were intriguing and lead us to an in-depth analysis of trial-averaged responses. In **Figure 3.11A, B and C** I depict trial-averaged responses of single neurons that were presented in **Figure 3.10A, B and C** with single traces. Reelin$^+$ neuron RE33 showed reliable responses to the odors amyl acetate and benzaldehyde, but did not respond to the presentation of the five other stimuli including air (**Figure 3.11A**). On the contrary, CB$^+$ neuron CB01 exhibited clear stimulus-evoked transients to the presentation of five out of six odors (**Figure 3.11B**). Similarly, five out of six odors activated GAD$^+$ neuron GAD08 (**Figure 3.11C**). Changes in fluorescence amplitude were smaller for GAD08 than for RE33 and CB01 (note the different scaling), supporting the finding of larger odor-evoked responses in the Reelin$^+$- and CB$^+$-population.

The trial-averaged responses of all neurons in an imaging area can be summarized in a heat map, shown here with RE33 and all other Reelin$^+$ neurons of this area as representative example (**Figure 3.11D**). This heat map reveals that the Reelin$^+$ population responded stronger to some odors than other, e.g. amyl acetate drove activity in a substantial fraction of neurons. Additionally, the heat map provides further information, revealing that some neurons in this area such as RE33 responded very selectively to only one or two odors, whereas other neurons showed a broader response pattern responding to most of the presented odors (e.g. RE34). These responses of individual neurons to the number of odors that successfully elicited responses can be quantified for all three cell types. Based on these quantifications, further differences in the odor-responsiveness can be observed (**Figure 3.11E**). The cell fraction of Reelin$^+$ neurons that did not show odor-evoked calcium transients was 7.5%. The largest cell fraction with 22.6% was activated by two odors, with smaller cell fractions responding to three or four odors (21.9% and 18.2%, respectively). 3.8% of all Reelin$^+$ neurons responded completely unselectively to all six odors presented. CB$^+$ neurons were more evenly distributed, with a larger cell fraction of 10.5% not responding to any of the odors, and a larger cell fraction of 9.1% responding unselectively to all of the odors. The largest cell fraction in the population of CB$^+$ neurons was activated by three different odors (19.3%). GABAergic neurons revealed a striking difference in their response pattern. The

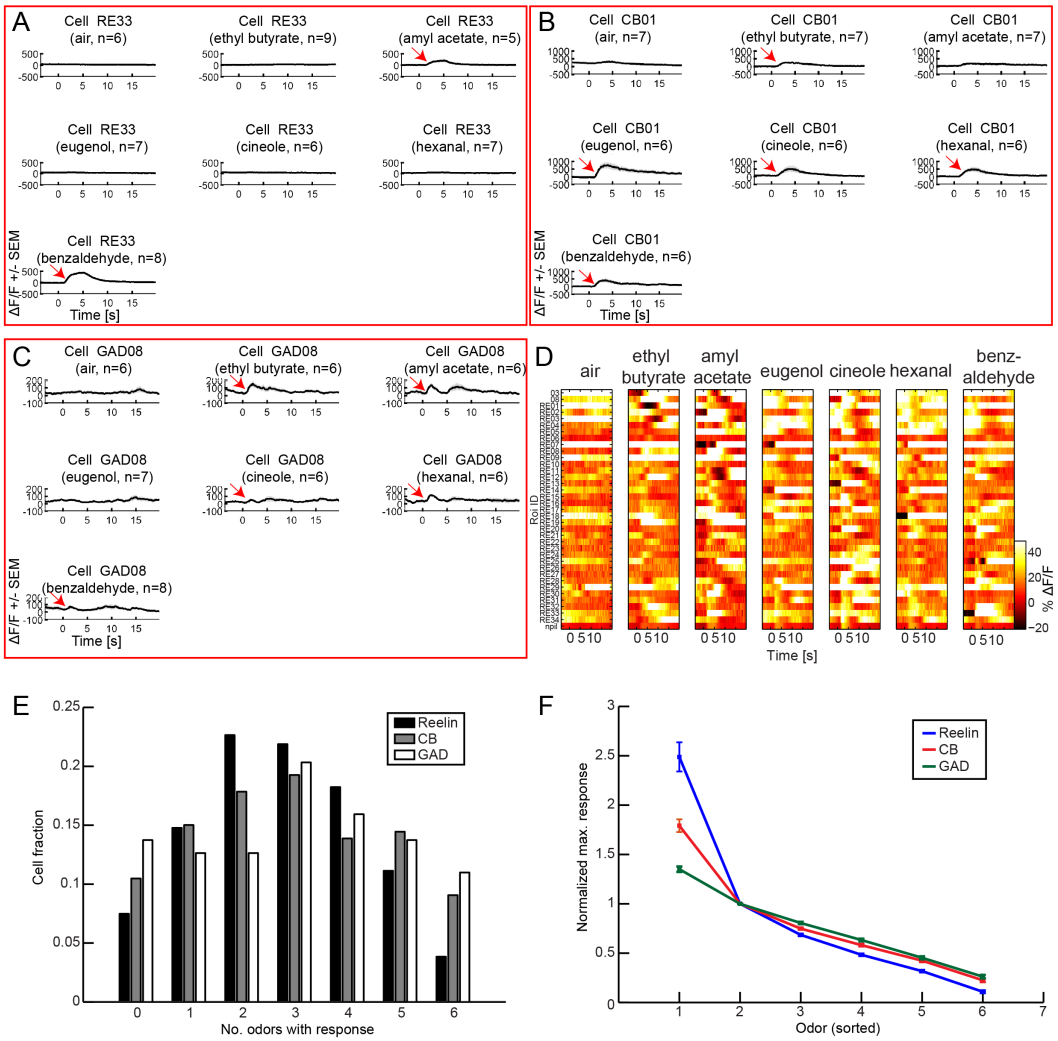

Figure 3.11. Reelin$^+$, CB$^+$ and GAD$^+$ neurons exhibit different selectivity in their response to odors Representative examples of neurons taken from imaging areas depicted in **Figure 3.10A, B and C**. Odor and number of trials per odor are indicated on top, red arrows mark trial-averaged odor-evoked calcium transients. (**A**) Peristimulus time plots of Reelin$^+$ neuron responding to two out of six odors. (**B**) Peristimulus time plots of CB$^+$ neuron responding to five out of six odors. (**C**) Peristimulus time plots of GAD$^+$ neuron responding to five out of six odors. (**D**) Average odor-evoked population activity of all Reelin$^+$ neurons present in **Figure 3.10A** displayed as heat map. (**E**) Graph showing the fraction of neurons with no response (0) or at least one event to one or more odors in different cell types. Most Reelin$^+$ neurons respond to two or three odors, and most GAD$^+$ neurons respond to three or more odors. CB$^+$ neurons are more evenly distributed. (**F**) Selectivity of trial-averaged odor responses. Odors are sorted according to trial-averaged response amplitude and normalized to the second-best response. Reelin$^+$ neurons exhibit the highest selectivity. Data analyzed jointly with Dr. Henry Lütcke.

distribution was strongly shifted towards higher number of odors that activated GAD$^+$ neurons, with more than 60% of all GABAergic neurons being responsive

to three or more odors (20.3% to 3 odors, 15.9% to 4 odors, 13.7% to 5 odors and 11.0% to 6 odors). Therefore, Reelin$^+$ neurons are more narrowly tuned to specific odors, whereas GABAergic neurons reveal a broader response profile. CB$^+$ neurons respond significantly different to both the other groups, with a tuning curve in between.

In an additional analytical approach, odors can be sorted according to the trial-averaged response amplitude, such that the odor eliciting the highest amplitude is the first in a row and considered to be the odor driving a particular neuron the 'best'. Responses are normalized to the 'second-best' odor for clearer visualization (**Figure 3.11F**). The larger the decrease between the peak response to the 'best' odor to the normalized peak response to the 'second-best' odor, the higher the selectivity. According to this analysis, Reelin$^+$ neurons exhibit the highest selectivity to the 'best' odor (Reelin versus CB and Reelin versus GAD: $p < 0.001$, t-test, Bonferroni corrected). CB$^+$ neurons are less selective, and GAD$^+$ are the least selective, providing additional support for the previous finding (CB versus GAD, for sorted odor no. 1-6: $p = 0.000$, $p = 0.000$, $p = 0.003$, $p = 0.173$, $p = 0.164$, t-test, Bonferroni corrected).

3.2.5 Correlation analysis of odor-evoked activity

The following data analysis is based on a subset of the neuronal cell population presented so far, without distinguishing between different cell types (9 mice, 25 imaging areas, 951 neurons). It can be assumed that the majority of neurons presented in the following belongs to the population of Reelin$^+$ neurons, as the depth of recording was mainly <200 µm. The experimental data acquisition performed by me has been accomplished, however data analysis of the complete data set performed by our collaboration partners is still ongoing.

As I illustrated in the introduction, one of the major advantages of two-photon calcium imaging is the possibility to record firing patterns of neurons with known spatial organization, allowing correlations for individual neurons between response characteristic and cell soma location. Color-coding the trial-averaged odor-evoked population activity results in the map of an example imaging area, revealing no obvious spatial organization. Neurons responding to the different stimuli are distributed across the imaging area and do not cluster in a particular zone (**Figure 3.12A**). Each ROI can be described by its odor RF map,

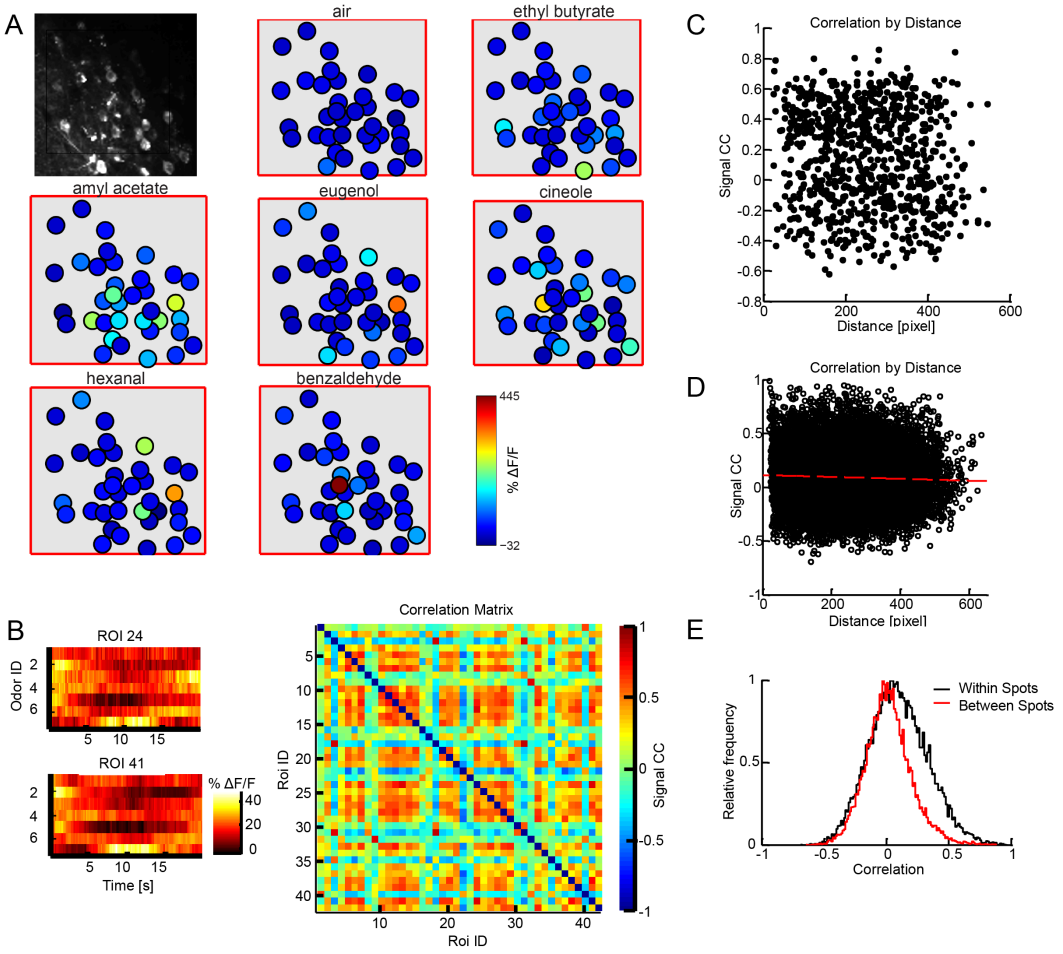

Figure 3.12. Spatial correlation is higher for neurons of the same imaging area (**A**) Average odor-evoked population activity maps of an imaging area in a wild-type mouse demonstrating no obvious spatial organization. (**B**) Odor RFs maps of two representative example ROIs display the average activity evoked by the seven stimuli (six odors plus air) over time. To the right, correlation matrix of odor RF maps between neurons to measure the similarity. The signal CC is color-coded, with red indicating high correlation between RFs. (**C**) Correlation by distance as measured in pixels within one imaging area. (**D**) Correlation by distance as measured in pixels for all spots. No apparent spatial organization on the order of individual imaging areas can be observed. (**E**) Correlations between neurons from different spots. Neurons within an imaging area are more similar to each other than randomly selected neurons from different areas. Abbreviations: CC, correlation coefficient, ROI, region of interest. Data analyzed jointly with Dr. Henry Lütcke.

which displays the average activity evoked by the six odors plus air over the time after stimulus onset (**Figure 3.12B**). Cross-correlating all odor RF maps of each ROI within an imaging area yields a correlation matrix, where the signal correlation coefficient (CC) can be of any value ranging between -1 (perfect anti-correlation) and +1 (perfect correlation). The correlation matrix indicates a

low correlation between odor RFs maps of ROIs, indicating rather independent firing of the neurons in this example of an imaging area (**Figure 3.12B, right panel**). As the numbering of ROIs does not follow a particular pattern and is uncorrelated to the distance between ROIs, we also analysed the correlation by distance. By expressing distance between neurons in pixels, we found no apparent spatial organization, both for single imaging areas (**Figure 3.12C**) and for all imaging areas combined (**Figure 3.12D**). Therefore, this preliminary data indicates that neurons with similar RFs are not clustered on the order of individual imaging areas. However, we found evidence that distribution of odor RF maps might not be entirely random. Correlations are normally distributed for cells from different imaging areas, but neurons within an imaging area are more similar to each other than randomly selected neurons from different imaging areas (**Figure 3.12E**). This finding might be correlated to the anatomical organization within the LEC, as different imaging areas covered mostly dorsal and posterior parts of the LEC, but were nevertheless spatially distributed to a certain extent. More positively correlated pairs of neurons within the same area might be indicative of subnetworks of neurons with similar odor-preference. We will further substantiate these findings with the ongoing analysis and will also disentangle possibly individual spatial organizations in the different neuronal populations.

3.3 Electrophysiological and morphological characterization of LEC neurons

We were also interested in electrophysiological and morphological properties of neurons in LII in the LEC. In particular, we wanted to investigate properties of neurons that were shown to be odor-responsive. We concentrated on principal neurons in LIIa that send axonal projections to the dentate gyrus and on GABAergic neurons in LIIa. To our knowledge, this is the first study that provides electrophysiological and morphological characterization of LEC LII neurons *in vivo* that were shown to respond to odor stimulation. For this part of the study, I performed injections, surgeries, immunostainings, calcium imaging, and two-photon imaging. All electrophysiological recordings and all reconstructions of recorded neurons were done by Dr. Sarah Melzer.

3.3.1 Regular spiking neurons that project to the hippocampus are odor-responsive

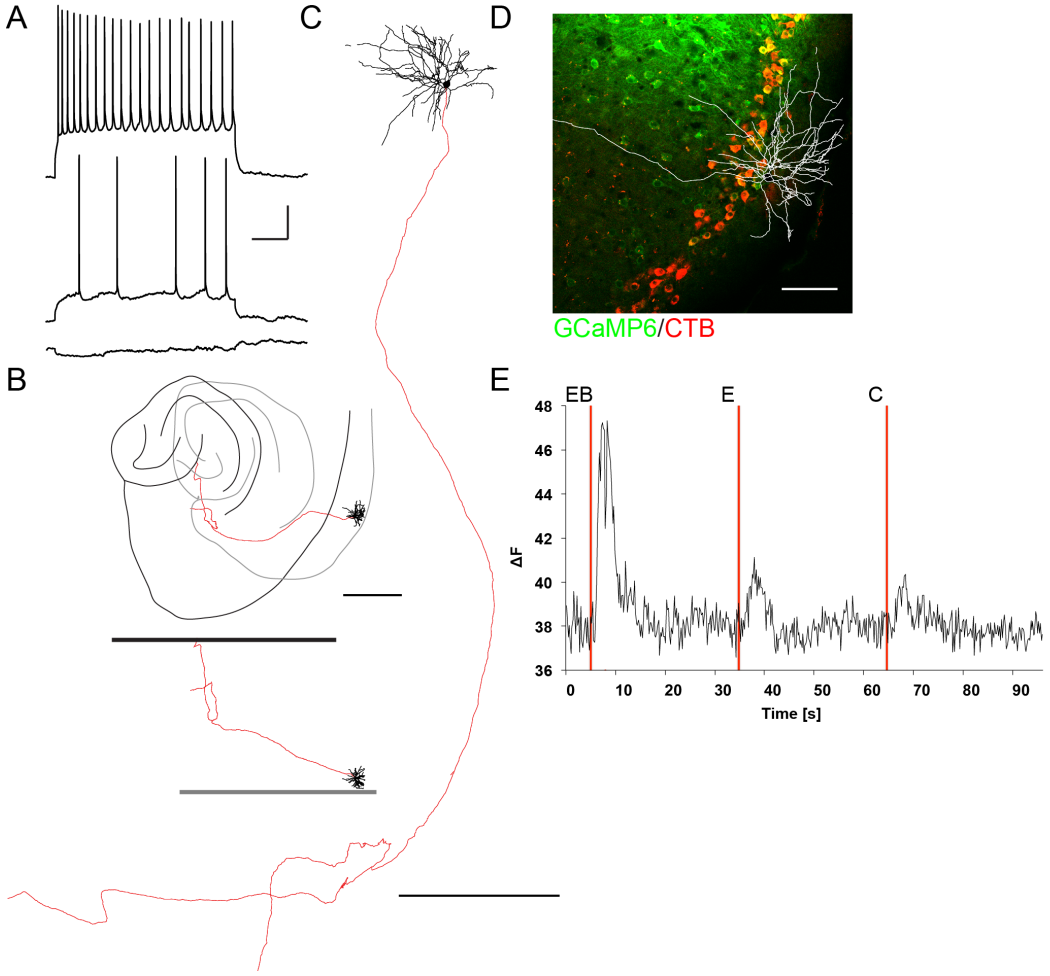

Figure 3.13. Regular spiking neurons that project to the hippocampus are odor-responsive (**A**) *In vivo* firing pattern of whole-cell patched odor-responsive CTB$^+$ cell in LIIa. (**B**) Reconstructed neuron (cell body and dendrites in black) with good recovery of the axon (red) that projects to the hippocampus. 2D image shows a ventral (grey) and a dorsal (black) outline of the hippocampus and LEC. Cell body and dendrites are localized more ventrally, whereas the axon extends to dorsal areas. The reconstructed neuron is shown along the dorsal-ventral axis (top) and along the posterior-anterior axis (bottom). Scale bar, 800 µm. (**C**) Higher magnification of the reconstructed cell. Scale bar, 400 µm. (**D**) *Ex vivo* confocal image of CTB$^+$ neurons confirms the localization of the cell in upper LIIa of the LEC. Scale bar, 100 µm. (**E**) Calcium transient of the patched neuron upon odor stimulation with three different odors. Abbreviations: EB, ethyl butyrate; E, eugenol; C, cineole. Data produced jointly with Dr. Sarah Melzer.

To label principal neurons projecting to the hippocampus in LII in the LEC, we used the same approach as for calcium imaging and I injected AAV.GCaMP6

into the LEC and CTB555 into the DG (5 wild-type mice). The patch pipette could be visualized under the microscope by adding Texas-Red to the intracellular solution and by setting the laser excitation wavelength to 900 nm. We probed the odor-responsiveness of GCaMP6$^+$/CTB$^+$ neurons in 3-4 trials consisting each of three different odor stimulations. Having determined that a neuron responded reliably to the presentation of odors, one neuron per mouse was whole-cell patched, the firing pattern recorded and the cell filled with biocytin for subsequent reconstruction. **Figure 3.13A** shows the *in vivo* firing pattern of a whole-cell patched odor-responsive CTB$^+$ cell in LIIa. This neuron was regular spiking and revealed spiny dendrites extensively arborizing in LI and LIIa and an axonal projection into *stratum lacunosum-moleculare* in the hippocampus (**Figure 3.13B**). The 2D projection of the reconstructed neuron is shown with the outline of the ventral and dorsal hippocampus and the LEC. The spatial extent of this neuron was so large that for the reconstruction of the axon, 37 slices of 50 µm thickness were taken into account. The ventral slice depicts the level of the cell body and the dorsal slice the level of the axon terminal. The view along the posterior-anterior axis as shown in the lower panel indicates that the axonal terminal reached the hippocampus at a far more dorsal level than the cell body was located. A higher magnification of the neuron is presented in **Figure 3.13C**, which is overlain in **Figure 3.13D** with a confocal image of the brain slice containing the cell body to confirm the localization of the cell in upper LIIa. The calcium transient certifies the odor-responsiveness of the patched neuron, with a major increase in fluorescence intensity upon presentation of ethyl butyrate, and smaller increases upon stimulation with two other odors (eugenol and cineole) (**Figure 3.13E**).

Four additional reconstructed CTB$^+$ odor-responsive cells are shown in **Figure 3.14** with corresponding firing pattern, higher magnification of the reconstruction and overview of the parahippocampal regions. These additional neurons were regular spiking or bursty spiking neurons. For two of these neurons, the axon could be reconstructed for just a short distance, but the other two neurons also reveal axonal projections that reach as far as the presubiculum. Axonal branches can be detected in three out of four neurons and they are mainly localized in superficial layers in the EC and in the presubiculum. The dendritic trees radiate out from the soma in all directions and is mainly confined to superficial layers LI and LII. Basal dendrites are not as pronounced as dendrites extending towards the pia. In the appendix, additional principal neurons are

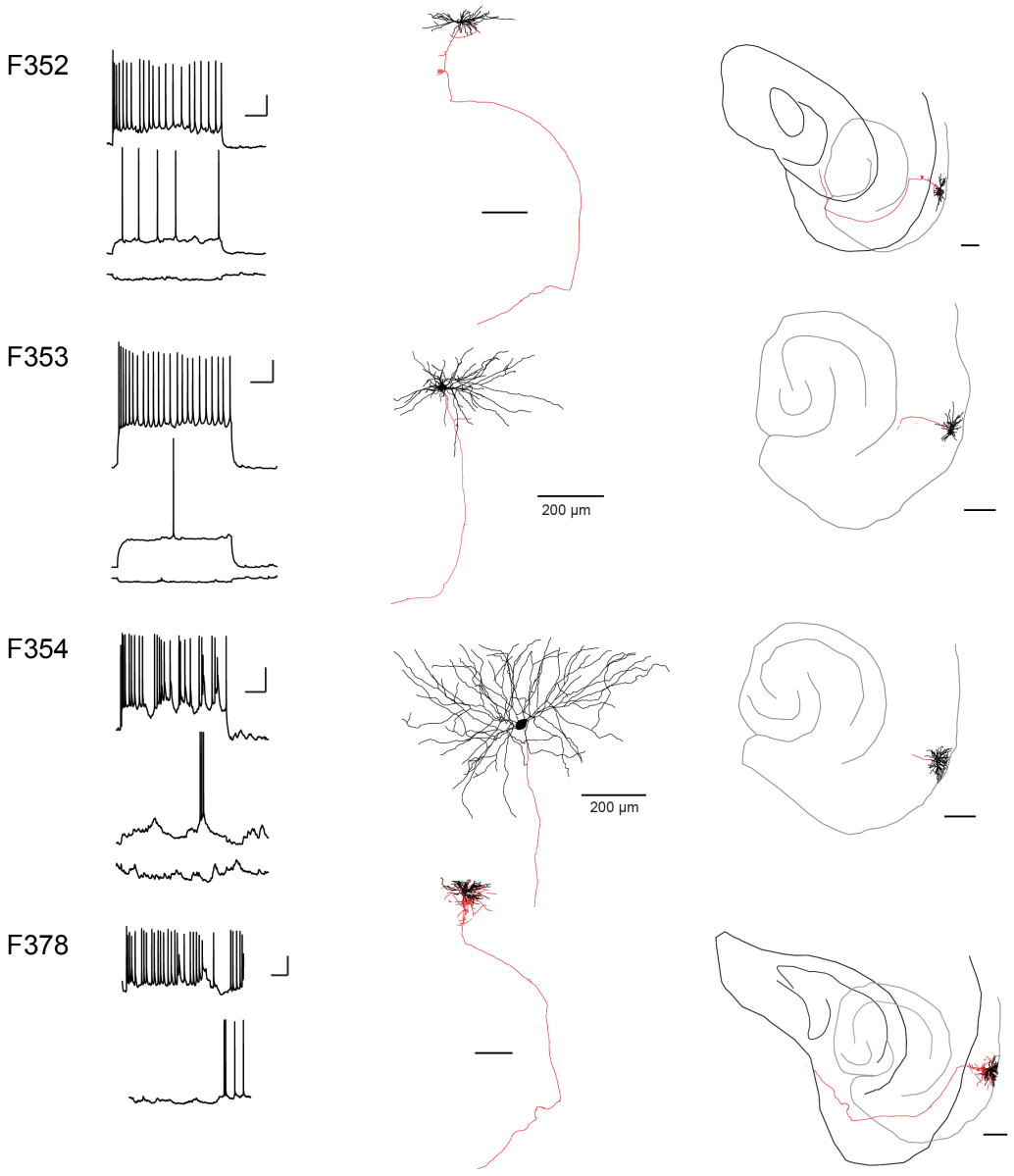

Figure 3.14. Odor responsive CTB⁺ cells in LIIa of the LEC are regular spiking or burst-spiking projecting neurons. Four additional reconstructed odor-responsive cells are shown with corresponding firing pattern (left panels), higher magnification of the reconstruction and overview of the hippocampus and LEC with outlines at the level of the cell body (grey) and at the axon terminals (black). Axons are shown in red, dendrites in black. Scale bars, 20 mV, 200 ms (firing pattern), 400 µm (reconstructions, if not indicated otherwise). Data produced jointly with Dr. Sarah Melzer.

depicted that were not tested for odor responsiveness (**Appendix Figure 3**).

3.3.2 Different types of *GAD67*$^{+}$ neurons are odor-responsive in layer IIa of the LEC

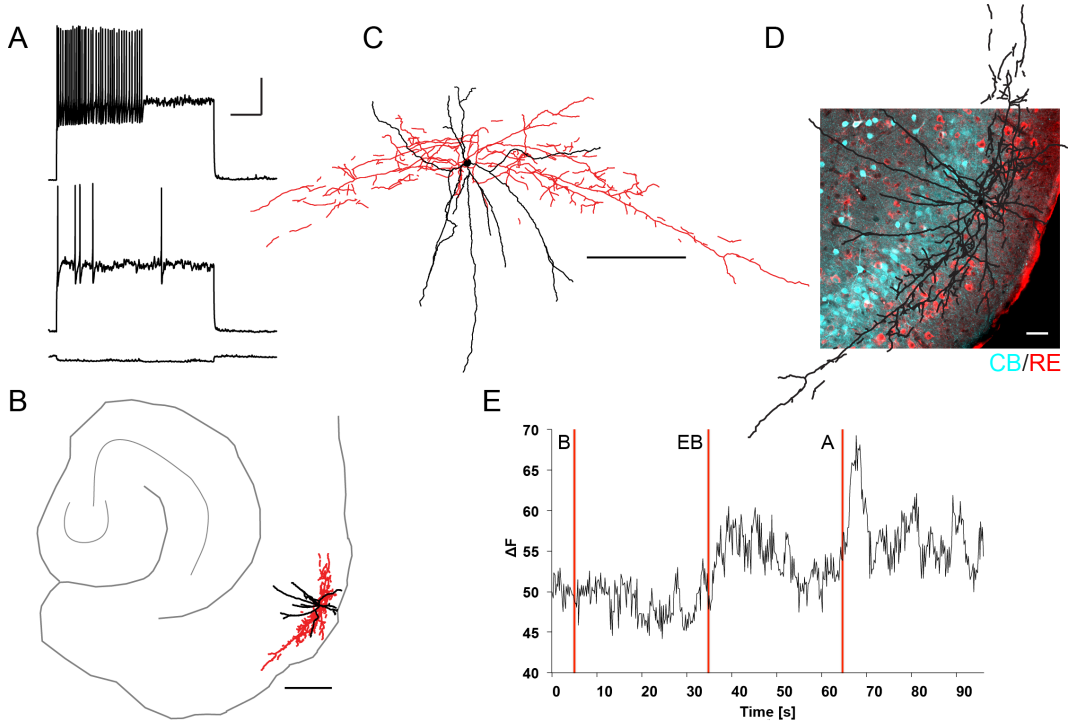

Figure 3.15. Fast-spiking basket-like GABAergic neuron in the LEC responds to various odors (**A**) *In vivo* firing pattern of whole-cell patched odor-responsive cell in LIIa. Scale bars, 20 mV, 200 ms. (**B**) Biocytin-filling and reconstruction of odor-responsive neuron reveals dendrites in superficial and deeper layers (black) and basket-like axonal arborization (red) in LII. 2D projection from top view is shown with outlines of the hippocampus and LEC at the level of the cell body. Scale bar, 400 µm. (**C**) Higher magnification of the reconstructed cell. Scale bar, 200 µm.(**D**) Immunostaining with CB and Reelin confirms the localization of the cell in LIIa of the LEC. Scale bar, 50 µm. (**E**) Calcium transient of the patched neuron upon odor stimulation with three different odors. Abbreviations: B, benzaldehyde; EB, ethyl butyrate; A, amyl acetate. Data produced jointly with Dr. Sarah Melzer.

Next to excitatory output neurons, we also wanted to characterize local GABAergic neurons. Therefore, I injected AAV.flex.GCaMP6 into the LEC of *GAD67*^{Cre} mice. Specific labeling in Cre-expressing, GABAergic neurons enabled us to target selectively the inhibitory neuronal population in LIIa. In **Figure 3.15A**, I present an example of a fast-spiking cell (FS-cell) with the corresponding *in vivo* recorded firing pattern. Biocytin-filling and reconstruction of this odor-responsive neuron reveals dendrites spread across superficial and deeper layers and basket-like axonal arborization in LII as shown with the outlines of the hippocampus and the LEC in **Figure 3.15B** or as higher magnification in

Figure 3.15C. Brain slices were immunostained with Reelin and CB to confirm the localization of the patched neuron in LIIa, close to the border to LIIb. The overlay indicates that axonal arborization is more prominent in LIIa than LIIb (**Figure 3.15D**). The odor stimulation with three different odors led to prominent increase in fluorescence intensity after presentation of two of these odors (**Figure 3.15E**).

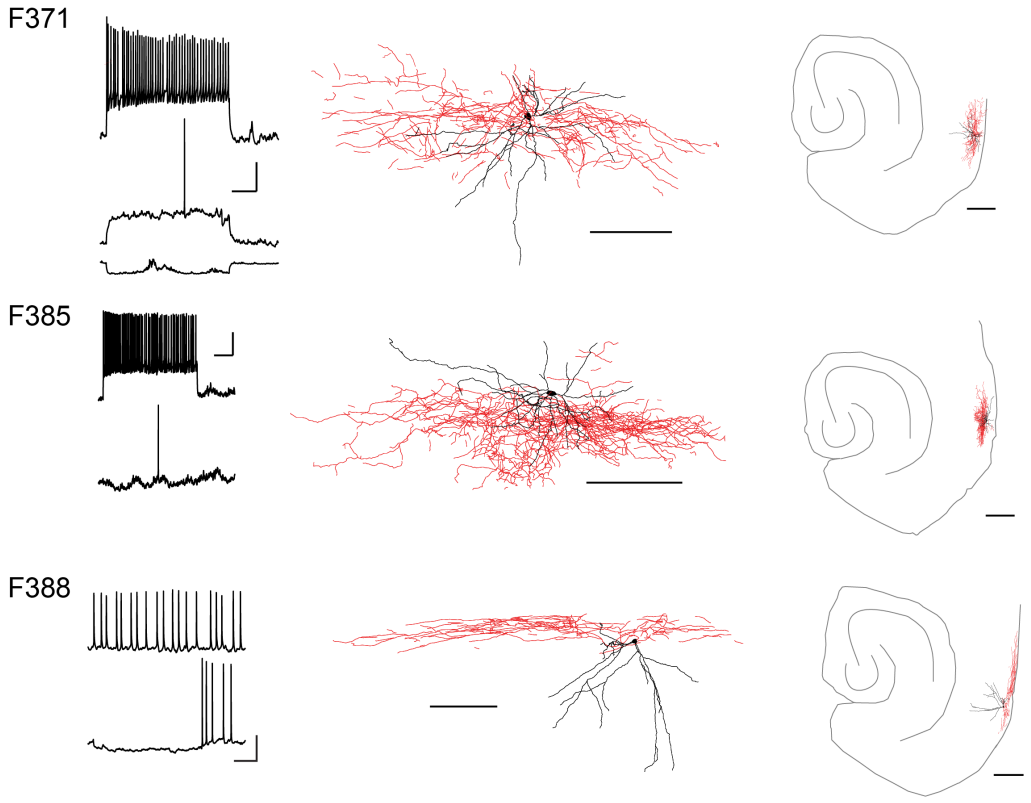

Figure 3.16. Different types of *GAD67*$^{+}$ cells are odor-responsive in LIIa of the LEC. Three additional reconstructed odor-responsive cells are shown with corresponding firing pattern (left panels), higher magnification of the reconstruction and overview of the hippocampus and LEC. Axons are shown in red, dendrites in black. Scale bars, 20 mV, 200 ms (firing pattern), 200 µm (higher magnification reconstruction), 400 µm (overview). Data produced jointly with Dr. Sarah Melzer.

In addition to this fast-spiking neuron, several other types of GABAergic neurons were found to be odor-responsive (**Figure 3.16**). They showed different firing patterns, resembling both fast-spiking as well as irregular spiking and classical accommodating neurons. Common to all was extensive axonal arborizations in the superficial layers of the LEC, although with varying spatial extent. Dendrites extended into deeper layers or spread equally in all directions. In the appendix, additional GABAergic neurons are depicted that were not tested for odor responsiveness (**Appendix Figure 4**). In conclusion, GABAergic neurons in LII LEC

exhibited various firing patterns and diverse morphologies. In consideration of my findings of a heterogeneous expression of protein markers (compare section **3.1.5**), these results further support the notion of different GABAergic subtypes in superficial LEC. Intriguingly, we could show that odor-evoked responses were elicited in GABAergic neurons with different electrophysiological and morphological characteristics.

4 DISCUSSION

In this study, I investigated the neuronal composition in the LEC and the differential involvement of specific neuronal subpopulations in odor processing. The main results can be summarized as follows: First, excitatory neurons in LII, which can be differentiated according to the expression of different molecular markers, target distinct brain regions. Reelin$^+$ neurons project to the DG, whereas CB$^+$ neurons provide feedback to the OB, the PIR and the contralateral LEC. Second, GABAergic neurons in superficial layers of the LEC are heterogeneous based on the expression of molecular markers. The largest proportion of GABAergic neurons can be distinguished by the expression of 5HT3aR. Third, odor-responsive principal neurons in LIIa are regular or burst-spiking and project to the hippocampus. Odor-responsive GABAergic neurons are fast-spiking, non-fast spiking or classical accommodating with a dense axonal arborization in superficial layers. Fourth, the response to odors is markedly different in Reelin$^+$, CB$^+$ and GABAergic neurons. Excitatory Reelin$^+$ neurons exhibit a higher selectivity to different odors compared to the selectivity of excitatory CB$^+$ neurons. On the contrary, inhibitory GABAergic neurons reveal a broad and unselective response pattern. In this chapter, I will comment on these findings and discuss their impact on the prospective functional role of the LEC.

4.1 Reelin and CB expression delineates two sublayers in layer II

Based on molecular markers, I distinguished two excitatory cell types in LII, namely Reelin$^+$ neurons and CB$^+$ neurons. The distribution of excitatory neurons expressing these marker proteins is spatially organized, with Reelin$^+$ neurons forming a continuous band of densely packed neurons in LIIa and CB$^+$ neurons being spatially segregated in LIIb. CB$^+$ neurons tend to cluster to-

gether forming islands, which results in a modular appearance in LIIb. Such islands have been described previously in LII (Fujimaru and Kosaka, 1996; Amaral et al., 1987) and also the parcellation of LEC LII into two segregated sublayers has been suggested (Fujimaru and Kosaka, 1996). Recently the expression of CB and Reelin in the MEC was correlated with LII pyramidal cell morphology and stellate cell morphology, respectively (Kitamura et al., 2014; Ray et al., 2014). These studies described the MEC LII arrangement as band of Reelin$^+$ neurons, in which islands of CB$^+$ neurons are nested. As stellate cells in the MEC are the equivalent to fan cells in the LEC, this indicates that similar neuronal composition in LEC and MEC results in different spatial arrangements in both areas: Reelin$^+$ neurons are located superficial to CB$^+$ neurons in the LEC. The functional implication of this modular organization in the MEC is still unclear. A technical highly demanding study succeeded to perform *in vivo* functional imaging in MEC neurons in mice navigating a virtual linear track (Heys et al., 2014). With this approach, the authors were able to show that grid cells are physically clustered compared to non-grid cells. This study indicates that specifically CB$^+$ neurons that are arranged in islands exhibit the grid-like spatial firing pattern. However, both CB$^+$ neurons as well as Reelin$^+$ neurons have been hypothesized to be the neuronal correlate of grid cells (Domnisoru et al., 2013). Furthermore, the existence of CB$^+$ islands in LII of the LEC, where cells show only weak spatial modulation (Hargreaves et al., 2005; Deshmukh and Knierim, 2011; Neunuebel et al., 2013), challenges a direct link between the anatomical organization of LII in the MEC and the occurrence of the grid cell firing pattern (Ray et al., 2014). The complexity of odors composed of hundreds of single-molecule odors is so high-dimensional that it is hard to imagine how such diverse input could map onto a discrete 3-dimensional spatial organization.

In summary, I found two different types of excitatory neurons marked by the expression of Reelin or CB that reveal a distinct spatial organization in LII in the LEC that resembles partly the cellular arrangement described in the MEC. To further analyze LEC LII neurons, I investigated their connectivity with the hippocampus and olfactory structures throughout the brain.

4.1.1 Reelin$^+$ neurons are part of a feed-forward neural network

Following injection of the retrograde tracer FG into the DG of *GAD67*^{EGFP} mice, I found almost all retrogradely labeled neurons in LEC LII to be Reelin$^+$/GAD67$^-$. Diffuse and much weaker FG signal was present in LIIb, rarely co-localized with CB$^+$ neurons. The intensity of this FG-labeling was not comparable in strength to the labeling that was present in LIIa and could only be visualized with increased laser power. In LIII, the intensity of FG-labeling was stronger, although still not comparable to the intensity level in LIIa. Following injections of another retrograde tracer, namely CTB, into the DG for calcium imaging experiments, retrogradely labeled cells were restricted to LIIa in the LEC and no diffuse signal in LIIb or intense labeling in LIII could be detected. In light of the observation that injection spots with CTB are spatially better restricted compared to those with FG, I suggest that CB$^+$ do not project to the hippocampus and that FG-labeling in LIII reflects the known projections of LEC LIII neurons to CA1 (Witter et al., 1986; Canto et al., 2008). Currently, it is assumed that FG is taken up unselectively both by excitatory and inhibitory neurons, and we could confirm previous reports of inhibitory neurons in LEC LII projecting to the DG. This finding lends further support to the idea that the perforant path is not purely excitatory but also consists of an inhibitory component (Germroth et al., 1989; Schwerdtfeger et al., 1990; Melzer et al., 2012).

Overall, I can conclude that excitatory Reelin$^+$ neurons but not CB$^+$ neurons in the LEC form the perforant path to the DG, with a minor contribution of GABAergic long-range projecting neurons. Therefore, Reelin$^+$ neurons provide the neural basis for signal transmission between the cortex and the DG. In the LEC, as relay station between cortex and hippocampus, they act as part of a feed-forward neural network, transmitting sensory content like odor identity from the sensory periphery to the core of the memory system, the hippocampus.

4.1.2 CB$^+$ neurons provide feedback and project contralaterally

For excitatory CB$^+$ neurons in LIIb in the LEC, I have identified several target regions. Retrogradely labeled CB$^+$ neurons were found following injection of

retrograde tracers into OB, PIR and contralateral LEC.

The number of retrogradely labeled neurons in superficial layers was the densest following injections into the OB, with most of them located in LIIb, and fewer in LIIa and LIII. In the most ventral part of the LEC, single CTB^+ neurons were also distributed across LIV and LV. This is consistent with previous reports, where LEC neurons projecting to the OB were found to be situated in LII as well as in LIV in rat (de Olmos et al., 1978) or LII/LIII and LIV/LV in mice (Shipley and Adamek, 1984; Witter and Groenewegen, 1986). Although different techniques for retrograde labeling were used, the results are in agreement with my findings. However, I extended the findings in respect to an important additional aspect, namely the expression of molecular markers in projecting neurons. In LIIb, 63% of all CTB^+ neurons were CB^+, indicating that CB^+ neurons in LIIb form a significant part of the feedback network between LEC and OB. However, most probably an additional neuronal population exists that also projects from LEC to OB. This population is also excitatory, as I did not observe $CTB^+/EGFP^+$ neurons in LIIb. This finding further supports my observation that LEC LIIb consists of at least two types of excitatory neurons, namely CB^+ and CB^- neurons (compare **section 3.1**). Although significantly less than LIIb, LIIa contained as well a small fraction of retrogradely labeled neurons. About 25% of these neurons in LIIa were $Reelin^+$. This raises the possibility that single $Reelin^+$ neurons might project both to the DG as well as to the OB.

With respect to an anterior-posterior gradient, I observed a strong tendency of CTB^+ neurons being located in anterior regions of the LEC following retrograde tracer injections into the OB. Lower numbers of labeled cells in the most caudal sections were also observed by de Olmos et al. (1978) and Shipley and Adamek (1984). This connectivity pattern could indicate the anterior LEC to provide strong feedback to the OB, but whether this pattern correlates with a functional separation between anterior and posterior LEC is not known. However, it is reminiscent of the PIR, where a similar differential innervation of the OB is observed. In the PIR, there is indeed a double-dissociation between anterior and posterior PIR, with the former encoding odor structure and the latter odor quality (Gottfried et al., 2006).

Following injections of the retrograde tracer CTB into the PIR, most labeled cells were located in LIII and LV, and fewer in LIIb. The number of labeled neurons in LII and LIII was higher in dorsal parts compared to the number in ventral parts

of the LEC. These findings are consistent with previous reports in cat and rat (Witter and Groenewegen, 1986; Insausti et al., 1997) and the correctness of the injection spot could be confirmed by the presence of ipsilateral CTB^+ mitral cells and contralateral CTB^+ neurons in the anterior PIR (Haberly and Price, 1978). Of note, I found that a large proportion of the retrogradely labeled neurons in LIIb were CB^+ neurons.

In consideration of the finding that a substantial fraction of CB^+ neurons in LIIb projects to the OB, we were intrigued by the idea that single CB^+ neurons might project to both the OB and the PIR. Indeed, I could show that single neurons in LIIb in LEC can target both regions simultaneously, and that about half of them are CB^+. This is in contrast to a study by Chapuis and colleagues, where no double-labeled cells in LEC were observed following injections of retrograde tracer virus into OB and PIR (Chapuis et al., 2013). This discrepancy might be explained by the different animal model, as they used rat instead of mice in their study. Also the use of rabies virus as retrograde tracer in contrast to our approach using CTB could contribute to the different findings. It can be speculated that the virus approach by Chapuis and colleagues did not lead to efficient labeling in the target regions, which is supported by the fact that in this study eight and four injections sites were chosen for the OB and the PIR, respectively, and the injection volume was extremely high compared to the volume I used (Chapuis et al., 2013). In my experiment, I noticed that labeling of cells projecting to the PIR was more prevalent in dorsal parts of the LEC, whereas labeling of cells targeting the OB was rather detectable in ventral parts. Nevertheless, there was an intermediate stripe that contained neurons projecting to both regions and images in the paper by Chapuis and colleagues reveal an organization similar to what I observed in the mouse. Therefore, I conclude that the relative small number of retrogradely labeled cells using the viral tracing approach could be the reason for not finding double-labeled cells in their study.

Noteworthy, I also detected neurons in the hippocampus that project to OB and PIR simultaneously. Cell bodies of these double-labeled neurons were located in CA1 *stratum oriens*, which is particularly interesting as *stratum oriens* is supposed to contain only GABAergic neurons (Freund and Buzsaki, 1996). Already de Olmos et al. (1978) suggested that a projection from the temporal part of CA1 to OB exists, but they were unsure of this projection due to the large size of their injection spots. Additional evidence for cells in the hippocampus projecting to the OB was provided by van Groen and Wyss (1990), who confirmed their

findings with both anterograde and retrograde injections. Neurons projecting to the OB were located more often in non-pyramidal layers *stratum oriens* and *stratum radiatum* than in the pyramidal cell layer (van Groen and Wyss, 1990). I have extended these findings by showing that single neurons in CA1 can project simultaneously to OB and PIR, but it remains to be elucidated whether these neurons are excitatory or inhibitory. Preliminary data by Dr. Elke Fuchs rather argues against GABAergic long-range projections.

In line with previous reports, retrograde tracer injection into LEC revealed labeled neurons in several brain regions including ipsilateral PIR, endopiriform nucleus, insula, mitral cell layer in OB, MEC, and subiculum as well as contralateral PIR, MEC and LEC (Insausti et al., 1997; Kerr et al., 2007). In the contralateral LEC, the majority of labeled cells was located in LIIb and LIII and preliminary analysis revealed that CB^+ neurons in LIIb contribute to this LEC-LEC projections. In rats, CB^+ neurons in MEC LII were already suggested to project to the contralateral MEC (Varga et al., 2010) and I plan to investigate the contribution of CB^+ to this projection in the mouse in more detail.

In summary, these findings attribute a unique role to CB^+ neurons in LEC LIIb. Via far-reaching axonal projections, they are in the position to excite neurons in at least three different regions in the brain, namely in OB, PIR and contralateral LEC. Accordingly, they might have an important function in the transmission of olfactory content, with a particular emphasis on feedback transmission to olfactory structures and the communication across hemispheres. I have provided evidence that single CB^+ neurons target at least two of these regions - OB and PIR - simultaneously, and it remains to be investigated if such connectivity also exists for contralateral LEC and PIR or OB, respectively.

In this part of the study, I made use of two well-established techniques, namely retrograde labeling with FG and CTB and the evaluation of neuronal marker protein expression determined by immunohistochemical experiments. In this respect, I would like to name two main technical considerations. With reference to the injections of retrograde tracers, the spatial boundaries of the injection site is the most important aspect to consider. All injection sites were thoroughly checked to include only data where injections were restricted to the target region and the amount of tracer injected was kept to a minimum. With respect to immunostainings, note that the antibody against CB has limited penetration capacity, which can lead to lower labeling efficacy with increasing distance from

the slice surface. As a result of diffuse dendritic and axonal labeling of the CB^+ neuronal network in LIIb, identification of labeled cell bodies was sometimes hindered. Nevertheless, I consider the given numbers of CB^+ neurons as good estimations. To confirm the given percentages of CB^+ neurons projecting to different target areas, the experiments could be repeated in $CB^{Cre\text{-}Rosa26}$ reporter mice.

4.2 Layer II GABAergic neurons comprise a heterogeneous group of inhibitory neurons

Shortly after the discovery of the particular relevance of the LEC in AD, numerous studies tried to characterize the neuronal cell population in the EC with a particular emphasize on GABAergic neurons regarding the expression of known molecular markers. Different techniques such as the so-called mirror technique (Miettinen et al., 1996, 1997) or colchicine treatment for arrest of anterograde transport in combination with immunohistochemistry (Köhler and Chan-Palay, 1983; Köhler et al., 1986; Wouterlood et al., 2000) were applied. These studies often came to contradictory results with respect to the GABAergic nature of neurons. One of the major drawbacks of these studies was the low labeling efficacy of antibodies against GAD67, which results easily in underestimating the size of the GABAergic population. Thus, the availability of the GAD^{EGFP} mouse (Tamamaki et al., 2003) provides a big advantage in our study as GABAergic neurons are easily detectable due to bright EGFP fluorescence and therefore the risk of underestimating the GABAergic population is greatly reduced. This might explain that in contradiction to some reports (Wouterlood and Pothuizen, 2000; Wouterlood et al., 2000), but in line with other reports (Miettinen et al., 1997), I found that the majority of both SOM^+ and CR^+ neurons were GABAergic ($EGFP^+$).

Investigating the distribution of the marker proteins PV, SOM, and CR, which define subpopulations of cortical neurons, revealed that none of these markers is expressed in a large proportion of GABAergic neurons in superficial layers in LEC. For all observations, note that these immunohistochemical experiments were performed in adult mice, however, changes in the expression level throughout lifetime can occur. For example, it is known that the expression level of SOM

decreases in EC during development (Forloni et al., 1990), whereas numbers of PV^+, CB^+ and CR^+ neurons in human EC increase postnatal (Grateron et al., 2003). PV, however, has been shown to exhibit activity-dependent expression levels (Donato et al., 2013). Therefore, immunohistochemical analysis provides a snapshot of neuronal populations expressing selected marker proteins above detection threshold. In LI, the percentage of PV^+, SOM^+ and CR^+ neurons, respectively, was below 4% for each subpopulation and in LIIa, each of these three markers was detected in less than 20% of all GABAergic neurons. In LIIb, a slightly larger proportion of GABAergic neurons expressed these markers with about 30% expressing PV, 27% expressing CR and 14% expressing SOM. I confirmed previous reports of dense PV^+ baskets surrounding excitatory cell bodies (Jones and Buhl, 1993; Wouterlood et al., 1995). In LII in the LEC, these baskets can be observed both in LIIa and LIIb, enfolding and presumably targeting both $Reelin^+$ as well as CB^+ neurons.

In consideration of the known distribution of PV^+ neurons in the MEC, this finding is of particular interest. Excitatory neurons in the MEC are under strong inhibitory control, which is mainly provided by PV^+ neurons that constitute 50% of the GABAergic population in LII (Jones and Buhl, 1993; Wouterlood et al., 1995; Buetfering et al., 2014). My findings imply that in the LEC, this inhibitory influence on excitatory neurons mediated by PV^+ neurons is reduced. Notably, in the LEC PV^+ neurons were more abundant in LIII than in LII (data not shown), which leaves the possibility of different connectivities across layers.

In other brain regions than the EC, Reelin and CB are often found to be expressed in GABAergic neurons (Rogers, 1992; Ramos-Moreno et al., 2006; Pohlkamp et al., 2013). However, in the EC these marker proteins have mainly been used to distinguish between two distinct populations of excitatory neurons. Nevertheless, Reelin and CB expression is also detected in a certain proportion of the GABAergic population in the EC. Interestingly, LIIa does not only show a high percentage of excitatory neurons expressing Reelin, but also an abundance of GABAergic neurons tested positive for Reelin expression. A similar pattern is observed in LIIb, where not only excitatory neurons express CB, but also about 40% of the GABAergic population. To date, we cannot say if this distinct distribution of GABAergic cell types is of functional significance.

Due to the availability of the *5-HT3*^{EGFP} mouse line (Inta et al., 2008), the expression of 5HT3aR in the LEC could be investigated. This was previously hindered

as no antibody against 5HT3aR exists to date. 5HT3aR is present exclusively in GABAergic neurons (Morales and Bloom, 1997; Ferezou et al., 2002), hence, no staining against GAD67 was performed for the reasons mentioned above. To calculate the percentage of 5HT3aR$^+$ neurons of the total GABAergic population, the numbers of GABAergic neurons per layer as counted in *GAD67*^{EGFP} mice were taken as a reference. With this approach, I could circumvent the problem of insufficient labeling using the antibody against GAD67. In light of the high number of slices that were counted in *GAD67*^{EGFP} mice and that were taken into account for calculating the average number of GABAergic neurons per layer, I believe that this approach is valid and that the derived numbers are reliable. This assumption is further supported by the fact that the summation of all 5HT3aR$^+$, PV$^+$ and SOM$^+$ neurons per layer never exceeded 100% of the total GABAergic population, in line with the finding that 5HT3AR-expressing cells are distinct from neurons expressing either PV or SOM (Ferezou et al., 2002).

Therefore, GABAergic neurons in LI and LII of the LEC belong to a variety of molecularly defined subtypes, and the GABAergic neuron population of the LEC seems to display rather unique features compared to the MEC with respect to prevalence and distribution of molecularly defined inhibitory subtypes.

4.3 Two-photon calcium imaging of odor-evoked responses in Reelin$^+$, CB$^+$ and GAD$^+$ neurons

Using two-photon calcium imaging, I have provided evidence that excitatory neurons expressing Reelin or CB as well as GABAergic inhibitory neurons respond to odor stimuli. Most importantly, I was able to distinguish neuronal response patterns of the three different cell types and could therefore investigate the functional involvement in odor processing separately.

4.3.1 Functional dissociation between Reelin$^+$ and CB$^+$ neurons in layer II

Reelin$^+$ neurons exhibited the highest selectivity to single odors and revealed stable and reliable odor-evoked responses over multiple trials. More than 90%

of Reelin$^+$ neurons responded to at least one of the six presented odors, which highlights their importance in olfactory processing and the transmission of odor information to the hippocampus. Noteworthy, the temporal ordering of olfactory information is impaired in animals with ventral CA1 lesions (Hunsaker et al., 2008) and olfactory working memory seems to depend on the ventral but not the dorsal hippocampus (Kesner et al., 2011). Both findings are in line with stronger projection patterns of the LEC to ventral compared to dorsal hippocampus (Kerr et al., 2007) and therefore point towards the LEC as a central relay station for olfactory information processing. Furthermore, the functionality of the connection between LEC and specifically ventral DG, as the direct target of Reelin$^+$ neurons, was shown to be crucially involved in successful odor pattern separation (Weeden et al., 2014). The dorsal DG was not required in this task, which further supports the view of stronger connectivity between the odor-transmitting LEC and the ventral hippocampus. The high percentage of Reelin$^+$ neurons responding to odors and their pronounced selectivity to respond to distinct odors most likely reflect a contribution to pattern separation in the DG. If this high responsiveness of Reelin$^+$ neurons is mediated solely by the combinatorial nature of the inputs from OB and PIR, or if this is also a result of intracortical association fibers connecting excitatory neurons among each other, remains to be elucidated. The connectivity among principal neurons seems to be absent (Couey et al., 2013) or low (observation from our own department) in MEC LII, but no study to date has elucidated LII connectivity in the LEC. Preliminary results indicate a low level of direct excitatory connections between adjacent principal cells, presumably of the fan type (Abstract FENS 2014 by Nilssen et al., 2014).

Sensory perception is not only driven by feed-forward projections, but can also substantially be modulated by feedback projections of higher order brain areas, so-called top down control. For the population of CB$^+$ neurons, I have shown that they project to PIR, OB and contralateral LEC and to interpret the functional data of CB$^+$ neurons, I would like to elaborate on the projections between other olfactory structures and the OB. Axonal projections of principal neurons originating in the PIR or the anterior olfactory nucleus are particularly dense in the granule cell layer and prominent in the glomerular layer in the OB (Matsutani, 2010; Boyd et al., 2012; Markopoulos et al., 2012). As granule cells in the OB are GABAergic neurons, this projection pattern indicates that bulbar interneurons are the primary target of cortical feedback projections. Indeed, it was shown that cortical feedback projections originating in the PIR (Boyd et al., 2012) or the

anterior olfactory nucleus (Markopoulos et al., 2012) excite inhibitory neurons in the OB. This excitation of granule cells results in an amplification of odor-evoked inhibition of mitral cells. Using calcium imaging to monitor the activity in presynaptic boutons of cortical feedback fibers revealed a diffuse projection pattern: PIR neurons tuned to different odors targeted individual glomeruli without discrimination (Boyd et al., 2015). Activation of granule cells in the OB by cortical projections appears to be a general connectivity scheme in the olfactory system (Davis and Macrides, 1981; Markopoulos et al., 2012). Therefore, it appears likely that CB$^+$ neurons in LIIb of the LEC, that I have shown to target the OB, make synapses onto inhibitory granule cells without distinct topographical organization. Thereby, the feedback provided by CB$^+$ neurons could contribute to the decorrelation of mitral cell activity, which in turn would lead to an improved discriminability of the input the LEC receives from the OB. PIR neurons targeting the OB have been suggested to exert such function (Boyd et al., 2015).

Next, I showed that CB$^+$ neurons target the PIR. Functional modulation of odor-evoked activity in the PIR mediated by feedback projections originating in the LEC was shown consistently in the past (Bernabeu et al., 2006; Mouly and Di Scala, 2006; Chapuis et al., 2013). In particular, a main inhibitory effect of the LEC on the PIR, and also other connected brain areas like the amygdala, was noted. This is indicative of LEC neurons exerting control over inhibitory neurons in the target areas. In addition, the LEC was suggested to establish an anticipatory top-down modulation on the PIR, as significant input from the LEC to the olfactory system was present prior to the onset of the odor stimulation (Kay and Freeman, 1998). Although it is unlikely to find neuronal correlates of alert expectancy in anesthetized animals, CB$^+$ neurons are a good candidate to contribute to the modulation of odor-evoked activity in the PIR. The interpretations in the lesion studies presented in the introduction of this thesis (Staubli et al., 1984, 1986; Otto et al., 1991; Otto and Eichenbaum, 1992; Ferry et al., 1996; Wirth et al., 1998; Ferry et al., 2006) have focused on the connectivity between LEC and hippocampus, but the discussed projections between LEC and PIR might help to solve the often contradictory findings reported in the above cited publications.

In comparison to the low percentage of neurons showing odor-evoked responses in the PIR, I recorded a high percentage of neurons that was activated by the presentation of odorant stimuli in the LEC. 92.5% of all Reelin$^+$ and 89.5% of all CB$^+$ neurons exhibited reliable odor-evoked transients, but only 35% of all

neurons in the PIR were activated by odor stimulation as described by Stettler and Axel (2009). Additionally, it has been suggested that LEC single units are more narrowly tuned to single odors than neurons in the PIR, but as recording sites were distributed across all layers in the LEC and recordings did not differentiate between distinct neuronal subtypes, these findings are not easily reconciled with the specificity of Reelin$^+$ or CB$^+$ neurons (Xu and Wilson, 2012). Therefore, a comparative study using similar odors and odor concentrations to evoke responses in PIR and LEC would be necessary to quantify differences in odor-evoked neuronal responses.

4.3.2 GABAergic neurons in layer II provide global inhibition

Local inhibitory circuits are assumed to shape sensory information processing in the brain, e.g. lateral inhibition is proposed to enhance odor discrimination by decorrelating mitral cell activity patterns in the OB (Arevian et al., 2008; Wiechert et al., 2010). Furthermore, inhibition has been shown to accelerate the ability to discriminate odors (Abraham et al., 2010). I showed that GABAergic neurons in the LEC are more broadly tuned to odors than excitatory neurons. Broad tuning to the prevalent stimuli has been observed in multiple cortical areas. PV$^+$ neurons in the OB display broad tuning to odors (Kato et al., 2013; Miyamichi et al., 2013) and selectively inactivating PV$^+$ neurons linearly enhanced mitral cell odor-evoked responses while maintaining mitral cell odor preferences (Kato et al., 2013). In the visual cortex, PV$^+$ neurons have been reported to transform response properties of pyramidal neurons in a linear fashion without altering tuning width (Atallah et al., 2012; Wilson et al., 2012) (but compare Runyan et al., 2010; Lee et al., 2012), and in the MEC, PV$^+$ neurons were shown to exhibit low spatial selectivity (Buetfering et al., 2014). This is consistent with our results showing low odor tuning of GABAergic neurons in the LEC. However, my immunohistochemical experiments revealed that superficial LEC layers comprise a heterogeneous group of inhibitory neurons based on the expression of molecular markers, therefore it is also of interest to compare my results to findings regarding not only PV$^+$ neurons but also other types of GABAergic neurons. Results obtained in the visual cortex indicate that not only PV$^+$ neurons, but also SOM$^+$ and VIP$^+$ neurons might be broadly tuned for orientation (Kerlin et al., 2010). As I observed single neurons with reliable inhibitory responses, i.e. a decrease in the calcium transient following odor stimulation

(data not shown), it is noteworthy that SOM$^+$ neurons in the barrel cortex were shown to decrease their firing with active or passive whisker sensing (Gentet et al., 2012). My results show that the largest cell fraction of GABAergic neurons in LEC LII is 5HT3aR$^+$ (**section 3.1.5**). Firing properties of this cell type and their responses to stimuli are just starting to be analyzed, but results derived in barrel cortex indicate that they share many characteristic features with PV$^+$ neurons (Gentet et al., 2010, 2012; Petersen and Crochet, 2013). Our results support this notion and based on our data, I suggest that 5HT3aR$^+$ neurons might exhibit similar broad tuning width as PV$^+$ neurons.

In summary, GABAergic neurons in LII LEC exhibit a broader response tuning than their excitatory counterparts and thereby reveal firing characteristics that are in line with previous findings in the OB and various other sensory brain areas. In the future, it will be crucial to investigate the connectivity of GABAergic neurons in the LEC both among themselves as well as with excitatory neurons to further elucidate the specific functions that GABAergic subtypes exert in the LEC microcircuit.

4.3.3 Technical limitations

Due to the invasive nature of the surgical procedure to gain access to the LEC, it was not feasible to implant chronic windows and to observe neuronal plasticity or to combine calcium imaging with the performance of the animal in a behavioral olfactory task. With the techniques available, it was necessary to tilt the mouse to the side and to keep it anesthetized during data acquisition. Several studies have directly compared odor-evoked responses in the OB in the awake state and under anesthesia. Mitral cells were shown to represent odors sparser and with higher temporal dynamics during wakefulness, resulting in improved discriminability of odor representations (Rinberg et al., 2006; Kato et al., 2012; Wachowiak et al., 2013). This observation might underly strongly increased activity in inhibitory granule cells, which are broadly tuned during wakefulness, but rather inactive during anesthesia (Cazakoff et al., 2014; Kato et al., 2012; Wachowiak et al., 2013). Interestingly, an opposing change between the awake and the anesthetized state was found in cortical feedback from principal neurons in PIR. In presynaptic boutons of these cortical feedback fibers targeting the OB wakefulness resulted in stronger odor-evoked excitation and broader response tuning (Boyd et al., 2015). Despite the possibility that wakefulness might induce

changes in the activity pattern of LEC neurons, it is unlikely that this will erase cell type-specific differences in odor-evoked response patterns. Therefore, the main finding of this study, i.e. distinct response properties of molecularly defined neurons in LEC, is very likely to hold in awake animals.

Another technical difficulty arises to the observed effect of 'nuclear filling'. To date, cellular mechanisms responsible for this phenomenon have not been extensively investigated. As I noted that this correlate of cytomorbidity exhibited an earlier onset in the LEC than in other brain areas (personal observations and compare Chen et al., 2013b), I suggest that increased susceptibility is a possible consequence of the higher metabolic rate in LEC neurons (Hevner and Wong-Riley, 1992; Solodkin and Van Hoesen, 1996; Khan et al., 2013). Restricting the waiting time after injection to eight days as compared to weeks or months reported by others (Chen et al., 2013b) helped me to overcome this obstacle. It should also be noted that excitatory and inhibitory neurons might differ in their calcium levels and that the presence of calcium buffers such as PV, CR and CB might influence recorded calcium transients in an unknown manner (Franconville et al., 2011). Nevertheless, two-photon calcium imaging is a valuable tool in visualizing activity in neuronal circuits and technical progress and the development of new, infrared shifted calcium indicators will help to push boundaries and enable recordings in unforeseen depths (see review by Ji, 2014).

4.4 Odor-responsive neurons projecting to the DG resemble fan cells

Combining retrograde tracer injections into the DG with targeted two-photon calcium imaging and *in vivo* whole-cell patch-clamp recordings in the LEC, we were able to characterize LII projection neurons electrophysiologically and morphologically. All neurons were located in LIIa, as indicated by their CTB-labeling, the depth of their location in the cortex, and post-hoc immunostainings. We recorded and reconstructed eleven neurons in LIIa, five of which were also imaged for odor-evoked responses. Common to all of these neurons is a spiny apical dendritic tree, which radiates out from the soma in horizontal and ascending direction, with the largest diameter close to the pia or at the level of the cell body. Basal dendrites are present, but often these are not as dense as apical

dendrites and their extent is mostly confined to LIIa and LIIb, reaching the border to LIII. For 9 out of 11 reconstructed neurons it was possible to follow the main axon to the alveus. In fewer cases the axon could be followed passing through the presubiculum and into the DG. If axon collaterals were detected, these were mostly localized in superficial layers and the presubiculum. The morphology of reconstructed neurons characterizes them as fan cells, one of three (Tahvildari and Alonso, 2005) or four (Canto and Witter, 2011) morphologically distinct principal cell types in LII in rat LEC. Using intracellular staining, Lingenhöhl and Finch (1991) showed that LII spiny neurons project to the subiculum. Additionally, they found widespread axonal branches. However, in the LEC of mice we found that axon collaterals were of similar width as the extent of the dendritic field.

Morphologically, fan cells resemble stellate cells in MEC, but stellate cells have more extensive descending dendrites. Fan cells can be distinguished based on physiological differences, as they lack persistent rhythmic subthreshold oscillations and time-dependent inward rectification typically seen in MEC stellate cells (Tahvildari and Alonso, 2005). Electrophysiological recordings in this current study classified principal neurons in LIIa as regular-spiking or burst-spiking projecting neurons. Importantly, both the firing patterns as well as the morphologies of the reconstructed neurons corroborate the observation of a rather homogeneous group of principal cells projecting to the DG. In consideration of the dendritic arborization, these neurons are ideally located to receive information from neurons having axonal terminals in LI-LIII. The observed axonal projections indicate a dual role for LIIa neurons. Their projections to the hippocampus form the perforant path, by which information is relayed to areas outside of the EC, whereas their local axon collaterals argue for intrinsic processing within the EC via associational connections.

4.5 Odor-responsive GABAergic neurons are electrophysiologically and morphologically diverse

Consistent with my finding of several GABAergic subpopulations based on the expression of molecular markers, the firing patterns and morphological recon-

structions of GABAergic neurons in LEC LII were diverse. This further argues for a heterogeneous group of GABAergic neurons in superficial layers in LEC. We recorded from fast-spiking as well as non fast-spiking neurons, both of which exhibited dense axonal arborization in superficial layers. The fast-spiking neuron depicted in **Figure 3.16** displays the typical basket-like axonal arborization of PV^+ neurons. However, we also encountered fast-spiking GABAergic neurons revealing a different morphology (**Figure 3.16** and **Appendix Figure 4**). On the basis of the low numbers of electrophysiologically recorded and biocytin-filled neurons *in vivo*, it is not possible to assign these neurons to distinct groups characterized by congruent firing patterns and morphologies.

As we observed dense axonal arborization in superficial layers, these GABAergic neurons are ideally suited to exert a strong inhibitory influence on the local microcircuit by targeting apical dendrites of excitatory neurons located in LII and LIII. It was shown that GABAergic neurons in LI receive direct synaptic contacts from mitral cells in the OB (Wouterlood et al., 1985), however, not much is known about the afferent and efferent connections of LII GABAergic neurons. We provided evidence that GABAergic neurons located in LII are odor-responsive, and based on their unselective response pattern, it can be hypothesized that these neurons receive excitatory input from local odor-responsive neurons tuned to different odors or direct input from mitral cells originating in different glomeruli.

The characterization of odor-responsive excitatory CB^+ neurons in LIIb *in vivo* was not feasible due to the depth of their location, therefore we decided to perform whole-cell patch-clamp recordings *in vitro*. These experiments are still ongoing.

4.6 Implications for olfactory impairment in Alzheimer's Disease

In light of our findings, it is of great interest to review the current state of knowledge about AD and its relation to olfactory perception. Olfactory dysfunction has been shown to precede other cognitive impairments in AD and can be detected as an impairment in odor detection, identification, and discrimination (Doty et al., 1987; Murphy, 1999). Remarkably, the earliest neuropathological changes re-

lated to AD occur in the EC (Braak and Braak, 1985). Specifically, the cells in LII in the EC forming the perforant path to the DG develop NFTs and the termination zone of the perforant path, the outer molecular layer in DG, shows the appearance of Aβ plaques (Hyman et al., 1984, 1986). This results in a denervation of the DG, effectively leading to a disruption of information transmission between the neocortex and the hippocampus. Consequently, it seems likely that the LEC is crucially involved in the impaired performance in odor identification, as it serves at least two roles in the process of perceiving and recognizing odors. The LEC receives direct input from the OB and the PIR, and passes this information on to the hippocampus, thereby establishing a pathway relevant for hippocampal-dependent odor memory (Staubli et al., 1984). In addition, the LEC projects back to both the OB and the PIR, developing a top-down control that was indicated to be critically involved in fine odor discrimination (Chapuis et al., 2013) and in modulating odor responses in the PIR (Chapuis et al., 2013; Mouly and Di Scala, 2006). Among several olfactory structures examined, it was indeed exclusively the LEC, where the deposition of Aβ plaques negatively correlated with olfactory task performance, namely investigation, habituation and discrimination (Wesson et al., 2010).

In animal models of AD, disturbed firing patterns of neurons were observed, in particular a hyperactivity in neurons located near Aβ plaques (Busche et al., 2008). In visual cortex, hyperactive neurons in the vicinity of plaques lose their selectivity (Grienberger et al., 2012), and place cells in hippocampus show an impairment in their spatial selectivity, which is correlated with the occurrence of Aβ plaques (Cacucci et al., 2008). A very recent study by Xu and colleagues extended this finding to the LEC and confirmed hyperactivity of neurons and disrupted firing activity in response to odors in an animal model of AD (Xu et al., 2015). As we could show in this study, Reelin$^+$ neurons in LIIa respond to odors with particularly high selectivity. If these neurons lost their selectivity with the emergence of Aβ plaques analogously to what was observed in visual cortex and hippocampus, this could result in an impairment of odor identification and discrimination as it is observed in AD. Surprisingly, Xu and colleagues did not observe a difference in single-unit odor responses and odor receptive fields (Xu et al., 2015). However, their recording sites were distributed across all layers in LEC and did not specifically target LII. It would be highly interesting to investigate specifically the firing pattern of Reelin$^+$ neurons in this mouse model of AD, as these neurons pass olfactory information directly onto the DG. Both in

humans with AD and in a mouse model of AD, the level of Reelin expression in LII excitatory neurons was decreased and also in the hippocampus, where Reelin is most likely released by these neurons (Ramos-Moreno et al., 2006), detectable levels of Reelin were reduced (Chin et al., 2007). Additionally, firing properties of fan cells, the morphological correlate of Reelin$^+$ neurons, were severely altered in an AD mouse model (Marcantoni et al., 2014). These findings strongly indicate that Reelin$^+$ neurons might suffer from a loss of function during AD pathogenesis.

Additionally, based on our calcium imaging data a second mechanistic explanation for impaired olfactory acuity can be put forward. This data revealed that the GABAergic population in LEC LII responds broadly to various odors and, in general, inhibition is assumed to exert a gain control and increase tuning selectivity in postsynaptic principal neurons (see review by Isaacson and Scanziani, 2011). Early in the entorhinal pathology related to AD, non-principal neurons containing PV or CB exhibit morphological alterations mainly in LII (Mikkonen et al., 1999) and the number of SOM$^+$ and CR$^+$ neurons is substantially decreased (Saiz-Sanchez et al., 2012). At more advanced stages of the disease, a comparable, but less pronounced decrease in numbers was also observed for PV$^+$ and inhibitory CB$^+$ neurons (Saiz-Sanchez et al., 2012). Potentially, this reduction in the level of inhibitory neurons could result in an alteration of the firing pattern of Reelin$^+$ neurons and subsequently reduce odor selectivity.

Although to date we do not know the actual mechanism that leads to a progressive impairment to discriminate and identify odors in AD, there is evidence that neuropathology starts in the LEC and spreads from there to other functionally connected structures (Braak and Braak, 1991; Khan et al., 2013). This early involvement of the LEC in the progression of AD highlights the theoretical importance and the potential diagnostic utility of detecting pathological changes in LEC and functional changes in olfaction. These tests could include olfactory tasks with a memory component depending on LEC function (Kesslak et al., 1988; Murphy, 1999) and magnetic resonance imaging to detect early volume reduction or hyperactivity in the EC (deToledo Morrell et al., 2004; Khan et al., 2013). Therefore, unraveling LEC function with respect to pathological impairments in AD holds a great clinical potential.

4.7 Outlook

I presented preliminary data about the spatial correlation in the network response to odor stimulation. In the PIR, the spatial organization of glomeruli located in the OB is not preserved and neurons responding to the same odor are intermingled with neurons responding to different odors, resulting in a 'salt and paper' layout (Stettler and Axel, 2009). Disregarding different neuronal subtypes in the LEC, we found no obvious spatial correlation of neurons with similar odor preference within single imaging areas, but a tendency for neurons within the same imaging area to be stronger correlated than neurons of different imaging areas. This is an interesting finding, as it might indicate the existence of subnetworks in the LEC representing some odors stronger than others. Therefore, we will continue to analyze the data set, focusing on the differentiation between neuronal types and their individual spatial organization. Considering the modular organization of CB^+ neurons and the so far unknown functional relevance of such cell islands both in MEC and LEC, it is intriguing to speculate that CB^+ neurons belonging to the same islands might reveal stronger correlation in their response to odors.

Moreover, we are contemplating how single odors are represented in the dispersed network of active neurons in the LEC and by which mechanism odor identity is unambiguously encoded to allow readout of odor information by subsequent brain areas. Preliminary analysis indicates that the presented stimulus can be predicted based on the observed activity of the neuronal population. The applied decoding approach revealed that the activity of single neurons in a network as well as the activity of the whole population show high classification accuracy, compared to shuffled data. It is conceivable that a sub-set of highly discriminating neurons drives the high population decoding accuracy, but further analysis is needed to confirm this conjecture.

Additionally, it will be essential to substantiate preliminary reports about the connectivity within the LEC network. The different neuronal subtypes are still awaiting detailed characterization, relating electrophysiological parameters and morphological descriptions with the expression of molecular markers. This characterization is ongoing in our department and by using the *CB*^{Cre} mouse line injected with CTB in the DG and flex.GCaMP6 in the LEC, it will become possible to perform pair recordings *in vitro* to study the connectivity between $Reelin^+$ and CB^+ neurons in LII in the LEC. Further experiments could aim for selec-

tively activating or silencing different neuronal subtypes by optogenetic means to functionally dissect the LEC circuit.

4.8 Concluding remarks

The current study sheds light on the cellular composition of the LEC and the differential involvement of specific cell types in olfactory information processing. We have provided evidence that odor information is transmitted to the hippocampus via Reelin$^+$, fan cell-like neurons in LIIa. Feedback projections to olfactory structures and to the contralateral LEC are established by CB$^+$ neurons that are also odor-responsive, but exhibit a broader response profile than Reelin$^+$ neurons. GABAergic neurons in LII provide general inhibition and it remains to be investigated if they contribute to odor selectivity in excitatory neurons or if they mostly exert gain control. Overall, I have highlighted the importance of the LEC in the olfactory pathway. Hopefully, future studies trying to elucidate the unique functional role of the LEC will consider our findings regarding the different cell types and will try to distinguish between neuronal players. In the long run, detailed knowledge about the LEC, its neuronal composition and its involvement in olfactory processing will contribute to an increased understanding of neurological disorders with a particular emphasis on the etiology of AD.

Bibliography

Abraham, N. M., Egger, V., Shimshek, D. R., Renden, R., Fukunaga, I., Sprengel, R., Seeburg, P. H., Klugmann, M., Margrie, T. W., Schaefer, A. T., and Kuner, T. (2010). Synaptic inhibition in the olfactory bulb accelerates odor discrimination in mice. *Neuron*, 65(3):399–411.

Agster, K. L. and Burwell, R. D. (2009). Cortical efferents of the perirhinal, postrhinal, and entorhinal cortices of the rat. *Hippocampus*, 19(12):1159–1186.

Agster, K. L. and Burwell, R. D. (2013). Hippocampal and subicular efferents and afferents of the perirhinal, postrhinal, and entorhinal cortices of the rat. *Behav. Brain Res.*

Akerboom, J., Chen, T. W., Wardill, T. J., Tian, L., Marvin, J. S., Mutlu, S., Calderon, N. C., Esposti, F., Borghuis, B. G., Sun, X. R., Gordus, A., Orger, M. B., Portugues, R., Engert, F., Macklin, J. J., Filosa, A., Aggarwal, A., Kerr, R. A., Takagi, R., Kracun, S., Shigetomi, E., Khakh, B. S., Baier, H., Lagnado, L., Wang, S. S. H., Bargmann, C. I., Kimmel, B. E., Jayaraman, V., Svoboda, K., Kim, D. S., Schreiter, E. R., and Looger, L. L. (2012). Optimization of a GCaMP Calcium Indicator for Neural Activity Imaging. *Journal of Neuroscience*, 32(40):13819–13840.

Akerboom, J., Rivera, J. D. V., Guilbe, M. M. R., Malavé, E. C. A., Hernandez, H. H., Tian, L., Hires, S. A., Marvin, J. S., Looger, L. L., and Schreiter, E. R. (2009). Crystal structures of the GCaMP calcium sensor reveal the mechanism of fluorescence signal change and aid rational design. *J. Biol. Chem.*, 284(10):6455–6464.

Alzheimer, A., Stelzmann, R. A., Schnitzlein, H. N., and Murtagh, F. R. (1995). *An English translation of Alzheimer's 1907 paper, "Uber eine eigenartige Erkankung der Hirnrinde".*, volume 8. Wiley Subscription Services, Inc., A Wiley Company.

Amaral, D. G., Insausti, R., and Cowan, W. M. (1987). The entorhinal cortex of the monkey: I. Cytoarchitectonic organization. *J. Comp. Neurol.*, 264(3):326–355.

Apicella, A., Yuan, Q., Scanziani, M., and Isaacson, J. S. (2010). Pyramidal cells in piriform cortex receive convergent input from distinct olfactory bulb glomeruli. *Journal of Neuroscience*, 30(42):14255–14260.

Arevian, A. C., Kapoor, V., and Urban, N. N. (2008). Activity-dependent gating of lateral inhibition in the mouse olfactory bulb. *Nature Neuroscience*, 11(1):80–87.

Atallah, B. V., Bruns, W., Carandini, M., and Scanziani, M. (2012). Parvalbumin-Expressing Interneurons Linearly Transform Cortical Responses to Visual Stimuli. *Neuron*, 73(1):159–170.

Beckstead, R. M. (1978). Afferent connections of the entorhinal area in the rat as demonstrated by retrograde cell-labeling with horseradish peroxidase. *Brain Res.*, 152(2):249–264.

Belluscio, L. and Katz, L. C. (2001). Symmetry, stereotypy, and topography of odorant representations in mouse olfactory bulbs. *Journal of Neuroscience*, 21(6):2113–2122.

Bernabeu, R., Thiriet, N., Zwiller, J., and Di Scala, G. (2006). Lesion of the lateral entorhinal cortex amplifies odor-induced expression of c-fos, junB, and zif 268 mRNA in rat brain. *Synapse*, 59(3):135–143.

Blumhagen, F., Zhu, P., Shum, J., Schärer, Y.-P. Z., Yaksi, E., Deisseroth, K., and Friedrich, R. W. (2011). Neuronal filtering of multiplexed odour representations. *Nature*, 479(7374):493–498.

Boeijinga, P. H. and Lopes da Silva, F. H. (1989). Modulations of EEG activity in the entorhinal cortex and forebrain olfactory areas during odour sampling. *Brain Res.*, 478(2):257–268.

Boyd, A. M., Kato, H. K., Komiyama, T., and Isaacson, J. S. (2015). Broadcasting of Cortical Activity to the Olfactory Bulb. *CellReports*, 10(7):1032–1039.

Boyd, A. M., Sturgill, J. F., Poo, C., and Isaacson, J. S. (2012). Cortical feedback control of olfactory bulb circuits. *Neuron*, 76(6):1161–1174.

Braak, H. and Braak, E. (1985). On Areas of Transition Between Entorhinal Allocortex and Temporal Isocortex in the Human-Brain - Normal Morphology and Lamina-Specific Pathology in Alzheimers-Disease. *Acta Neuropathol.*, 68(4):325–332.

Braak, H. and Braak, E. (1991). Neuropathological stageing of Alzheimer-related changes. *Acta Neuropathol.*, 82(4):239–259.

Buck, L. and Axel, R. (1991). A novel multigene family may encode odorant receptors: a molecular basis for odor recognition. *Cell*, 65(1):175–187.

Buetfering, C., Allen, K., and Monyer, H. (2014). Parvalbumin interneurons provide grid cell-driven recurrent inhibition in the medial entorhinal cortex. *Nature Neuroscience*, 17(5):710–718.

Burwell, R. D. and Amaral, D. G. (1998a). Cortical afferents of the perirhinal, postrhinal, and entorhinal cortices of the rat. *J. Comp. Neurol.*, 398(2):179–205.

Burwell, R. D. and Amaral, D. G. (1998b). Perirhinal and postrhinal cortices of the rat: interconnectivity and connections with the entorhinal cortex. *J. Comp. Neurol.*, 391(3):293–321.

Busche, M. A., Eichhoff, G., Adelsberger, H., Abramowski, D., Wiederhold, K.-H., Haass, C., Staufenbiel, M., Konnerth, A., and Garaschuk, O. (2008). Clusters of Hyperactive Neurons Near Amyloid Plaques in a Mouse Model of Alzheimer's Disease. *Science*, 321(5896):1686–1689.

Buzsaki, G. (2004). Large-scale recording of neuronal ensembles. *Nature Neuroscience*, 7(5):446–451.

Cacucci, F., Yi, M., Wills, T. J., Chapman, P., and O'Keefe, J. (2008). Place cell firing correlates with memory deficits and amyloid plaque burden in Tg2576 Alzheimer mouse model. *Proceedings of the National Academy of Sciences*, 105(22):7863–7868.

Canto, C. B. and Witter, M. P. (2011). Cellular properties of principal neurons in the rat entorhinal cortex. I. The lateral entorhinal cortex. *Hippocampus*, 22(6):1256–1276.

Canto, C. B., Wouterlood, F. G., and Witter, M. P. (2008). What Does the Anatomical Organization of the Entorhinal Cortex Tell Us? *Neural Plasticity*, 2008:1–18.

Caron, S. J. C., Ruta, V., Abbott, L. F., and Axel, R. (2013). Random convergence of olfactory inputs in the Drosophila mushroom body. *Nature*, 497(7447):113–+.

Cazakoff, B. N., Lau, B. Y. B., Crump, K. L., Demmer, H. S., and Shea, S. D. (2014). Broadly tuned and respiration-independent inhibition in the olfactory bulb of awake mice. *Nature Publishing Group*, 17(4):569–576.

Cetin, A., Komai, S., Eliava, M., Seeburg, P. H., and Osten, P. (2007). Stereotaxic gene delivery in the rodent brain. *Nature Protocols*, 1(6):3166–3173.

Chabaud, P., Ravel, N., Wilson, D. A., Mouly, A. M., Vigouroux, M., Farget, V., and Gervais, R. (2000). Exposure to behaviourally relevant odour reveals differential characteristics in rat central olfactory pathways as studied through oscillatory activities. *Chem. Senses*, 25(5):561–573.

Chapuis, J., Cohen, Y., He, X., Zhang, Z., Jin, S., Xu, F., and Wilson, D. A. (2013). Lateral Entorhinal Modulation of Piriform Cortical Activity and Fine Odor Discrimination. *Journal of Neuroscience*, 33(33):13449–13459.

Chen, J. L., Carta, S., Soldado-Magraner, J., Schneider, B. L., and Helmchen, F. (2013a). Behaviour-dependent recruitment of long-range projection neurons in somatosensory cortex. *Nature*.

Chen, Q., Cichon, J., Wang, W., Qiu, L., Lee, S.-J. R., Campbell, N. R., DeStefino, N., Goard, M. J., Fu, Z., Yasuda, R., Looger, L. L., Arenkiel, B. R., Gan, W.-B., and Feng, G. (2012). Imaging Neural Activity Using Thy1-GCaMP Transgenic Mice. *Neuron*, 76(2):297–308.

Chen, T.-W., Wardill, T. J., Sun, Y., Pulver, S. R., Renninger, S. L., Baohan, A., Schreiter, E. R., Kerr, R. A., Orger, M. B., Jayaraman, V., Looger, L. L., Svoboda, K., and Kim, D. S. (2013b). Ultrasensitive fluorescent proteins for imaging neuronal activity. *Nature*, 499(7458):295–300.

Chin, J., Massaro, C. M., Palop, J. J., Thwin, M. T., Yu, G. Q., Bien-Ly, N., Bender, A., and Mucke, L. (2007). Reelin Depletion in the Entorhinal Cortex of Human Amyloid Precursor Protein Transgenic Mice and Humans with Alzheimer's Disease. *Journal of Neuroscience*, 27(11):2727–2733.

Couey, J. J., Witoelar, A., Zhang, S.-J., Zheng, K., Ye, J., Dunn, B., Czajkowski, R., Moser, M.-B., Moser, E. I., Roudi, Y., and Witter, M. P. (2013). Recurrent inhibitory circuitry as a mechanism for grid formation. *Nature Publishing Group*, pages 1–9.

Davis, B. J. and Macrides, F. (1981). The organization of centrifugal projections from the anterior olfactory nucleus, ventral hippocampal rudiment, and piriform cortex to the main olfactory bulb in the hamster: an autoradiographic study. *J. Comp. Neurol.*, 203(3):475–493.

de Olmos, J., Hardy, H., and Heimer, L. (1978). The afferent connections of the main and the accessory olfactory bulb formations in the rat: an experimental HRP-study. *J. Comp. Neurol.*, 181(2):213–244.

DeFelipe, J. (1997). Types of neurons, synaptic connections and chemical characteristics of cells immunoreactive for calbindin-D28K, parvalbumin and calretinin in the neocortex. *J. Chem. Neuroanat.*, 14(1):1–19.

DeFelipe, J., Alonso-Nanclares, L., and Arellano, J. I. (2002). Microstructure of the neocortex: Comparative aspects. *J. Neurocytol.*, 31(3-5):299–316.

Denk, W., Strickler, J. H., and Webb, W. W. (1990). Two-photon laser scanning fluorescence microscopy. *Science*.

Deshmukh, S. S. and Knierim, J. J. (2011). Representation of non-spatial and spatial information in the lateral entorhinal cortex. *Front. Behav. Neurosci.*, 5:69.

deToledo Morrell, L., Stoub, T. R., Bulgakova, M., Wilson, R. S., Bennett, D. A., Leurgans, S., Wuu, J., and Turner, D. A. (2004). MRI-derived entorhinal volume is a good predictor of conversion from MCI to AD. *NBA*, 25(9):1197–1203.

Domnisoru, C., Kinkhabwala, A. A., and Tank, D. W. (2013). Membrane potential dynamics of grid cells. *Nature*, 495(7440):199–204.

Donato, F., Rompani, S. B., and Caroni, P. (2013). Parvalbumin-expressing basket-cell network plasticity induced by experience regulates adult learning. *Nature*, 504(7479):272–276.

Doty, R. L., Reyes, P. F., and Gregor, T. (1987). Presence of both odor identification and detection deficits in Alzheimer's disease. *Brain Res. Bull.*, 18(5):597–600.

Eichenbaum, H., Fagan, A., Mathews, P., and Cohen, N. J. (1988). Hippocampal system dysfunction and odor discrimination learning in rats: impairment or facilitation depending on representational demands. *Behav. Neurosci.*, 102(3):331–339.

Eichenbaum, H., Morton, T. H., Potter, H., and Corkin, S. (1983). Selective olfactory deficits in case H.M. *Brain*, 106 (Pt 2):459–472.

Engert, F. and Bonhoeffer, T. (1999). Dendritic spine changes associated with hippocampal long-term synaptic plasticity. *Nature*, 399(6731):66–70.

Ferezou, I., Cauli, B., Hill, E. L., Rossier, J., Hamel, E., and Lambolez, B. (2002). 5-HT3 receptors mediate serotonergic fast synaptic excitation of neocortical vasoactive intestinal peptide/cholecystokinin interneurons. *Journal of Neuroscience*, 22(17):7389–7397.

Ferry, B., Ferreira, G., Traissard, N., and Majchrzak, M. (2006). Selective involvement of the lateral entorhinal cortex in the control of the olfactory memory trace during conditioned odor aversion in the rat. *Behav. Neurosci.*, 120(5):1180–1186.

Ferry, B., Oberling, P., Jarrard, L. E., and Di Scala, G. (1996). Facilitation of conditioned odor aversion by entorhinal cortex lesions in the rat. *Behav. Neurosci.*, 110(3):443–450.

Fisek, M. and Wilson, R. I. (2014). Stereotyped connectivity and computations in higher-order olfactory neurons. *Nature Neuroscience*, 17(2):280–288.

Forloni, G., Hohmann, C., and Coyle, J. (1990). Developmental Expression of Somatostatin in Mouse-Brain .1. Immunocytochemical Studies. *Brain Res. Dev. Brain Res.*, 53(1):6–25.

Franconville, R., Revet, G., Astorga, G., Schwaller, B., and Llano, I. (2011). Somatic calcium level reports integrated spiking activity of cerebellar interneurons in vitro and in vivo. *Journal of Neurophysiology*, 106(4):1793–1805.

Franks, K. M. and Isaacson, J. S. (2006). Strong single-fiber sensory inputs to olfactory cortex: implications for olfactory coding. *Neuron*, 49(3):357–363.

Freund, T. F. and Buzsaki, G. (1996). Interneurons of the hippocampus. *Hippocampus*, 6(4):347–470.

Friedrich, R. W. (2013). Neuronal computations in the olfactory system of zebrafish. *Annu. Rev. Neurosci.*, 36:383–402.

Friedrich, R. W. and Laurent, G. (2004). Dynamics of Olfactory Bulb Input and Output Activity During Odor Stimulation in Zebrafish. *Journal of Neurophysiology*, 91(6):2658–2669.

Fuchs, E. C., Zivkovic, A. R., Cunningham, M. O., Middleton, S., LeBeau, F. E. N., Bannerman, D. M., Rozov, A., Whittington, M. A., Traub, R. D., Rawlins, J. N. P., and Monyer, H. (2007). Recruitment of parvalbumin-positive interneurons determines hippocampal function and associated behavior. *Neuron*, 53(4):591–604.

Fujimaru, Y. and Kosaka, T. (1996). The distribution of two calcium binding proteins, calbindin D-28K and parvalbumin, in the entorhinal cortex of the adult mouse. *Neurosci. Res.*, 24(4):329–343.

Fyhn, M., Molden, S., Witter, M. P., Moser, E. I., and Moser, M.-B. (2004). Spatial Representation in the Entorhinal Cortex. *Science, New Series*, 305(5688):1258–1264.

Gavériaux-Ruff, C. and Kieffer, B. L. (2007). Conditional gene targeting in the mouse nervous system: Insights into brain function and diseases. *Pharmacol. Ther.*, 113(3):619–634.

Gentet, L. J., Avermann, M., Matyas, F., Staiger, J. F., and Petersen, C. C. H. (2010). Membrane Potential Dynamics of GABAergic Neurons in the Barrel Cortex of Behaving Mice. *Neuron*, 65(3):422–435.

Gentet, L. J., Kremer, Y., Taniguchi, H., Huang, Z. J., Staiger, J. F., and Petersen, C. C. H. (2012). Unique functional properties of somatostatin-expressing GABAergic neurons in mouse barrel cortex. *Nature Neuroscience*, 15(4):607–612.

Germroth, P., Schwerdtfeger, W. K., and Buhl, E. H. (1989). GABAergic neurons in the entorhinal cortex project to the hippocampus. *Brain Res.*, 494(1):187–192.

Giocomo, L. M., Moser, M.-B., and Moser, E. I. (2011). Computational Models of Grid Cells. *Neuron*, 71(4):589–603.

Göbel, W. and Helmchen, F. (2007). New Angles on Neuronal Dendrites In Vivo. *Journal of Neurophysiology*, 98(6):3770–3779.

Göbel, W., Kampa, B. M., and Helmchen, F. (2007). Imaging cellular network dynamics in three dimensions using fast 3D laser scanning. *Nat Meth*, 4(1):73–79.

Gómez-Isla, T., Price, J. L., McKeel, D. W., Morris, J. C., Growdon, J. H., and Hyman, B. T. (1996). Profound loss of layer II entorhinal cortex neurons occurs in very mild Alzheimer's disease. *J. Neurosci.*, 16(14):4491–4500.

Gong, S., Doughty, M., Harbaugh, C. R., Cummins, A., Hatten, M. E., Heintz, N., and Gerfen, C. R. (2007). Targeting Cre recombinase to specific neuron populations with bacterial artificial chromosome constructs. *Journal of Neuroscience*, 27(37):9817–9823.

Gottfried, J. A., Smith, A. P. R., Rugg, M. D., and Dolan, R. J. (2004). Remembrance of odors past: human olfactory cortex in cross-modal recognition memory. *Neuron*, 42(4):687–695.

Gottfried, J. A., Winston, J. S., and Dolan, R. J. (2006). Dissociable codes of odor quality and odorant structure in human piriform cortex. *Neuron*, 49(3):467–479.

Grateron, L., Cebada-Sanchez, S., Marcos, P., Mohedano-Moriano, A., Insausti, A. M., Muñoz, M., Arroyo-Jimenez, M. M., Martinez-Marcos, A., Artacho-Perula, E., Blaizot, X., and Insausti, R. (2003). Postnatal development of calcium-binding proteins immunoreactivity (parvalbumin, calbindin, calretinin) in the human entorhinal cortex. *J. Chem. Neuroanat.*, 26(4):311–316.

Greenberg, D. S. and Kerr, J. N. D. (2009). Automated correction of fast motion artifacts for two-photon imaging of awake animals. *Journal of Neuroscience Methods*, 176(1):1–15.

Grewe, B. F., Langer, D., Kasper, H., Kampa, B. M., and Helmchen, F. (2010). High-speed in vivo calcium imaging reveals neuronal network activity with near-millisecond precision. *Nat Meth*, 7(5):399–405.

Grienberger, C., Rochefort, N. L., Adelsberger, H., Henning, H. A., Hill, D. N., Reichwald, J., Staufenbiel, M., and Konnerth, A. (2012). Staged decline of neuronal function in vivo in an animal model of Alzheimer's disease. *Nature Communications*, 3.

Gruntman, E. and Turner, G. C. (2013). Integration of the olfactory code across dendritic claws of single mushroom body neurons. *Nature Publishing Group*, 16(12):1821–1829.

Haberly, L. B. and Price, J. L. (1977). The axonal projection patterns of the mitral and tufted cells of the olfactory bulb in the rat. *Brain Res.*, 129(1):152–157.

Haberly, L. B. and Price, J. L. (1978). Association and commissural fiber systems of the olfactory cortex of the rat. *J. Comp. Neurol.*, 178(4):711–740.

Habets, A. M., Lopes da Silva, F. H., and de Quartel, F. W. (1980a). Autoradiography of the olfactory-hippocampal pathway in the cat with special reference to the perforant path. *Exp Brain Res*, 38(3):257–265.

Habets, A. M., Lopes da Silva, F. H., and Mollevanger, W. J. (1980b). An olfactory input to the hippocampus of the cat: field potential analysis. *Brain Res.*, 182(1):47–64.

Hafting, T., Fyhn, M., Molden, S., Moser, M.-B., and Moser, E. I. (2005). Microstructure of a spatial map in the entorhinal cortex. *Nature*, 436(7052):801–806.

Hargreaves, E. L., Rao, G., Lee, I., and Knierim, J. J. (2005). Major Dissociation Between Medial and Lateral Entorhinal Input to Dorsal Hippocampus. *Science*, 308(5729):1792–1794.

Heimer, L. (1968). Synaptic distribution of centripetal and centrifugal nerve fibres in the olfactory system of the rat. An experimental anatomical study. *J. Anat.*, 103(Pt 3):413–432.

Helmchen, F. and Denk, W. (2005). Deep tissue two-photon microscopy. *Nat Meth*, 2(12):932–940.

Herry, C., Ciocchi, S., Senn, V., Demmou, L., Müller, C., and Lüthi, A. (2008). Switching on and off fear by distinct neuronal circuits. *Nature*, 454(7204):600–606.

Hevner, R. F. and Wong-Riley, M. T. (1992). Entorhinal cortex of the human, monkey, and rat: metabolic map as revealed by cytochrome oxidase. *J. Comp. Neurol.*, 326(3):451–469.

Heys, J. G., Rangarajan, K. V., and Dombeck, D. A. (2014). The Functional Micro-organization of Grid Cells Revealed by Cellular-Resolution Imaging. *Neuron*, pages 1–12.

Hintiryan, H., Gou, L., Zingg, B., Yamashita, S., Lyden, H. M., Song, M. Y., Grewal, A. K., Zhang, X., Toga, A. W., and Dong, H.-W. (2012). Comprehensive connectivity of the mouse main olfactory bulb: analysis and online digital atlas. *Front Neuroanat*, 6:30.

Horikawa, K., Yamada, Y., Matsuda, T., Kobayashi, K., Hashimoto, M., Matsuura, T., Miyawaki, A., Michikawa, T., Mikoshiba, K., and Nagai, T. (2010). Spontaneous network activity visualized by ultrasensitive Ca2+ indicators, yellow Cameleon-Nano. *Nat Meth*, 7(9):729–732.

Huber, D., Gutnisky, D. A., Peron, S., O'Connor, D. H., Wiegert, J. S., Tian, L., Oertner, T. G., Looger, L. L., and Svoboda, K. (2012). Multiple dynamic representations in the motor cortex during sensorimotor learning. *Nature*, 484(7395):473–478.

Hunsaker, M. R., Chen, V., Tran, G. T., and Kesner, R. P. (2013). The medial and lateral entorhinal cortex both contribute to contextual and item recognition memory: A test of the binding ofitems and context model. *Hippocampus*, 23(5):380–391.

Hunsaker, M. R., Fieldsted, P. M., Rosenberg, J. S., and Kesner, R. P. (2008). Dissociating the roles of dorsal and ventral CA1 for the temporal processing of spatial locations, visual objects, and odors. *Behav. Neurosci.*, 122(3):643–650.

Hyman, B. T., Van Hoesen, G. W., Damasio, A. R., and Barnes, C. L. (1984). Alzheimer's Disease: Cell-Specific Pathology Isolates the Hippocampal Formation. *Science, New Series*, 225(4667):1168–1170.

Hyman, B. T., Van Hoesen, G. W., Kromer, L. J., and Damasio, A. R. (1986). Perforant pathway changes and the memory impairment of Alzheimer's disease. *Annals of Neurology*, 20(4):472–481.

Igarashi, K. M., Ieki, N., An, M., Yamaguchi, Y., Nagayama, S., Kobayakawa, K., Kobayakawa, R., Tanifuji, M., Sakano, H., Chen, W. R., and Mori, K. (2012). Parallel mitral and tufted cell pathways route distinct odor information to different targets in the olfactory cortex. *Journal of Neuroscience*, 32(23):7970–7985.

Igarashi, K. M., Lu, L., Colgin, L. L., Moser, M.-B., and Moser, E. I. (2014). Coordination of entorhinal–hippocampal ensemble activity during associative learning. *Nature*, pages 1–20.

Insausti, R., Herrero, M. T., and Witter, M. P. (1997). Entorhinal cortex of the rat: cytoarchitectonic subdivisions and the origin and distribution of cortical efferents. *Hippocampus*, 7(2):146–183.

Inta, D., Alfonso, J., von Engelhardt, J., Kreuzberg, M. M., Meyer, A. H., van Hooft, J. A., and Monyer, H. (2008). Neurogenesis and widespread forebrain migration of distinct GABAergic neurons from the postnatal subventricular zone. *Proceedings of the National Academy of Sciences*, 105(52):20994–20999.

Inta, D., Monyer, H., Sprengel, R., Meyer-Lindenberg, A., and Gass, P. (2010). Mice with genetically altered glutamate receptors as models of schizophrenia: A comprehensive review. *Neuroscience & Biobehavioral Reviews*, 34(3):285–294.

Isaacson, J. S. and Scanziani, M. (2011). How Inhibition Shapes Cortical Activity. *Neuron*, 72(2):231–243.

Jefferis, G. S. X. E., Potter, C. J., Chan, A. M., Marin, E. C., Rohlfing, T., Maurer, C. R., and Luo, L. (2007). Comprehensive maps of Drosophila higher olfactory centers: spatially segregated fruit and pheromone representation. *Cell*, 128(6):1187–1203.

Ji, N. (2014). The Practical and Fundamental Limits of Optical Imaging in Mammalian Brains. *Neuron*, 83(6):1242–1245.

Jones, R. S. and Buhl, E. H. (1993). Basket-like interneurones in layer II of the entorhinal cortex exhibit a powerful NMDA-mediated synaptic excitation. *Neurosci Lett*, 149(1):35–39.

Jortner, R. A., Farivar, S. S., and Laurent, G. (2007). A simple connectivity scheme for sparse coding in an olfactory system. *J. Neurosci.*, 27(7):1659–1669.

Kato, H. K., Chu, M. W., Isaacson, J. S., and Komiyama, T. (2012). Dynamic sensory representations in the olfactory bulb: modulation by wakefulness and experience. *Neuron*, 76(5):962–975.

Kato, H. K., Gillet, S. N., Peters, A. J., Isaacson, J. S., and Komiyama, T. (2013). Parvalbumin-expressing interneurons linearly control olfactory bulb output. *Neuron*, 80(5):1218–1231.

Kay, L. M. and Freeman, W. J. (1998). Bidirectional processing in the olfactory-limbic axis during olfactory behavior. *Behav. Neurosci.*, 112(3):541–553.

Kerlin, A. M., Andermann, M. L., Berezovskii, V. K., and Reid, R. C. (2010). Broadly Tuned Response Properties of Diverse Inhibitory Neuron Subtypes in Mouse Visual Cortex. *Neuron*, 67(5):858–871.

Kerr, J. N. D., Greenberg, D., and Helmchen, F. (2005). Imaging input and output of neocortical networks in vivo. *Proc. Natl. Acad. Sci. U.S.A.*, 102(39):14063–14068.

Kerr, K. M., Agster, K. L., Furtak, S. C., and Burwell, R. D. (2007). Functional neuroanatomy of the parahippocampal region: The lateral and medial entorhinal areas. *Hippocampus*, 17(9):697–708.

Kesner, R. P., Hunsaker, M. R., and Ziegler, W. (2011). The role of the dorsal and ventral hippocampus in olfactory working memory. *Neurobiol Learn Mem*, 96(2):361–366.

Kesslak, J. P., Cotman, C. W., Chui, H. C., Van den Noort, S., Fang, H., Pfeffer, R., and Lynch, G. (1988). Olfactory tests as possible probes for detecting and monitoring Alzheimer's disease. *NBA*, 9(4):399–403.

Khan, U. A., Liu, L., Provenzano, F. A., Berman, D. E., Profaci, C. P., Sloan, R., Mayeux, R., Duff, K. E., and Small, S. A. (2013). Molecular drivers and cortical spread of lateral entorhinal cortex dysfunction in preclinical Alzheimer's disease. *Nature Publishing Group*.

Kitamura, T., Pignatelli, M., Suh, J., Kohara, K., Yoshiki, A., Abe, K., and Tonegawa, S. (2014). Island Cells Control Temporal Association Memory. *Science*.

Kjelvik, G., Evensmoen, H. R., Brezova, V., and Håberg, A. K. (2012). The human brain representation of odor identification. *Journal of Neurophysiology*, 108(2):645–657.

Klenoff, J. R. and Greer, C. A. (1998). Postnatal development of olfactory receptor cell axonal arbors. *J. Comp. Neurol.*, 390(2):256–267.

Köhler, C. and Chan-Palay, V. (1982). The distribution of cholecystokinin-like immunoreactive neurons and nerve terminals in the retrohippocampal region in the rat and guinea pig. *J. Comp. Neurol.*, 210(2):136–146.

Köhler, C. and Chan-Palay, V. (1983). Somatostatin and vasoactive intestinal polypeptide-like immunoreactive cells and terminals in the retrohippocampal region of the rat brain. *Anat. Embryol.*, 167(2):151–172.

Köhler, C., Eriksson, L., Davies, S., and Chan-Palay, V. (1986). Neuropeptide-Y Innervation of the Hippocampal Region in the Rat and Monkey Brain. *J. Comp. Neurol.*, 244(3):384–400.

Köhler, C., Wu, J. Y., and Chan-Palay, V. (1985). Neurons and terminals in the retrohippocampal region in the rat's brain identified by anti-gamma-aminobutyric acid and anti-glutamic acid decarboxylase immunocytochemistry. *Anat. Embryol.*, 173(1):35–44.

Kosel, K. C., Van Hoesen, G. W., and West, J. R. (1981). Olfactory bulb projections to the parahippocampal area of the rat. *J. Comp. Neurol.*, 198(3):467–482.

Kubota, Y. (2014). Untangling GABAergic wiring in the cortical microcircuit. *Current Opinion in Neurobiology*, 26:7–14.

Kurtz, R., Fricke, M., Kalb, J., Tinnefeld, P., and Sauer, M. (2006). Application of multiline two-photon microscopy to functional in vivo imaging. *Journal of Neuroscience Methods*, 151(2):276–286.

Lacy, J. W. and Stark, C. E. L. (2012). Intrinsic functional connectivity of the human medial temporal lobe suggests a distinction between adjacent MTL cortices and hippocampus. *Hippocampus*, 22(12):2290–2302.

Lechleiter, J. D., Lin, D.-T., and Sieneart, I. (2002). Multi-Photon Laser Scanning Microscopy Using an Acoustic Optical Deflector. *Biophysical Journal*, 83(4):2292–2299.

Lee, S.-H., Kwan, A. C., Zhang, S., Phoumthipphavong, V., Flannery, J. G., Masmanidis, S. C., Taniguchi, H., Huang, Z. J., Zhang, F., Boyden, E. S., Deisseroth, K., and Dan, Y. (2012). Activation of specific interneurons improves V1 feature selectivity and visual perception. *Nature*, 488(7411):379–383.

Leybaert, L., de Meyer, A., Mabilde, C., and Sanderson, M. J. (2005). A simple and practical method to acquire geometrically correct images with resonant scanning-based line scanning in a custom-built video-rate laser scanning microscope. *J Microsc*, 219(Pt 3):133–140.

Lingenhöhl, K. and Finch, D. M. (1991). Morphological characterization of rat entorhinal neurons in vivo: soma-dendritic structure and axonal domains. *Exp Brain Res*, 84(1):57–74.

Lu, L., Leutgeb, J. K., Tsao, A., Henriksen, E. J., Leutgeb, S., Barnes, C. A., Witter, M. P., Moser, M.-B., and Moser, E. I. (2013). Impaired hippocampal rate coding after lesions of the lateral entorhinal cortex. *Nature Publishing Group*.

Lütcke, H. and Helmchen, F. (2011). Two-photon imaging and analysis of neural network dynamics. *Rep. Prog. Phys.*, 74(8):086602.

Lütcke, H., Murayama, M., Hahn, T., Margolis, D. J., Astori, S., zum Alten Borgloh, S. M., Göbel, W., Yang, Y., Tang, W., Kügler, S., Sprengel, R., Nagai, T., Miyawaki, A., Larkum, M. E., Helmchen, F., and Hasan, M. T. (2010). Optical recording of neuronal activity with a genetically-encoded calcium indicator in anesthetized and freely moving mice. *Front. Neural Circuits*, 4:9.

Ma, D. L., Tang, Y. C., and Tang, F. R. (2008). Cytoarchitectonics and afferent/efferent reorganization of neurons in layers II and III of the lateral entorhinal cortex in the mouse pilocarpine model of temporal lobe epilepsy. *J. Neurosci. Res.*, 86(6):1324–1342.

Marcantoni, A., Raymond, E. F., Carbone, E., and Marie, H. (2014). Firing properties of entorhinal cortex neurons and early alterations in an Alzheimer's disease transgenic model. *Pflugers Arch - Eur J Physiol*, 466(7):1437–1450.

Margolis, D. J., Lütcke, H., Schulz, K., Haiss, F., Weber, B., gler, S. K. u., Hasan, M. T., and Helmchen, F. (2012). Reorganization of cortical population activity imaged throughout long-term sensory deprivation. *Nature Publishing Group*, pages 1–10.

Markopoulos, F., Rokni, D., Gire, D. H., and Murthy, V. N. (2012). Functional properties of cortical feedback projections to the olfactory bulb. *Neuron*, 76(6):1175–1188.

Markram, H., Toledo-Rodriguez, M., Wang, Y., Gupta, A., Silberberg, G., and Wu, C. (2004). Interneurons of the neocortical inhibitory system. *Nat Rev Neurosci*, 5(10):793–807.

Martin, C., Beshel, J., and Kay, L. M. (2007). An Olfacto-Hippocampal Network Is Dynamically Involved in Odor-Discrimination Learning. *Journal of Neurophysiology*, 98(4):2196–2205.

Matsutani, S. (2010). Trajectory and terminal distribution of single centrifugal axons from olfactory cortical areas in the rat olfactory bulb. *Neuroscience*, 169(1):436–448.

Melzer, S., Michael, M., Caputi, A., Eliava, M., Fuchs, E. C., Whittington, M. A., and Monyer, H. (2012). Long-Range-Projecting GABAergic Neurons Modulate Inhibition in Hippocampus and Entorhinal Cortex. *Science*, 335(6075):1506–1510.

Meyer, H. S., Schwarz, D., Wimmer, V. C., Schmitt, A. C., Kerr, J. N. D., Sakmann, B., and Helmstaedter, M. (2011). Inhibitory interneurons in a cortical column form hot zones of inhibition in layers 2 and 5A. *Proceedings of the National Academy of Sciences*, 108(40):16807–16812.

Miettinen, M., Koivisto, E., Riekkinen, P., and Miettinen, R. (1996). Coexistence of parvalbumin and GABA in nonpyramidal neurons of the rat entorhinal cortex. *Brain Res.*, 706(1):113–122.

Miettinen, M., Pitkänen, A., and Miettinen, R. (1997). Distribution of calretinin-immunoreactivity in the rat entorhinal cortex: coexistence with GABA. *J. Comp. Neurol.*, 378(3):363–378.

Mikkonen, M., Alafuzoff, I., Tapiola, T., Soininen, H., and Miettinen, R. (1999). Subfield- and layer-specific changes in parvalbumin, calretinin and calbindin-D28K immunoreactivity in the entorhinal cortex in Alzheimer's disease. *NSC*, 92(2):515–532.

Mittmann, W., Wallace, D. J., Czubayko, U., Herb, J. T., Schaefer, A. T., Looger, L. L., Denk, W., and Kerr, J. N. D. (2011). Two-photon calcium imaging of

evoked activity from L5 somatosensory neurons in vivo. *Nature Publishing Group*, 14(8):1089–1093.

Miyamichi, K., Amat, F., Moussavi, F., Wang, C., Wickersham, I., Wall, N. R., Taniguchi, H., Tasic, B., Huang, Z. J., He, Z., Callaway, E. M., Horowitz, M. A., and Luo, L. (2011). Cortical representations of olfactory input by trans-synaptic tracing. *Nature*, 472(7342):191–196.

Miyamichi, K., Shlomai-Fuchs, Y., Shu, M., Weissbourd, B. C., Luo, L., and Mizrahi, A. (2013). Dissecting local circuits: parvalbumin interneurons underlie broad feedback control of olfactory bulb output. *Neuron*, 80(5):1232–1245.

Miyawaki, A., Llopis, J., Heim, R., McCaffery, J. M., Adams, J. A., Ikura, M., and Tsien, R. Y. (1997). Fluorescent indicators for Ca2|[plus]|based on green fluorescent proteins and calmodulin. *Nature*, 388(6645):882–887.

Mombaerts, P., Wang, F., Dulac, C., Chao, S. K., Nemes, A., Mendelsohn, M., Edmondson, J., and Axel, R. (1996). Visualizing an olfactory sensory map. *Cell*, 87(4):675–686.

Morales, M. and Bloom, F. E. (1997). The 5-HT3 receptor is present in different subpopulations of GABAergic neurons in the rat telencephalon. *J. Neurosci.*, 17(9):3157–3167.

Mouly, A. M. and Di Scala, G. (2006). Entorhinal cortex stimulation modulates amygdala and piriform cortex responses to olfactory bulb inputs in the rat. *Neuroscience*, 137(4):1131–1141.

Murphy, C. (1999). Loss of olfactory function in dementing disease. *Physiol. Behav.*, 66(2):177–182.

Murthy, M., Fiete, I., and Laurent, G. (2008). Testing odor response stereotypy in the Drosophila mushroom body. *Neuron*, 59(6):1009–1023.

Neunuebel, J. P., Yoganarasimha, D., Rao, G., and Knierim, J. J. (2013). Conflicts between Local and Global Spatial Frameworks Dissociate Neural Representations of the Lateral and Medial Entorhinal Cortex. *Journal of Neuroscience*, 33(22):9246–9258.

Nilssen, E., Kvello, P., and Witter, M. P. (2014). Local connectivity between prinicipal neurons in layer II of lateral entorhinal cortex. In *FENS*, Milano. NTNU.

Otto, T. and Eichenbaum, H. (1992). Complementary Roles of the Orbital Prefrontal Cortex and the Perirhinal Entorhinal Cortices in an Odor-Guided Delayed-Nonmatching-to-Sample Task. *Behav. Neurosci.*, 106(5):762–775.

Otto, T., Schottler, F., Staubli, U., Eichenbaum, H., and Lynch, G. (1991). Hippocampus and olfactory discrimination learning: effects of entorhinal cortex lesions on olfactory learning and memory in a successive-cue, go-no-go task. *Behav. Neurosci.*, 105(1):111–119.

Pearson, R. C. A., Esiri, M. M., Hiorns, R. W., Wilcock, G. K., and Powell, T. P. S. (1985). Anatomical Correlates of the Distribution of the Pathological Changes in the Neocortex in Alzheimer Disease. *Proc. Natl. Acad. Sci. U.S.A.*, 82(13):4531–4534.

Petersen, C. C. H. and Crochet, S. (2013). Synaptic computation and sensory processing in neocortical layer 2/3. *Neuron*, 78(1):28–48.

Petrulis, A., Alvarez, P., and Eichenbaum, H. (2005). Neural correlates of social odor recognition and the representation of individual distinctive social odors within entorhinal cortex and ventral subiculum. *Neuroscience*, 130(1):259–274.

Pohlkamp, T., Dávid, C., Cauli, B., Gallopin, T., Bouché, E., Karagiannis, A., May, P., Herz, J., Frotscher, M., Staiger, J. F., and Bock, H. H. (2013). Characterization and Distribution of Reelin-Positive Interneuron Subtypes in the Rat Barrel Cortex. *Cereb Cortex*.

Powell, T. P., Cowan, W. M., and Raisman, G. (1965). The central olfactory connexions. *J. Anat.*, 99(Pt 4):791–813.

Price, J. L. (1973). An autoradiographic study of complementary laminar patterns of termination of afferent fibers to the olfactory cortex. *J. Comp. Neurol.*, 150(1):87–108.

Proust, M. (1919). *Du côté de chez Swann* . Gaillimard, Paris.

Ramón y Cajal, S. (1902). Sobre un ganglio especial de la corteza esfeno - occipital. *Trab del Lab de Invest Biol Univ Madrid*, 1:189–120.

Ramos-Moreno, T., Galazo, M. J., Porrero, C., Martínez-Cerdeño, V., and Clascá, F. (2006). Extracellular matrix molecules and synaptic plasticity: im-

munomapping of intracellular and secreted Reelin in the adult rat brain. *Eur J Neurosci*, 23(2):401–422.

Ray, S., Naumann, R., Burgalossi, A., Tang, Q., Schmidt, H., and Brecht, M. (2014). Grid-Layout and Theta-Modulation of Layer 2 Pyramidal Neurons in Medial Entorhinal Cortex. *Science*.

Ressler, K. J., Sullivan, S. L., and Buck, L. B. (1993). A zonal organization of odorant receptor gene expression in the olfactory epithelium. *Cell*, 73(3):597–609.

Ressler, K. J., Sullivan, S. L., and Buck, L. B. (1994). Information coding in the olfactory system: evidence for a stereotyped and highly organized epitope map in the olfactory bulb. *Cell*, 79(7):1245–1255.

Rinberg, D., Koulakov, A., and Gelperin, A. (2006). Sparse odor coding in awake behaving mice. *Journal of Neuroscience*, 26(34):8857–8865.

Rogers, J. H. (1992). Immunohistochemical Markers in Rat Cortex - Colocalization of Calretinin and Calbindin-D28k with Neuropeptides and Gaba .1. *Brain Res.*, 587(1):147–157.

Rothschild, G., Nelken, I., and Mizrahi, A. (2010). Functional organization and population dynamics in the mouse primary auditory cortex. *Nature Neuroscience*, 13(3):353–360.

Rubin, B. D. and Katz, L. C. (1999). Optical imaging of odorant representations in the mammalian olfactory bulb. *Neuron*, 23(3):499–511.

Rudy, B., Fishell, G., Lee, S., and Hjerling-Leffler, J. (2011). Three groups of interneurons account for nearly 100GABAergic neurons. *Dev Neurobiol*, 71(1):45–61.

Runyan, C. A., Schummers, J., Van Wart, A., Kuhlman, S. J., Wilson, N. R., Huang, Z. J., and Sur, M. (2010). Response Features of Parvalbumin-Expressing Interneurons Suggest Precise Roles for Subtypes of Inhibition in Visual Cortex. *Neuron*, 67(5):847–857.

Saiz-Sanchez, D., Ubeda-Bañon, I., De la Rosa-Prieto, C., and Martinez-Marcos, A. (2012). Differential expression of interneuron populations and correlation with amyloid-β deposition in the olfactory cortex of an AβPP/PS1

transgenic mouse model of Alzheimer's disease. *J. Alzheimers Dis.*, 31(1):113–129.

Schwerdtfeger, W. K., Buhl, E. H., and Germroth, P. (1990). Disynaptic olfactory input to the hippocampus mediated by stellate cells in the entorhinal cortex. *J. Comp. Neurol.*, 292(2):163–177.

Scoville, W. B. and Milner, B. (1957). Loss of recent memory after bilateral hippocampal lesions. *J. Neurol. Neurosurg. Psychiatr.*, 20(1):11–21.

Serizawa, S., Ishii, T., Nakatani, H., Tsuboi, A., Nagawa, F., Asano, M., Sudo, K., Sakagami, J., Sakano, H., Ijiri, T., Matsuda, Y., Suzuki, M., Yamamori, T., Iwakura, Y., and Sakano, H. (2000). Mutually exclusive expression of odorant receptor transgenes. *Nature Neuroscience*, 3(7):687–693.

Serizawa, S., Miyamichi, K., Nakatani, H., Suzuki, M., Saito, M., Yoshihara, Y., and Sakano, H. (2003). Negative feedback regulation ensures the one receptor-one olfactory neuron rule in mouse. *Science*, 302(5653):2088–2094.

Shipley, M. T. and Adamek, G. D. (1984). The connections of the mouse olfactory bulb: a study using orthograde and retrograde transport of wheat germ agglutinin conjugated to horseradish peroxidase. *Brain Res. Bull.*, 12(6):669–688.

Solodkin, A. and Van Hoesen, G. W. (1996). Entorhinal cortex modules of the human brain. *J. Comp. Neurol.*, 365(4):610–617.

Sosulski, D. L., Bloom, M. L., Cutforth, T., Axel, R., and Datta, S. R. (2011). Distinct representations of olfactory information in different cortical centres. *Nature*, 472(7342):213–216.

Soucy, E. R., Albeanu, D. F., Fantana, A. L., Murthy, V. N., and Meister, M. (2009). Precision and diversity in an odor map on the olfactory bulb. *Nature Publishing Group*, 12(2):210–220.

Staubli, U., Fraser, D., Kessler, M., and Lynch, G. (1986). Studies on retrograde and anterograde amnesia of olfactory memory after denervation of the hippocampus by entorhinal cortex lesions. *Behav. Neural Biol.*, 46(3):432–444.

Staubli, U., Ivy, G., and Lynch, G. (1984). Hippocampal denervation causes rapid forgetting of olfactory information in rats. *Proc. Natl. Acad. Sci. U.S.A.*, 81(18):5885–5887.

Stensola, H., Stensola, T., Solstad, T., Frøland, K., Moser, M.-B., and Moser, E. I. (2012). The entorhinal grid map is discretized. *Nature*, 492(7427):72–78.

Stettler, D. D. and Axel, R. (2009). Representations of Odor in the Piriform Cortex. *Neuron*, 63(6):854–864.

Stettler, D. D., Yamahachi, H., Li, W., Denk, W., and Gilbert, C. D. (2006). Axons and Synaptic Boutons Are Highly Dynamic in Adult Visual Cortex. *Neuron*, 49(6):877–887.

Steward, O. and Scoville, S. A. (1976). Cells of origin of entorhinal cortical afferents to the hippocampus and fascia dentata of the rat. *J. Comp. Neurol.*, 169(3):347–370.

Stewart, W. B., Kauer, J. S., and Shepherd, G. M. (1979). Functional organization of rat olfactory bulb analysed by the 2-deoxyglucose method. *J. Comp. Neurol.*, 185(4):715–734.

Stosiek, C., Garaschuk, O., Holthoff, K., and Konnerth, A. (2003). In vivo two-photon calcium imaging of neuronal networks. *Proc. Natl. Acad. Sci. U.S.A.*, 100(12):7319–7324.

Stranahan, A. M., Haberman, R. P., and Gallagher, M. (2011a). Cognitive decline is associated with reduced reelin expression in the entorhinal cortex of aged rats. *Cereb Cortex*, 21(2):392–400.

Stranahan, A. M., Salas-Vega, S., Jiam, N. T., and Gallagher, M. (2011b). Interference with reelin signaling in the lateral entorhinal cortex impairs spatial memory. *Neurobiol Learn Mem*, 96(2):150–155.

Tahvildari, B. and Alonso, A. (2005). Morphological and electrophysiological properties of lateral entorhinal cortex layers II and III principal neurons. *J. Comp. Neurol.*, 491(2):123–140.

Tamamaki, N., Yanagawa, Y., Tomioka, R., Miyazaki, J.-I., Obata, K., and Kaneko, T. (2003). Green fluorescent protein expression and colocalization with calretinin, parvalbumin, and somatostatin in the GAD67-GFP knock-in mouse. *J. Comp. Neurol.*, 467(1):60–79.

Tang, Q., Burgalossi, A., Ebbesen, C. L., Ray, S., Naumann, R., Schmidt, H., Spicher, D., and Brecht, M. (2014). Pyramidal and Stellate Cell Specificity

of Grid and Border Representations in Layer 2 of Medial Entorhinal Cortex. *Neuron*, pages 1–30.

Theer, P., Hasan, M. T., and Denk, W. (2003). Two-photon imaging to a depth of 1000 microm in living brains by use of a Ti:Al2O3 regenerative amplifier. *Opt Lett*, 28(12):1022–1024.

Tian, L., Hires, S. A., Mao, T., Huber, D., Chiappe, M. E., Chalasani, S. H., Petreanu, L., Akerboom, J., McKinney, S. A., Schreiter, E. R., Bargmann, C. I., Jayaraman, V., Svoboda, K., and Looger, L. L. (2009). Imaging neural activity in worms, flies and mice with improved GCaMP calcium indicators. *Nat Meth*, 6(12):875–881.

Tolu, S., Avale, M. E., Nakatani, H., Pons, S., Parnaudeau, S., Tronche, F., Vogt, A., Monyer, H., Vogel, R., de Chaumont, F., Olivo-Marin, J. C., Changeux, J. P., and Maskos, U. (2010). A versatile system for the neuronal subtype specific expression of lentiviral vectors. *The FASEB Journal*, 24(3):723–730.

Tsao, A., Moser, M.-B., and Moser, E. I. (2013). Traces of Experience in the Lateral Entorhinal Cortex. *Current Biology*, pages 1–7.

Van Cauter, T., Camon, J., Alvernhe, A., Elduayen, C., Sargolini, F., and Save, E. (2013). Distinct roles of medial and lateral entorhinal cortex in spatial cognition. *Cereb Cortex*, 23(2):451–459.

van Groen, T. (2001). Entorhinal cortex of the mouse: cytoarchitectonical organization. *Hippocampus*, 11(4):397–407.

van Groen, T. and Wyss, J. M. (1990). Extrinsic projections from area CA1 of the rat hippocampus: olfactory, cortical, subcortical, and bilateral hippocampal formation projections. *J. Comp. Neurol.*, 302(3):515–528.

van Strien, N. M., Cappaert, N. L. M., and Witter, M. P. (2009). The anatomy of memory: an interactive overview of the parahippocampal–hippocampal network. *Nat Rev Neurosci*, 10(4):272–282.

Varga, C., Lee, S. Y., and Soltesz, I. (2010). Target-selective GABAergic control of entorhinal cortex output. *Nature Publishing Group*, 13(7):822–824.

Vassar, R., Chao, S. K., Sitcheran, R., Nuñez, J. M., Vosshall, L. B., and Axel, R. (1994). Topographic organization of sensory projections to the olfactory bulb. *Cell*, 79(6):981–991.

Vassar, R., Ngai, J., and Axel, R. (1993). Spatial segregation of odorant receptor expression in the mammalian olfactory epithelium. *Cell*, 74(2):309–318.

Wachowiak, M. and Cohen, L. B. (2001). Representation of odorants by receptor neuron input to the mouse olfactory bulb. *Neuron*, 32(4):723–735.

Wachowiak, M., Economo, M. N., Díaz-Quesada, M., Brunert, D., Wesson, D. W., White, J. A., and Rothermel, M. (2013). Optical dissection of odor information processing in vivo using GCaMPs expressed in specified cell types of the olfactory bulb. *Journal of Neuroscience*, 33(12):5285–5300.

Weeden, C. S. S., Hu, N. J., Ho, L. U. N., and Kesner, R. P. (2014). The role of the ventral dentate gyrus in olfactory pattern separation. *Hippocampus*, 24(5):553–559.

Wesson, D. W., Levy, E., Nixon, R. A., and Wilson, D. A. (2010). Olfactory Dysfunction Correlates with Amyloid- Burden in an Alzheimer's Disease Mouse Model. *Journal of Neuroscience*, 30(2):505–514.

White, L. E. (1965). Olfactory bulb projections of the rat. *The Anatomical Record*, 152(4):465–479.

Wiechert, M. T., Judkewitz, B., Riecke, H., and Friedrich, R. W. (2010). Mechanisms of pattern decorrelation by recurrent neuronal circuits. *Nature Publishing Group*, 13(8):1003–1010.

Wilson, D. I. G., Langston, R. F., Schlesiger, M. I., Wagner, M., Watanabe, S., and Ainge, J. A. (2013a). Lateral entorhinal cortex is critical for novel object-context recognition. *Hippocampus*.

Wilson, D. I. G., Watanabe, S., Milner, H., and Ainge, J. A. (2013b). Lateral entorhinal cortex is necessary for associative but not nonassociative recognition memory. *Hippocampus*, 23(12):1280–1290.

Wilson, N. R., Runyan, C. A., Wang, F. L., and Sur, M. (2012). Division and subtraction by distinct cortical inhibitory networks in vivo. *Nature*, 488(7411):343–348.

Wilson, R. C. and Steward, O. (1978). Polysynaptic activation of the dentate gyrus of the hippocampal formation: an olfactory input via the lateral entorhinal cortex. *Exp Brain Res*, 33(3-4):523–534.

Wirth, S., Ferry, B., and Di Scala, G. (1998). Facilitation of olfactory recognition by lateral entorhinal cortex lesion in rats. *Behav. Brain Res.*, 91(1-2):49–59.

Witter, M. P. and Groenewegen, H. J. (1986). Connections of the parahippocampal cortex in the cat. III. Cortical and thalamic efferents. *J. Comp. Neurol.*, 252(1):1–31.

Witter, M. P., Groenewegen, H. J., Lopes da Silva, F. H., and Lohman, A. H. (1989). Functional organization of the extrinsic and intrinsic circuitry of the parahippocampal region. *Progress in Neurobiology*, 33(3):161–253.

Witter, M. P., Room, P., Groenewegen, H. J., and Lohman, A. H. (1986). Connections of the parahippocampal cortex in the cat. V. Intrinsic connections; comments on input/output connections with the hippocampus. *J. Comp. Neurol.*, 252(1):78–94.

Wouterlood, F. G., Canto, C. B., Aliane, V., Boekel, A. J., Grosche, J., Härtig, W., Beliën, J. A. M., and Witter, M. P. (2007). Coexpression of vesicular glutamate transporters 1 and 2, glutamic acid decarboxylase and calretinin in rat entorhinal cortex. *Brain Struct Funct*, 212(3-4):303–319.

Wouterlood, F. G., Härtig, W., Brückner, G., and Witter, M. P. (1995). Parvalbumin-immunoreactive neurons in the entorhinal cortex of the rat: localization, morphology, connectivity and ultrastructure. *J. Neurocytol.*, 24(2):135–153.

Wouterlood, F. G., Mugnaini, E., and Nederlof, J. (1985). Projection of olfactory bulb efferents to layer I GABAergic neurons in the entorhinal area. Combination of anterograde degeneration and immunoelectron microscopy in rat. *Brain Res.*, 343(2):283–296.

Wouterlood, F. G. and Nederlof, J. (1983). Terminations of olfactory afferents on layer II and III neurons in the entorhinal area: degeneration-Golgi-electron microscopic study in the rat. *Neurosci Lett*, 36(2):105–110.

Wouterlood, F. G. and Pothuizen, H. (2000). Sparse colocalization of somatostatin- and GABA-immunoreactivity in the entorhinal cortex of the rat. *Hippocampus*, 10(1):77–86.

Wouterlood, F. G., van Denderen, J. C., van Haeften, T., and Witter, M. P. (2000). Calretinin in the entorhinal cortex of the rat: distribution, morphology, ultra-

structure of neurons, and co-localization with gamma-aminobutyric acid and parvalbumin. *J. Comp. Neurol.*, 425(2):177–192.

Wyss, J. M. (1981). An autoradiographic study of the efferent connections of the entorhinal cortex in the rat. *J. Comp. Neurol.*, 199(4):495–512.

Xu, W., Fitzgerald, S., Nixon, R. A., Levy, E., and Wilson, D. A. (2015). Early hyperactivity in lateral entorhinal cortex is associated with elevated levels of AβPP metabolites in the Tg2576 mouse model of Alzheimer's disease. *Experimental Neurology*, 264(C):82–91.

Xu, W. and Wilson, D. A. (2012). Odor-evoked activity in the mouse lateral entorhinal cortex. *NSC*, pages 1–9.

Yaksi, E., von Saint Paul, F., Niessing, J., Bundschuh, S. T., and Friedrich, R. W. (2009). Transformation of odor representations in target areas of the olfactory bulb. *Nature Neuroscience*, 12(4):474–482.

Yanovsky, Y., Ciatipis, M., Draguhn, A., Tort, A. B. L., and Brankačk, J. (2014). Slow oscillations in the mouse hippocampus entrained by nasal respiration. *Journal of Neuroscience*, 34(17):5949–5964.

Yoganarasimha, D., Rao, G., and Knierim, J. J. (2010). Lateral entorhinal neurons are not spatially selective in cue-rich environments. *Hippocampus*, 21(12):1363–1374.

Young, B. J., Otto, T., Fox, G. D., and Eichenbaum, H. (1997). Memory Representation within the Parahippocampal region (1997). *J. Neurosci.*, 17(13):5183–5195.

Zariwala, H. A., Borghuis, B. G., Hoogland, T. M., Madisen, L., Tian, L., De Zeeuw, C. I., Zeng, H., Looger, L. L., Svoboda, K., and Chen, T. W. (2012). A Cre-Dependent GCaMP3 Reporter Mouse for Neuronal Imaging In Vivo. *Journal of Neuroscience*, 32(9):3131–3141.

List of Figures

List of Tables

Acknowledgements

I would like to use the opportunity to thank several people who helped me in the course of this work. I am grateful to the continuous encouragement that I experienced during the last few years, and I am aware that this support cannot be taken for granted.

I am sincerely grateful to Prof. Hannah Monyer for putting her trust in me and for giving me the chance of a fresh start under much better circumstances. I truly appreciate this. I would also like to thank my doctor father Prof. Peter Seeburg for giving me the freedom to conduct my project both in- and outside of his department.

Dr. Elke Fuchs and Dr. Antonio Caputi taught me how to approach scientific investigations properly. Thank you for being always open to all my questions and willing to discuss countless obstacles with me. Dr. Günther Giese introduced me to the handling of the two-photon microscope and took care of its maintenance whenever I was in need of help to avoid smaller or bigger catastrophes. The construction of a custom-built olfactometer would not have been feasible without the valuable input and assistance from several colleagues at the MPImF, including Martin Lukat, Niklas Neef, Christian Kieser, Dr. Andreas Schäfer, and Dr. Jan Herb. Laura Winkel and Gwenaëlle Matthies supported me with any kind of organizational issues, especially the numerous prolongations of stipends and contracts. I thank Dr. Anne Herb for breeding mice and Ulrike Amtmann and Anja Kravchenko for help with immunostainings.

I thank the Max Planck Society for financial support and the “Hartmut Hoffmann-Berling International Graduate School of Molecular and Cellular Biology“ for offering numerous scientific courses and additional trainings to support my personal career development.

I would like to express my warm thanks to our collaboration partners in Zurich, Prof. Fritjof Helmchen and Dr. Henry Lütcke - it was a great pleasure to work with them on this project. In addition, I would also like to thank Sarah, who joined this project later. Discussions with her, the constant exchange about new ideas and about how to address some challenging problems were not only of great help to me, but they were also great fun. Thanks to the proof-readers of my thesis - Tina, Elke, Sarah, Roberta and Antonio. I am aware that this must have cost you quite some time and stretched your nerves! Roberta and Stephie - we shared so many wonderful moments, both in our office and all over Heidelberg. Thanks for becoming close friends and for making my days at the DKFZ so cheerful! Tina, you became so enthusiastically involved in my project. Thank you not only for your tremendous input, but also for all the non-scientific fun that we had. Eric, Michi, Magda and all the other current or past members of the lab - I really enjoyed working with you and I am grateful for this nice atmosphere that you all help creating!

Cathleen, Kristina and Anikó, you adopted me to the BMM department at the MPImF. You were always a little bit staggered by me and my mice, but your moral support was priceless for me.

Thekla, Silvana, Sophie and Micha - Thank you all for making my time in Heidelberg so special and for being part of my life. Now and in the future, no matter on which continent you will end up doing terrific research.

Basically the first day back then at university in K-Town, I met Anna, Doro, Johanna and Svenja. Thank you for sticking by me through thick and thin! Life at uni and in the world of science would have been much darker without you. Thanks also to Jenny, for a friendship that lasts about 20 years by now!

Thank you, Stefan, for not only tolerating my time-consuming work, but for supporting me in every respect that you possibly could. Even though I never wrote the project plan you had ask for...! Thanks for being by my side.

Thanks to my sisters Anke and Tanja and my brother Frank for taking my mind off work and for reminding me what really matters in life. The warmest thank you from the bottom of my heart goes to my parents for giving me all their support and their love, and the freedom to take my own decisions - both good and bad ones! Thank you for always being there for me.

Appendix

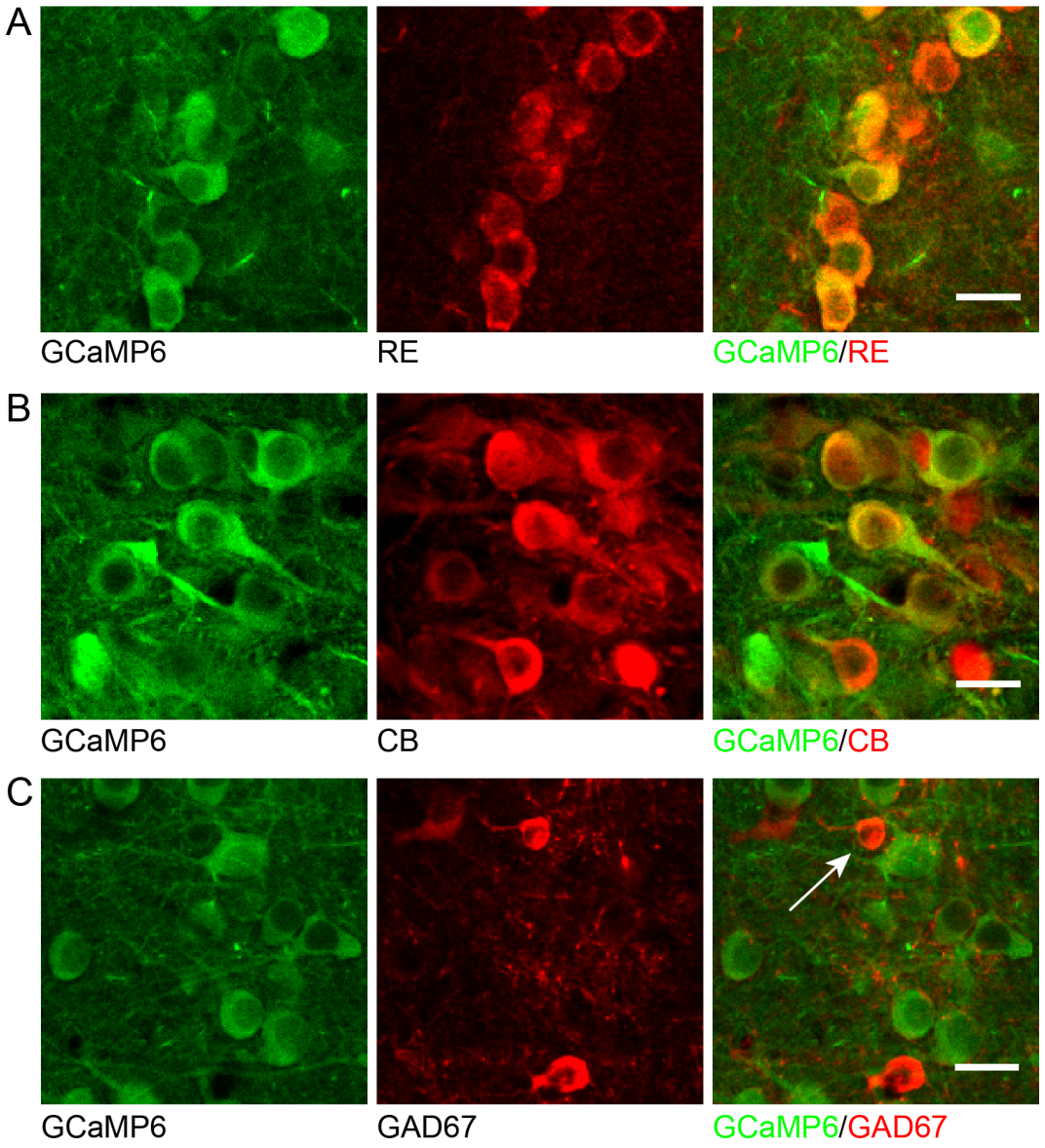

Figure 1. GCaMP6 is expressed in different neuronal cell types. The AAV.GCaMP6 labels cells that express Reelin (**A**), CB (**B**), and GAD67 (**C**). The expression level in Reelin$^+$ neurons is high, whereas there is a tendency for lower expression levels in GAD67$^+$ neurons. The arrow indicates a GCaMP6$^+$/GAD67$^+$ neuron. Scale bars, 20 µm. Abbreviations: CB, calbindin; RE, Reelin.

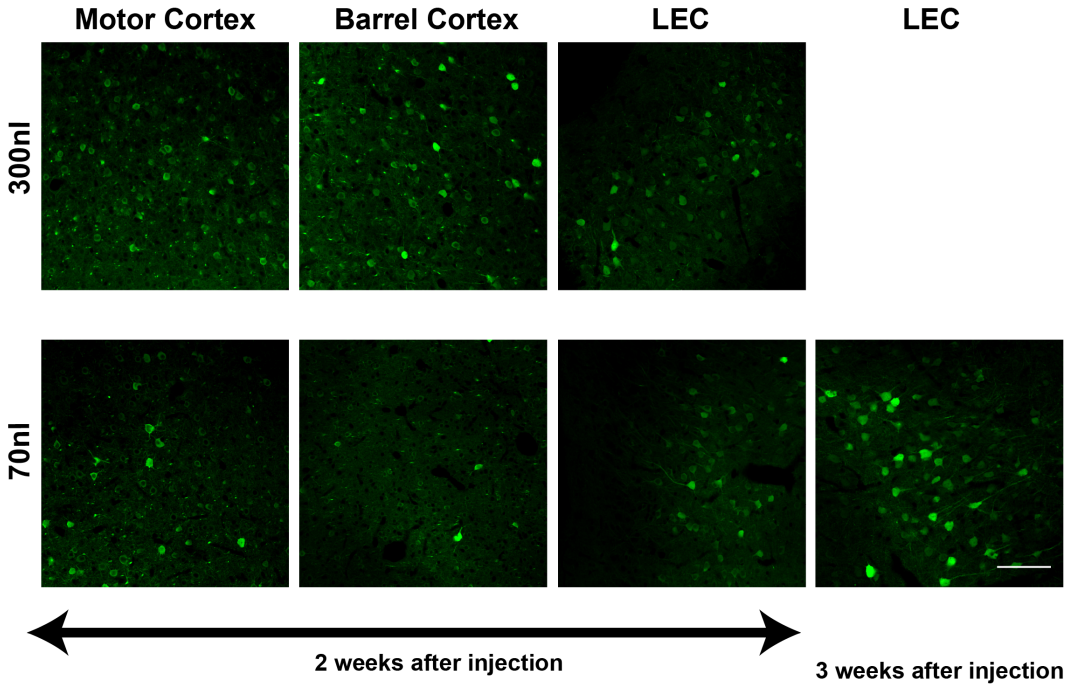

Figure 2. Neurons in the LEC are more susceptible to nuclear filling than in motor cortex and barrel cortex. Two weeks after injection of AAV.GCaMP6, neurons in the LEC tend to reveal nuclear filling, whereas most neurons in motor cortex and barrel cortex appear healthy. Three weeks after injection, basically all neurons in the LEC have filled nuclei. All areas show higher numbers of filled nuclei with 300 nl injection volume compared to 70 nl injection volume. Note that the brightness of the confocal images was kept low on purpose to avoid overexposing the image and thereby artificially increasing the number of neurons with filled nuclei. Scale bar, 100 µm.

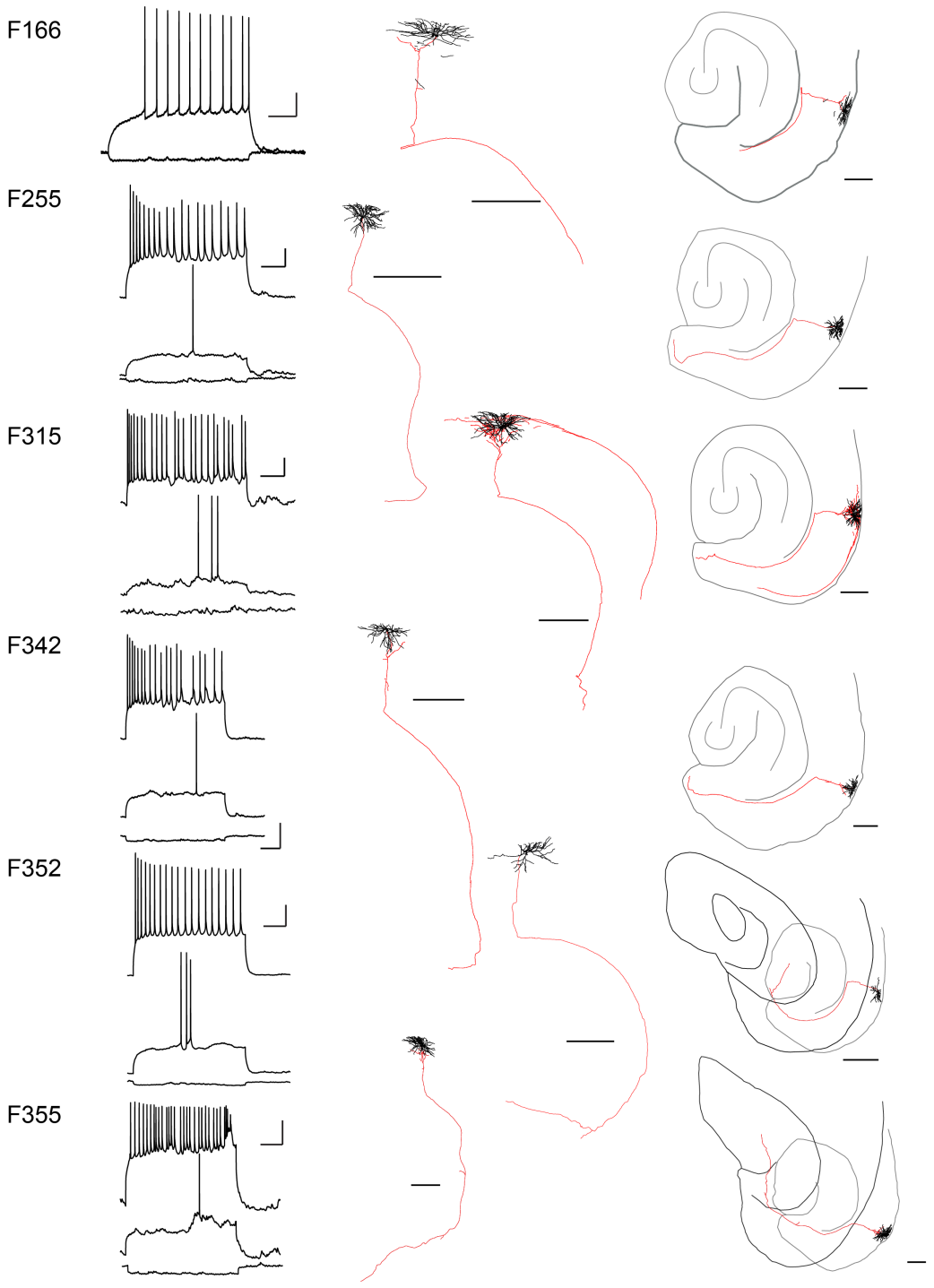

Figure 3. Excitatory cells in LEC LIIa that were not tested for odor-responsiveness are regular spiking or burst-spiking, have spiny dendrites and project towards alveus/presubiculum/hippocampus. Six reconstructed cells are shown with corresponding firing pattern (left panels), higher magnification of the reconstruction and overview of the hippocampus and the LEC with outlines at the level of the cell body (grey) and at the axon terminals (black). Axons are shown in red, dendrites in black, dendrites in black. Scale bars, 20 mV, 200 ms (firing pattern), 400 µm (reconstructions, if not indicated otherwise). Data produced jointly with Dr. Sarah Melzer.

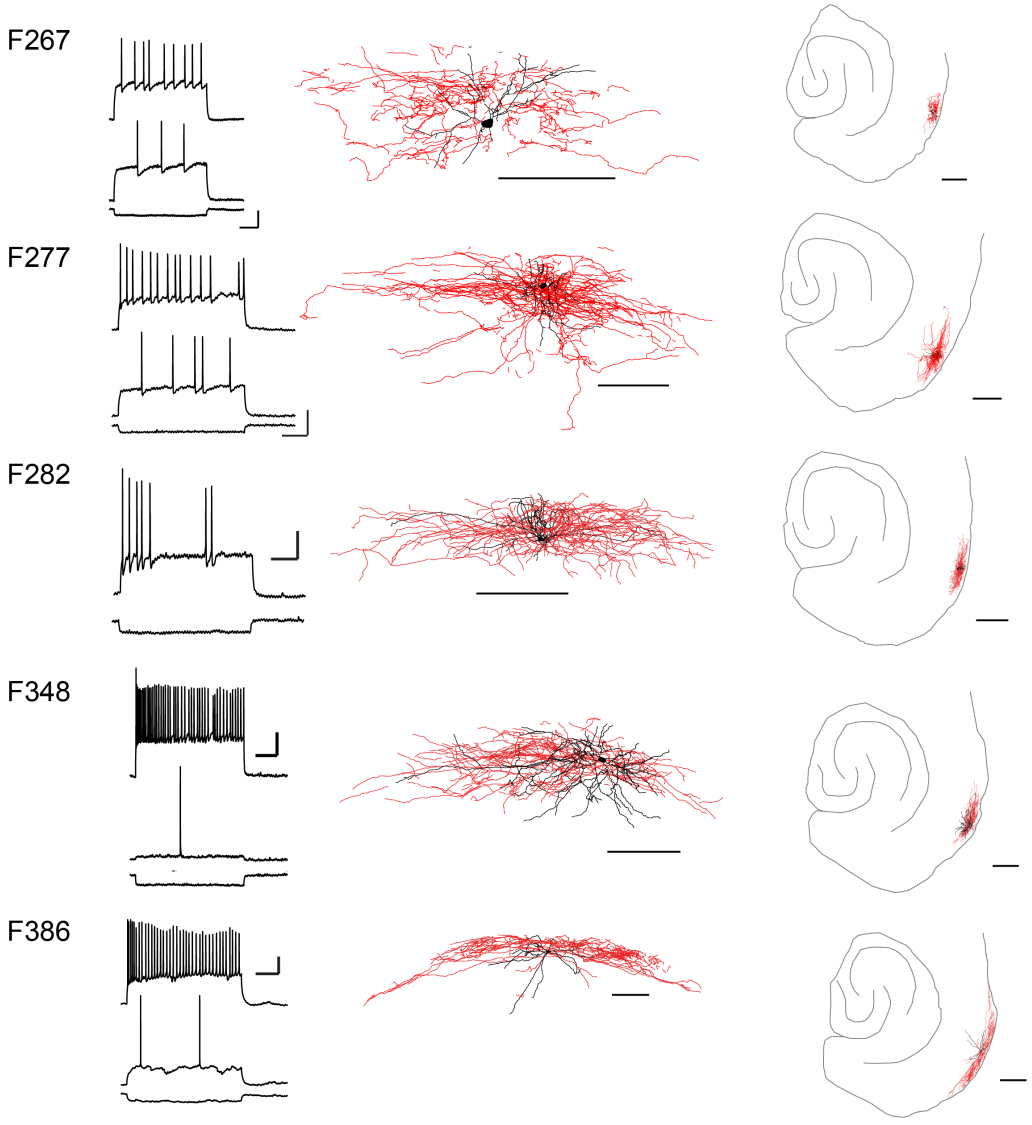

Figure 4. *In vivo* patched and filled *GAD67*^{EGFP} cells have different firing patterns and extensive axon arborizations in the superficial layers of the LEC. Five reconstructed cells are shown with corresponding firing pattern (left panels), higher magnification of the reconstruction and overview of the hippocampus and the LEC. Axons are shown in red, dendrites in black. Scale bars, 20 mV, 200 ms (firing pattern), 200 µm (higher magnification reconstruction), 400 µm (overview). Data produced jointly with Dr. Sarah Melzer.